INFORMATION TO USERS

This manuscript has been reproduced from the microfilm master. UMI films the text directly from the original or copy submitted. Thus, some thesis and dissertation copies are in typewriter face, while others may be from any type of computer printer.

The quality of this reproduction is dependent upon the quality of the copy submitted. Broken or indistinct print, colored or poor quality illustrations and photographs, print bleedthrough, substandard margins, and improper alignment can adversely affect reproduction.

In the unlikely event that the author did not send UMI a complete manuscript and there are missing pages, these will be noted. Also, if unauthorized copyright material had to be removed, a note will indicate the deletion.

Oversize materials (e.g., maps, drawings, charts) are reproduced by sectioning the original, beginning at the upper left-hand corner and continuing from left to right in equal sections with small overlaps. Each original is also photographed in one exposure and is included in reduced form at the back of the book.

Photographs included in the original manuscript have been reproduced xerographically in this copy. Higher quality 6" x 9" black and white photographic prints are available for any photographs or illustrations appearing in this copy for an additional charge. Contact UMI directly to order.

UMI®

Bell & Howell Information and Learning
300 North Zeeb Road, Ann Arbor, MI 48106-1346 USA
800-521-0600

KINETIC STUDIES OF ELECTRON TRANSFER FROM Q_A to Q_B IN THE PHOTOSYNTHETIC REACTION CENTER PROTEIN

by

JIALI LI

A dissertation submitted to the Gradute Faculty in Physics in partial fulfillment of the requirements for the degree of Doctor of Philosophy, The City Univercity of New York

1999

This manuscript has been read and accepted for the Graduate Faculty in Physics in the satisfaction of the dissertation requirement for the degree of Doctor of Philosophy.

6/2/99
Date

Chair of Examining Committee

6/8/99
Date

Executive Officer

R. Callender

J. Lombardi

A. Mcdermott

V. Patricevic

Supervisory Committee

THE CITY UNIVERSITY OF NEW YORK

ABSTRACT

KINETIC STUDIES OF ELECTRON TRANSFER FROM Q_A to Q_B IN PURPLE BACTERIA REACTION CENTERS

by

Jiali Li

Advisor: Professor Marilyn R. Gunner

Reaction center (RC) function and electron transfer kinetics were measured following changes in the protein environment at the Q_B site by mutation and changes in the Q_A^- energy level by quinone exchange.

A mutant with M220-M261 from the Q_A site substituted for L193-L227 in the Q_B site in *Rb. capsulatus* RCs were studied. Despite the huge change in the Q_B pocket, secondary quinone function still can be reconstituted. The UQ4 dissociation constant for the Q_B site in the mutant is only 2 times larger than in the wild type RCs. The electron transfer rate of the mutant from Q_A^- to Q_B is 14/s, 3 orders of magnitude slower than the wild type RCs. The equilibrium constant between $Q_A^-Q_B$ and $Q_AQ_B^-$ is bigger than 200 in the mutant compared to 10 in the wild type, showing a large stabilization of Q_B^-.

Electron transfer from $P^+Q_A^-Q_B$ to $P^+Q_AQ_B^-$ was measured in R-26 *Rb. sphaeroides* RCs where Q_A was substituted with different naphthoquinones

(NQ_A), Q_B was ubiquinone (UQ_B) in all cases. These substitutions change the redox midpoint potential of Q_A and therefore change the driving force (ΔG_{AB}) for electron transfer. The absorption change provides a direct monitor of the electron transfer from NQ_A^- to UQ_B. The electron transfer rate is heterogeneous. In RCs with 2-methyl-3-phytyl-1,4-naphthoquinone (MQ) substituted at Q_A, three rates are observed: $\tau_1 \approx 3\mu s \pm 0.9\mu s$, $\tau_2 = 80 \pm 20\mu s$, and $\tau_3 = 0.4 \pm 0.2ms$ at pH=8 and 22°C. Analysis of the time correlated spectra shows that the changes at τ_1 are mostly due to electron transfer, electron transfer and charge compensation are mixed in τ_2, while little or no electron transfer occurs at τ_3 in MQ_AUQ_B RCs. The activation energy for electron transfer is $\Delta G \approx 3.5$ kcal/Mol for both τ_1 and τ_2. With different NQs at Q_A, τ_1 is found to be free energy dependent with a reaction reorganization energy of 850±100 meV. The slower phase τ_2 is free energy independent.

ACKNOWLEDGMENT

I own special gratitude to my thesis advisor Professor Marilyn R. Gunner for her constant education, guidance, encouragement and support; for giving me an opportunity to work in the field of photosynthesis which I like so much.

I am very grateful to Dr. William J. Coleman for providing me the opportunity to study his interesting Q_AQ_A mutant, to Dr David M. Tiede for useful discussion and technical assistance on measuring electron transfer from Q_A to Q_B, to Dr. Eiji Takahashi and Colin Wraight for providing their mutant RCs and helpful discussions.

I would like to thank members of my examine committee, Professors Robert Callender, John Lombardi, Ann Mcdermott and Vladimir Petricevic for their valuable time and suggestions.

I very much thank Dr. Hua Deng for his valuable time and support, HongFeng Du for his help on electronic devices, Dan Gilroy for his help when I came to the lab, co-workers Qing Xu, Samir Lipovaca, Dmitri Karpman and Emil Alexov for their help and support.

Finally, I would like to thank my husband, Ma Sha, for his support and patience over the years. I also thank my parents, my family, and my teachers for their help throughout my school years.

TO MY PARENTS AND MY TEACHERS

TABLE OF CONTENTS

LIST OF TABLES

LIST OF FIGURES

1. Abbreviations:

P, or P870 bacteriochlorophyll dimer which is the electron donor in the reaction center protein

BPh_L, bacteriopheophytin near Q_A on the L branch of the protein

BPh_M, bacteriopheophytin near Q_B on the M branch

MQ, 2-methyl-3-phytyl-1,4-naphthoquinone

UQ, Ubiquinone-10: 2,3-dimethoxy-5-methyl-6-decaisopropyl-1,4-benzoquinone;

P^+Q^- difference spectrum is the absorption of P^+Q^- minus that of PQ;

Q^- spectrum is the semiquinone minus quinone spectrum;

k_{AB} is the rate constant of the electron transfer from $P^+Q_A^-$ to form $P^+Q_B^-$, this includes all associated processes.

Lifetimes for reactions:

τ_{AP} for $P^+Q_A^-$->PQ_A

τ_{BP} for $P^+Q_B^-$ ->PQ_B

τ_{AB} for $P^+Q_A^-Q_B$ ->$P^+Q_AQ_B^-$. τ_{AB} was analyzed as sum of 3 exponentials with lifetimes τ_1, τ_2 and τ_3 and respective amplitudes A_1, A_2 and A_3

DMNQ=2,3-Dimethyl-1,4-naphthoquinone

MK4=2-methyl-3-tetraisoprenyl-1,4-naphthoquinone

TMNQ=2,3,5-trimethyl-1,4-naphthoquinone

TEMNQ=2,3,6,7-tetramethy-1,4-naphthoquinone

Chapter 1
INTRODUCTION

Nature's most sophisticated and important solar energy storage system is found in photosynthetic organisms, including plants, algae and a variety of types of bacteria. Photosynthesis is arguably the most important biological process on earth. It is essential to life and it is the primary energy source of almost all the living world. These natural "technologies" have been developed over several billion years. So research into photosynthesis is vitally important. Through understanding it, we may learn to control the complexity of the photosynthetic processes. This knowledge may allow us to use the basic chemistry and physics of photosynthesis for many purposes, such as to enhance production of food, fiber and to enhance solar energy conversion, and the construction of molecular electronic devices.

The first steps of photosynthetic light-energy conversion: light absorption followed by a series of electron transfer reactions, takes place in protein complexes located in photosynthetic membranes. The membrane serves as a means of storing electrochemical free energy by allowing the creation of transmembrane proton ($\Delta\mu_H$) and electrical ($\Delta\psi$) gradients. The energy stored in the gradients can be used to drive energy requiring processes such as manufacturing ATP which are necessary to the life of the cell (1).

The photosynthetic apparatus used to perform the conversion is both complex and highly efficient. Two initial steps of photosynthesis are energy transfer and electron transfer. Light absorption results in the formation of the lowest excited singlet state of bacteriochlorophyll (BChl) of the light-

harvesting system. This electronic excitation energy is transferred to a special dimmer of BChl in the protein-cofactor complex called the reaction center (RC), where is the site of the initial photosynthetic electron transfer reactions.

1.1 Photosynthetic reaction center: Function and Structure

The success of studying photosynthetic electron transfer comes from the many technical advantages of working with the reaction centers from purple nonsulfur bacteria. The reaction centers of several species are readily isolated in high yield and in most cases are stable for days in the dark at room temperature or indefinitely when frozen (2, 3).

Studies of the electron transfer reaction have focused on the RC from *Rb. sphaeroides* strain R-26 since it was isolated from this source by Reed and Clayton in 1968 (4, 5). In addition, the structure of this RC is available at atomic resolution, permitting sophisticated analysis of the relationship between the protein's structure and its function. So this RC is a very good model for the study of functional, high efficiency, long range electron transfer in proteins.

With the x-ray diffraction data and other analytical techniques, the structure of the reaction center of *Rb. sphaeroides* R-26 was determined in considerable detail (Fig. 1.1). Like all reaction centers, this one consists of two main systems: the protein and the donor-acceptor complex. The protein is made up of three distinct subunits, L, M, and H, which have 281, 307, and 260 amino acids, respectively. The donor-acceptor complex is embedded

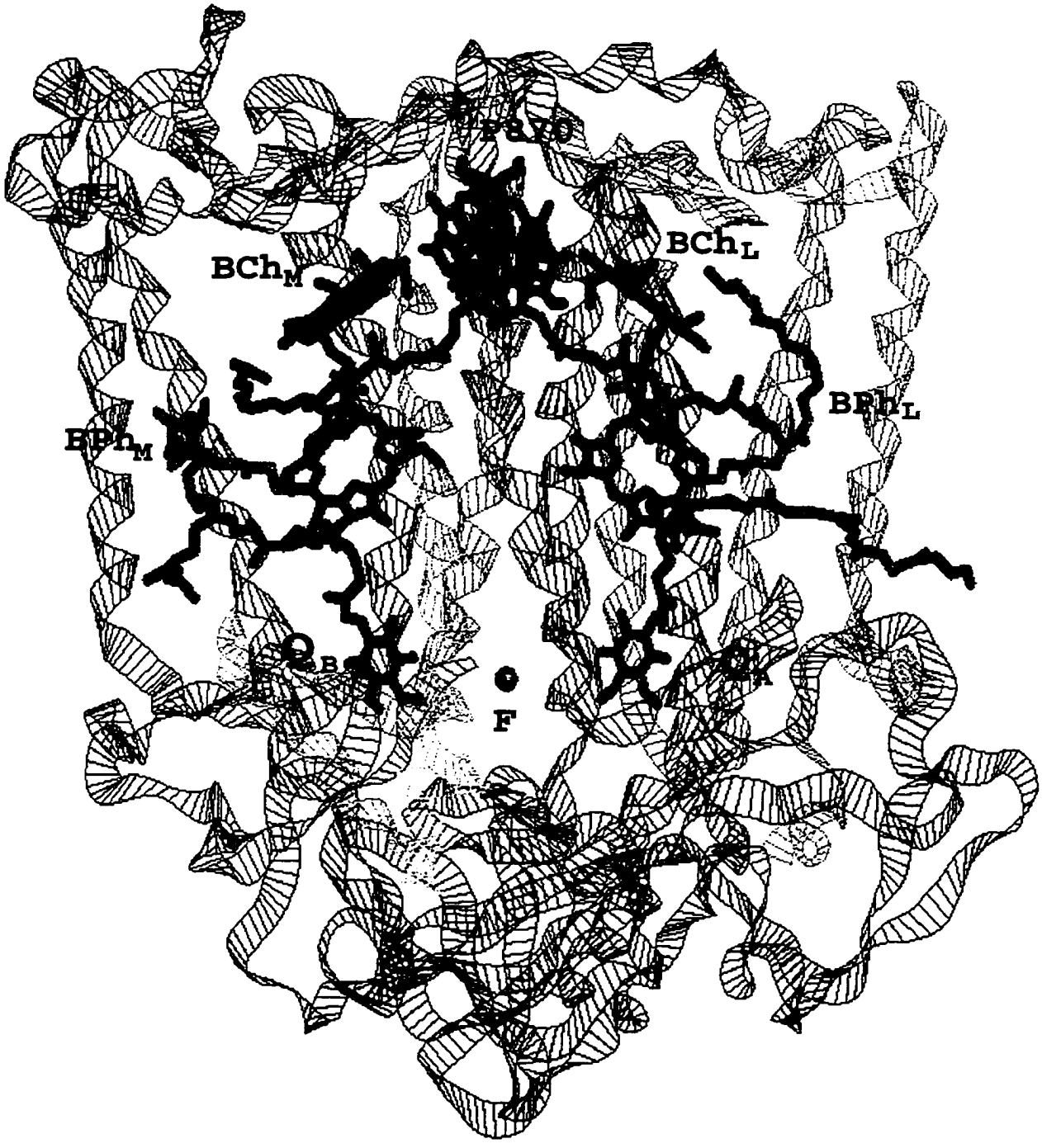

FIGURE 1.1. Structure of the reaction center protein of the purple bacterium *Rhodobacter sphaeroides.* The complex consists of three protein subunits called M, L and H.

primarily in the L and M components. The H protein has one hydrophobic helix that traverses the membrane and the L and M proteins each have five. The H protein also has a hydrophilic region that "caps" L and M proteins on the side of the membrane that faces the inside of the cell.

The donor-acceptor complex is a group of bound cofactors which is directly responsible for the activity of reaction center, absorbing light and participating in a series of electron transfer reactions. The cofactors contain four bacteriochlorophyls (BChl), two bacteriopheophytins (BPh), two ubiquinones, and a nonheme F_e^{2+}. Of the total molecular weight of the RC protein 52% is contributed by these cofactors (6). None of these cofactor molecules are covalently bound to the RC protein. Two of the BChls are close to the symmetry axis near the periplasmic side of the RC. They are in van der Waals contact and closely coupled, reacting as a single unit, known as the special pair ([BChl]$_2$,P870 or P). One of these two is associated with the L subunit and the other with the M subunit. The remaining two BChls are referred to as the bridging or accessory BChls. One is complexed with each subunit ($BChl_L$ and $BChl_M$). Similarly, one BPh is associated with each subunit (BPh_L and BPh_M). Q_A is in a loop from the M subunit, and Q_B is mostly surrounded by residues contributed from L. Only the iron, which is between and is closely associated with both ubiquinones, does not have a corresponding pair. The L subunit, the M subunit, and the donor-acceptor complex are related by an approximate two fold C_2 axis of symmetry (7, 8).

1.2. The Theory of Electron Transfer in Protein

Electron transfer is one of the most fundamental processes in chemistry and biology. Many levels of electron transfer theory incorporating semiclassical to fully quantum mechanical multi-mode approaches can be used to obtain a phenomenological description of electron transfer processes. In the non-adiabatic (weak coupling) limit, derived from quantum mechanical perturbation theory, the electron transfer rate is expressed in terms of Fermi's Golden Rule:

$$k_{et} = \frac{2\pi}{\hbar} V_R^2 (FC) \qquad (1.1)$$

where h is Planck's constant, V is the electronic coupling and FC is the Frank-Condon (vibrational overlap) factor. where V_R^2, the electron tunneling matrix element, is a measure of the quantum mechanical matrix element coupling reactant and product electronic wavefunctions. For nonadiabatic electron transfer, where the coupling is weak by definition, the overlap of donor and acceptor electronic wavefunctions will simply follow an exponential decay with distance:

$$V_R^2 = V_0^2 \exp(-\beta R) \qquad (1.2)$$

here V_0^2 is the maximum electronic coupling, R is the center of edge atom of donor to center of edge atom of acceptor, β is the exponential coefficient for decay of electronic coupling with R. The value of β lies in the range of 0.6-1.5 $Å^{-1}$ in condensed media as has been determined by both experiment and theory (9).

FC, the Frank-Condon weighted density of states, is the integrated overlap of donor and acceptor nuclear wavefunctions of equal energy. The Frank-

Condon factor is commonly expressed in terms of the driving force (-ΔG) of the reaction and the reorganization energy (λ). the reorganization energy consists of changes in bond lengths, bond angles, and distance or orientation of the donor, acceptor, and the medium. Quantum mechanical theories express the Frank-Condon factor in terms of vibrational modes of the participants, and how strongly these modes are coupled to the electron transfer event. The Marcus classic expression for overlap of classical harmonic oscillator wavefunctions with identical frequencies is:

$$FC = \frac{1}{\sqrt{4\pi\lambda k_B T}} \exp -[\frac{(-\Delta G^\circ - \lambda)^2}{4\lambda k_B \mathrm{T}}] \qquad (1.3)$$

here λ is the reorganization energy, which is the energy required to distort the nuclear configuration of the product state into the geometry of the reactant state without electron transfer. $-\Delta G^\circ$ is the free energy difference between reactant and product state.

There are three regions of interest in assessing the magnitude of the Frank-condon factor: (1) the normal, or activated region (-ΔG<λ) where the rate of electron transfer increases as the driving force increases; (2) the activationless region (-ΔG=λ) where the rate of electron transfer reaches its maximum for a given electronic coupling; and (3) the so-called inverted region (-ΔG>λ). Semiclassical theory predicts a rapid decrease in rate as the driving force increases in the inverted region, while quantum mechanical treatments predict a more gradual decrease in the rate with increasing -ΔG when high-frequency modes are coupled to the reaction.

Combining equation (2) to (4), the electron transfer rate is:

$$k_{et} = \frac{2\pi {V_0}^2}{\hbar\sqrt{4\pi\lambda k_B T}} e^{-\beta R} \exp -[\frac{(-\Delta G^\circ - \lambda)^2}{4\lambda k_B \mathrm{T}}] \qquad (1.4)$$

This relationship predicts that the rate of reaction will be maximal when $-\Delta G^{\circ} = \lambda$, and will fall off at smaller and larger values of ΔG° (Fig. 1.2). The activation energy E_A is a measure of FC and is given by

$$E_A = (-\Delta G^{\circ} - \lambda)^2 / 4\lambda \qquad (1.5)$$

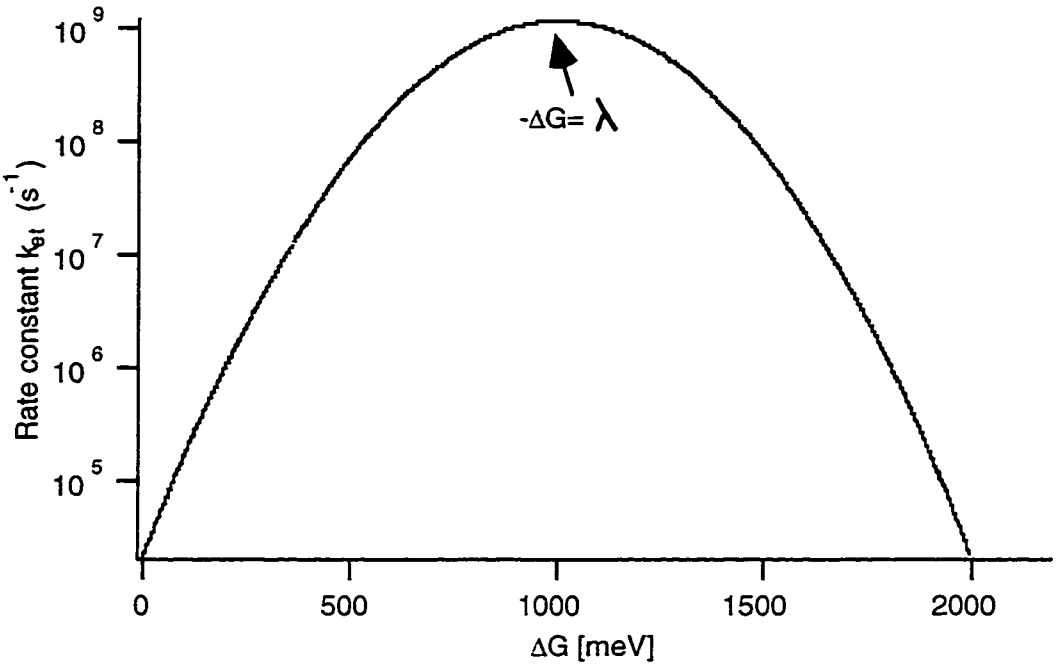

Figure 1.2. Free energy dependence of electron transfer rates. λ is assumed 1000meV here.

When $-\Delta G^{\circ} = \lambda$, equation (1.5) has $E_A = 0$, the reaction is "activationless" and essentially depends only on the electronic factors (V_0^2). In fact, the theoretical temperature dependence is slightly negative, due to the pre-exponential factor of Equation 1.4. As the temperature is lowered, this corresponds to the settling of the reactant state thermal distribution into the lowest vibrational levels. This yields the fastest rate, so the reaction speeds up as the system is cooled! The temperature dependence is approximately $T^{-1/2}$ (from Eq. 1.4) (9, 10).

The long-range electron transfer through proteins depends on several factors:

- the driving force, i.e. the redox potential difference, ΔG
- the distance between and relative orientation of the donor and acceptor
- the relaxation energy associated with the conformational changes that accompany the change of redox state.

1.3. Electron Transfer in Reaction Center Protein

It is well-established that the in vitro rates of the intra-protein electron transfer reactions and the yields of the various charge-separated intermediates are essentially the same as in vivo. The initial electron transfer reactions of photosynthesis have been best studied in the reaction centers of the purple nonsulfur bacteria (11, 12, 13, 14). Though many of the mechanistic details of the process remain unclear, the overall reactions are well known. Figure 1.3 summarizes the pathways and rates of the electron transfer reactions in this protein. Each of the intra-RC electron transfers has a characteristic driving force (varying from 0.06 to 1.2 eV), distance (from 7 to 25 Å (edge to edge)), and reaction rate (varying by 10^9). These reactions occur even at cryogenic temperatures (except the electron transfer from Q_A to Q_B in RCs cooled in the dark).

The reaction sequence starts when an electron on the primary electron donor, P, is promoted to the excited singlet state P^*. Thus a series of electron transfer reactions is initiated (Fig.1.3).

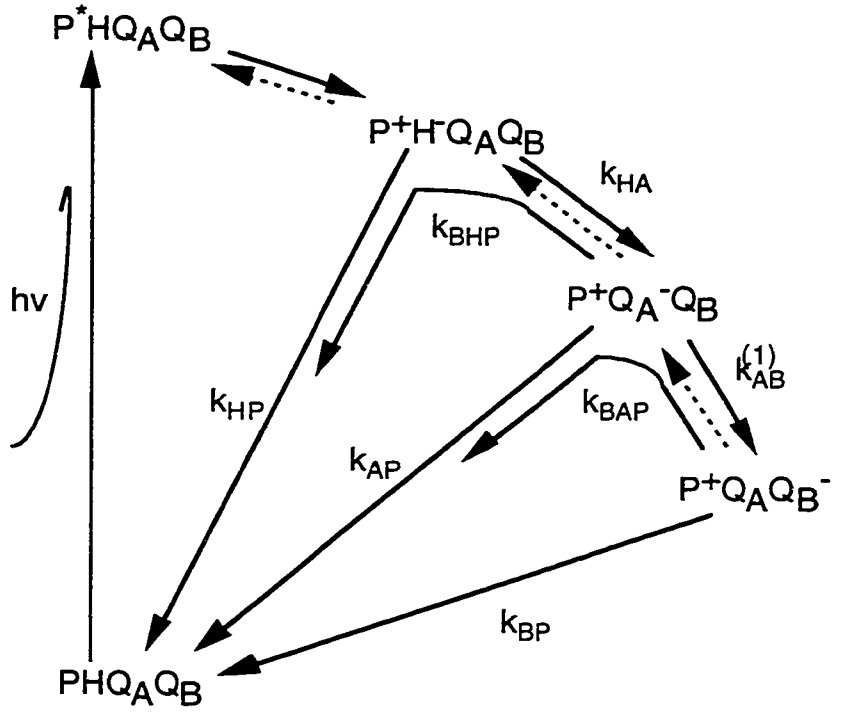

Figure 1.3. RC electron transfer pathways in the bacterial RCs. First an electron on P is promoted to the excited singlet state (P*) by absorption of a photon. Initial charge separation, over 15 Å to BPh with $-\Delta G \approx 160$ meV, occurs in 4 ps forming P^+BPh^-. In 200 picoseconds the electron moves to the tightly bound primary quinone Q_A, 10.1 Å from BPh with $-\Delta G \approx 670$ meV. The subsequent electron transfer from Q_A^- to the secondary quinone, Q_B, 14.5 Å from Q_A with $-\Delta G_{AB} \approx 60$ meV, has been measured to occur within 3-200 microseconds yielding $P^+Q_B^-$. If there is no exogenous donor to donate an electron to P^+, the electron on the acceptors will go back to P^+ in a charge recombining, back reaction. The back reactions from Q_A^- or Q_B^- to P^+ (22.5 and 23.4 Å respectively) each have two pathways: k_{BP} or k_{AP} where the electron goes back directly to P^+; and k_{BAP} or k_{BHP} where the electrons go back indirectly to P^+ via a higher energy state. The intermediate state is $P^+Q_A^-Q_B$ for $P^+Q_B^-$ and $P^+H^-Q_A$ for $P^+Q_A^-$.

A. Electron Transfers Between P and BPh

After excitation of P, the charge separation of $P^+BPh_L^-$ occurs in 4 ps over a distance of 10.1 Å (center of edge atom of P to center of edge atom of BPh_L). No reduction of BPh_M is observed. The electron transfer is activationless, with the rate increasing by 2 to 3 fold as the temperature is decreased to 5 K. The charge recombination of $P^+BPh_L^-$ to the ground state $PBPh_L$ occurs in $\tau \approx 20$ ns. The $-\Delta G^\circ$ is approximately 160 meV and $-\Delta G^\circ \approx \lambda$ for the native reaction. The reaction is unidirectional, with electrons going exclusively down the L branch of the reaction center (11).

B. The Electron Transfer From BPh^- to Q_A

This reaction occurs over about 10 Å with a life time of approximately 200 psec. More than 98% of the RCs that absorb a photon reach the state $P^+Q_A^-$ (15). The reaction $-\Delta G^\circ$ is about 670 meV. the reaction slows 3 to 4 fold as the temperature is increased from 5 to 300 K. When the native UQ_{10} is Q_A, the rate is the fastest and $-\Delta G^\circ \approx \lambda$. In the absence of Q_B and an electron donor to P^+, $P^+Q_A^-$ decays to the ground state at k_{AP}. In native *Rb. sphaeroides* reaction centers this occurs by direct electron transfer 22.5 Å across the protein. The decay time constant is 100 ms at 300 K and 33 ms below 100K (11). This rate increases as temperature lowered consistent with Marcus electron transfer theory (equation 1.4).

C. The electron transfer from Q_A to Q_B

In many respects, the electron transfer between the two quinones is the most complex reaction that occurs in the reaction center. Unlike the other electron transfers that occur between one-electron carriers in a nearly solid-state

configuration, Q_B is a two electron carrier and electron transfer is linked both to proton uptake and binding of quinone to the Q_B site.

The rate of electron transfer from Q_A to Q_B has been measured. It is about 5000 s^{-1} across the 14.5 Å distance. The $-\Delta G^{\circ}_{AB}$ between $Q_A^-Q_B$ and $Q_AQ_B^-$ has been determined in *Rb. sphaeroides* RCs by a variety of methods. All methods provide a $-\Delta G^{\circ}_{AB}$ value for electron transfer from Q_A- to Q_B of 60 to 80 meV at pH 7 to 8. The $-\Delta G^{\circ}_{AB}$ for the second reduction of Q_B ($Q_A^-Q_B^-$ to $Q_AQ_BH_2$) appears to be about 90 meV at pH 8.

D. Charge Recombination

If there is no exogenous donor to donate an electron to P^+, the electron on the quinone acceptors will go back to P^+ in a charge recombining, back reaction. The back reactions from Q_A^- or Q_B^- to P^+ each have two pathways: k_{BP} or k_{AP} where the electron goes back directly to P^+; and k_{BAP} or k_{BHP} where the electrons go back indirectly to P^+ via a higher energy state. (Fig. 1.3). The intermediate state is $P^+Q_A^-Q_B$,for $P^+Q_B^-$ and $P^+H^-Q_A$ for $P^+Q_A^-$. Electron transfer pathways and charge recombination kinetics associated with Q_A and Q_B can be calculated (Appendix 2). The computer simulated kinetics based on the analytical solution then can be used to help to understand reaction mechanism underlying the measured kinetic data. In the thermally activated, uphill reactions, the reaction rates are proportional to the free energy difference between the initial and intermediate states. Therefore these rates can provide a measure of the relative free energy of different states.

References

1. Cramer, W. A., and Knaff, D. B. (1991) *Energy Transduction in Biological Membranes: A Textbook of Bioenergetics*, Springer-Verlag, New York.
2. Feher, G., and Okamura, M. Y. (1978) in *The Photosynthetic Bacteria* (Clayton, R. K., and Sistrom, W. R., Eds.) pp 349-386, Plenum Press, New York.
3. Prince, R. C., and Youvan, D. C. (1987) *Biochim. Biophys. Acta 890*, 286-291.
4. Reed, D. W., and Clayton, R. K. (1968) *Biochim. Biophys. Res. Commun. 30*, 471.
5. Reed, D. W. (1969) *J. Biol. Chem. 244*, 4936.
6. Williams, J. C., Steiner, L. A., and Feher, G. (1986) *Proteins 1*, 312-325.
7. Deisenhofer, J., and Michel, H. (1989) *Science 245*, 1463-1473.
8. Okamoto, Y. (1994) *Biopolymers 34*, 529-539.
9. Moser, C. C., Keske, J. M., Warncke, K., Farid, R., and Dutton, P. L. (1992) *Nature 355*, 796-802.
10. Marcus, R. A., and Sutin, N. (1985) *Biochim. Biophys. Acta 811*, 265-322.
11. Gunner, M. R. (1991) *Current Topics in Bioenergetics 16*, 319-367.
12. Kirmaier, C., and Holten, D. (1987) *Photosynthesis Research 13*, 225-260.
13. Kirmaier, C., and Holten, D. (1993) in *The Photosynthetic Reaction Center* (Deisenhofer, J., and Norris, J. R., Eds.) pp 49-70, Academic Press, San Diego.
14. Feher, G., Allen, J. P., Okamura, M. Y., and Rees, D. C. (1989) *Nature 339*, 111-116.
15. Wraight, C. A., and Clayton, R. K. (1973) *Biochim. Biophys. Acta 333*, 246-260.

Chapter 2
Absorption Spectroscopy

2.1 Absorption Spectroscopy

Measurements of absorbance and of light-induced changes of absorbance have been very useful tools to study photosynthesis. This is one of the basic methods to obtain information about the characteristics of photosynthetic proteins. In absorption spectrophotometry, the fraction of incident light transmitted by a sample is measured over a selected range of wavelengths. Modern instruments measure the *transmittance* (T) and the *optical density* (O.D.), which are related by

$$O.D. = \log_{10} (1/T)$$

An O.D. range of 0-4 corresponds to a change T from 1 to 0.0001. The absorbance (A) is used to designate the contribution of absorption alone to optical density. The ideal absorbance of a dilute solute in a transparent solvent follows the Lambert-Bouguer-Beer law:

$$A = \varepsilon cd = \log_{10} (I_0/I_x)$$

where ε (Liters/mole-cm or ml/mM-cm) is the *molar extinction coefficient* of the solute at the wavelength of measurement, c (moles/Liter or mM/ml) is the molarity of the solute, and d (cm) is the optical pathlength. I_0 and I_x are the light intensities before and after passing through the sample. The concentration of a solute can be calculated by measuring A, when ε is known at the measurement wavelength. Fig. 2.1 shows the absorption spectra of

isolated RC from *Rhodobacter sphaeroides* taken by a spectrophotometer (SHIMADZU UV160U).

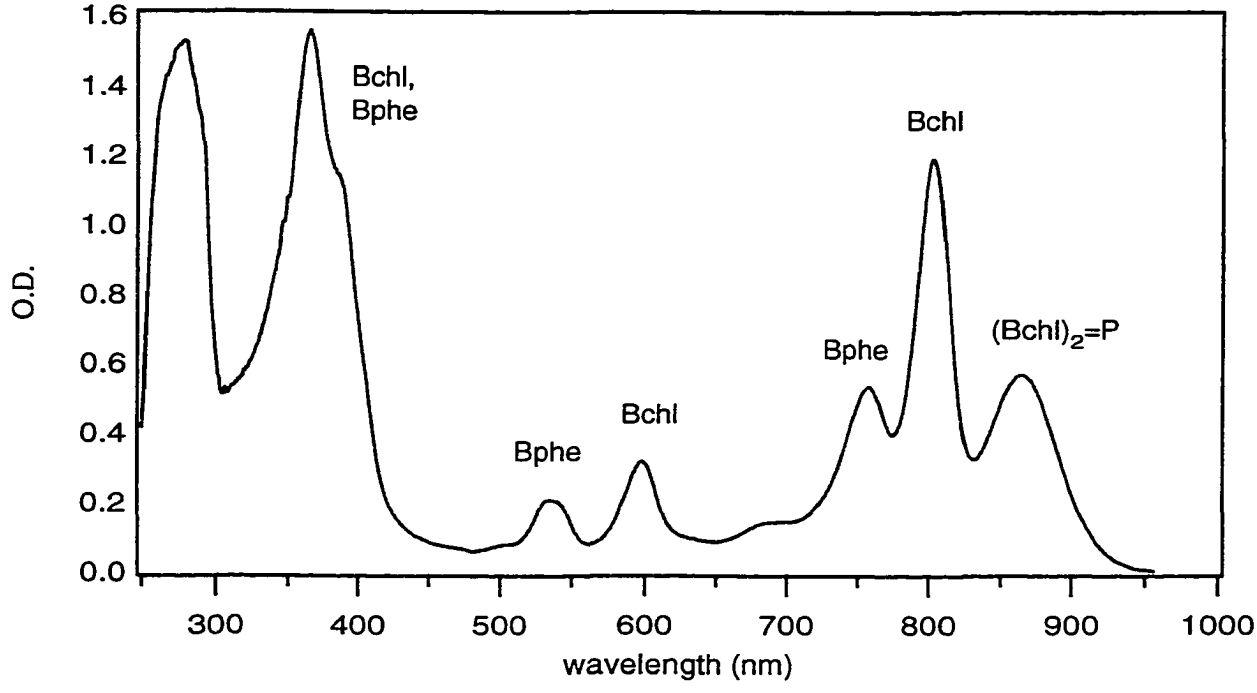

Fig. 2.1. Absorption spectra of reaction centers isolated from carotenoidless mutant *Rb. sphaeroides*. Bands due to bacteriochlorophyll (Bchl), bacteriopheophytin (Bphe), are labled.

2.2 Instrumentation

Flash photolysis is a major application of absorption spectroscopy. In this technique, the system of interest is irradiated with a short, intense light flash, and the short-lived intermediate states are identified and followed in real time by making fast optical absorption measurements.

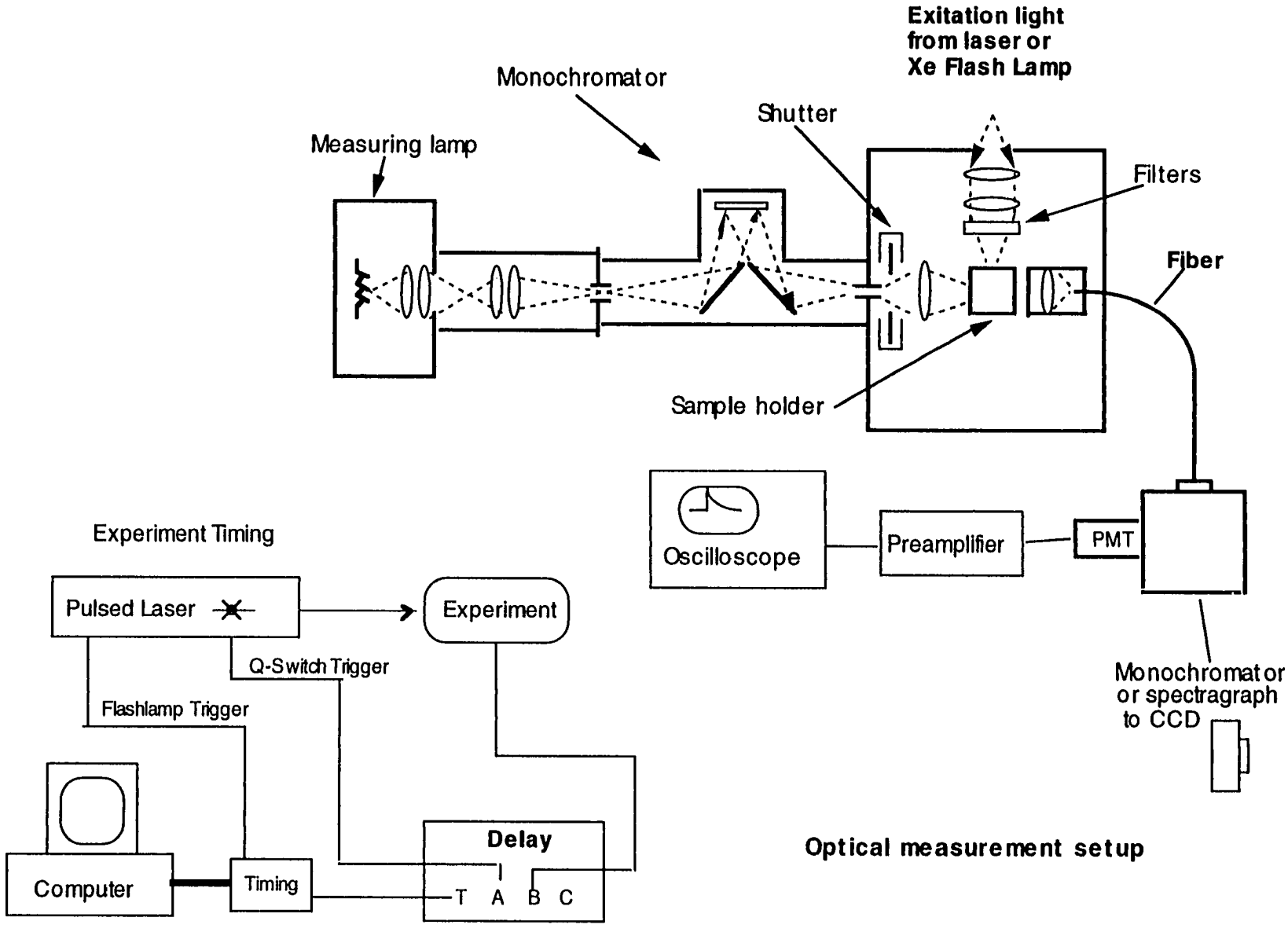

Optical measurement setup

Figure 2.2

Figure 2 .2 shows the typical instrumental set-up of our time resolved light-induced absorbance change experiment. Light-induced absorbance changes were measured using a flash spectrophotometer designed by the University of Pennsylvania Biomedical Instrumentation Group. Actinic light was provided by a 5 ns, 532 nm pulsed YAG laser pumping the fluorescent dye LDS 751 (Exciton). The peak of the fluorescence was at 750 nm. The measuring light, placed perpendicular to the excitation light, was from a 100W quartz-halogen-tungsten lamp (ORIEL) with appropriate neutral density and interference filters. A shutter placed before the RC sample was only opened during measurement. The transmitted light was detected using a Thorn EMI 9798QB or 9128B photomultiplier. The output from the photomultiplier was amplified by a Stanford Research System model SR445 or Comlinear Model E103 fast amplifier. For measurement of the $P^+Q_A^-Q_B$ to $P^+Q_AQ_B^-$ electron transfer, the amplified signal was sent to a LeCroy (model 9310M 300 MHz and 9304A 250 MHz) digital storage oscilloscopes recording and averaging different time scales.

Chapter 3

CHARACTERIZATION OF A SYMMETRIZED MUTANT RC WITH THE QB SITE MADE MORE LIKE QA.

ABSTRACT

Rb. capsulatus RCs from a photosynthetically competent reverent of the mutant with M220-M261 in the Q_A site substituted for L193-L227 in the Q_B site have been investigated. Despite the huge change in the Q_B pocket, secondary quinone function still can be reconstituted. The UQ4 dissociation constant for the Q_B site in the mutant is only 2 times larger than in the wild type RCs. The rate of charge recombination from $P^+Q_B^-$, k_{BP}, is less than 0.05 s^{-1} vs 1s^{-1} in wild type RCs at pH 7.3. The equilibrium constant between $Q_A^-Q_B$ and $Q_AQ_B^-$ is bigger than 200 in the mutant compared to 10 in the wild type, showing a large stabilization of Q_B-. In the wild type RCs, k_{BP} increases above pH 9.0 and decreases below pH 6. In the mutant, k_{BP} is pH independent from pH4.6-10.3. The electron transfer rate of the mutant from Q_A^- to Q_B ($k_{AB}^{(1)} \approx 14/s$) is 3 orders of magnitude slower compared to the wild type RCs (10^4 s^{-1}). Only 50% $P^+Q_B^-$ is formed, as determined by the back reaction kinetics, when the Q_B site is saturated with quinone, again supporting a very slow electron transfer rate from Q_A to Q_B. Given the stabilization of Q_B^- in the mutant, the charge recombination from $P^+Q_AQ_B^-$ to PQ_AQ_B may occur by a direct tunneling rather than by repopulating the $P^+Q_A^-$ state as in the wild type RCs.

INTRODUCTION

Rhodobacter(Rb.) capsulatus is one of the purple bacteria with an amino acid sequence which is very close to that of *Rb. sphaeroides* RCs [Williams, 1986 #77]. The electron transfer pathway, rates, and thermodynamics are almost the same for *Rb. capsulatus* and *Rb. sphaeroides* RCs. Furthermore, the methods to do mutations are well developed in *Rb. capsulatus*.

The isolated reaction center complex (RC) from the purple photosynthetic bacteria *Rb. capsulatus* has three protein subunits, L, M, and H, and four bacteriochlorophylls (BChl), two bacteriopheophytins (BPh) and two quinones, Q_A and Q_B. When a RC is activated by light, a special pair of BChls (P) is excited and an electron is transferred by way of BPh to Q_A forming the semiquinone (Q_A^-) producing the state $P^+Q_A^-Q_B$. Q_A^- reduces the quinone bound at the Q_B site to form $P^+Q_AQ_B^-$. The two quinones are both UQ_{10}. However, they are functionally different presumably because of differences in their binding sites. Q_A, tightly bound, in a relatively hydrophobic environment, is a one electron acceptor. Q_B, is loosely bound, in a more polar region, and functions as a sequential two electron acceptor.

The amino acid residues near the Q_B site are mainly from the L subunit of the protein surrounded by residues from the M and H subunits. Coleman et. al. produced a genetically engineered *Rb. capsulatus* RC where the 42 residues, M220 to M261, from the Q_A binding site replace the 35 residues, L193 to L227, in the Q_B binding site (1) (Figure 3.1). This produces a protein where many of the residues near Q_B have been replaced by residues

from the Q_A site. The original mutant was photosynthetically inactive. A6D1 is a photosynthetically active revertent (1) which retains the Q_A

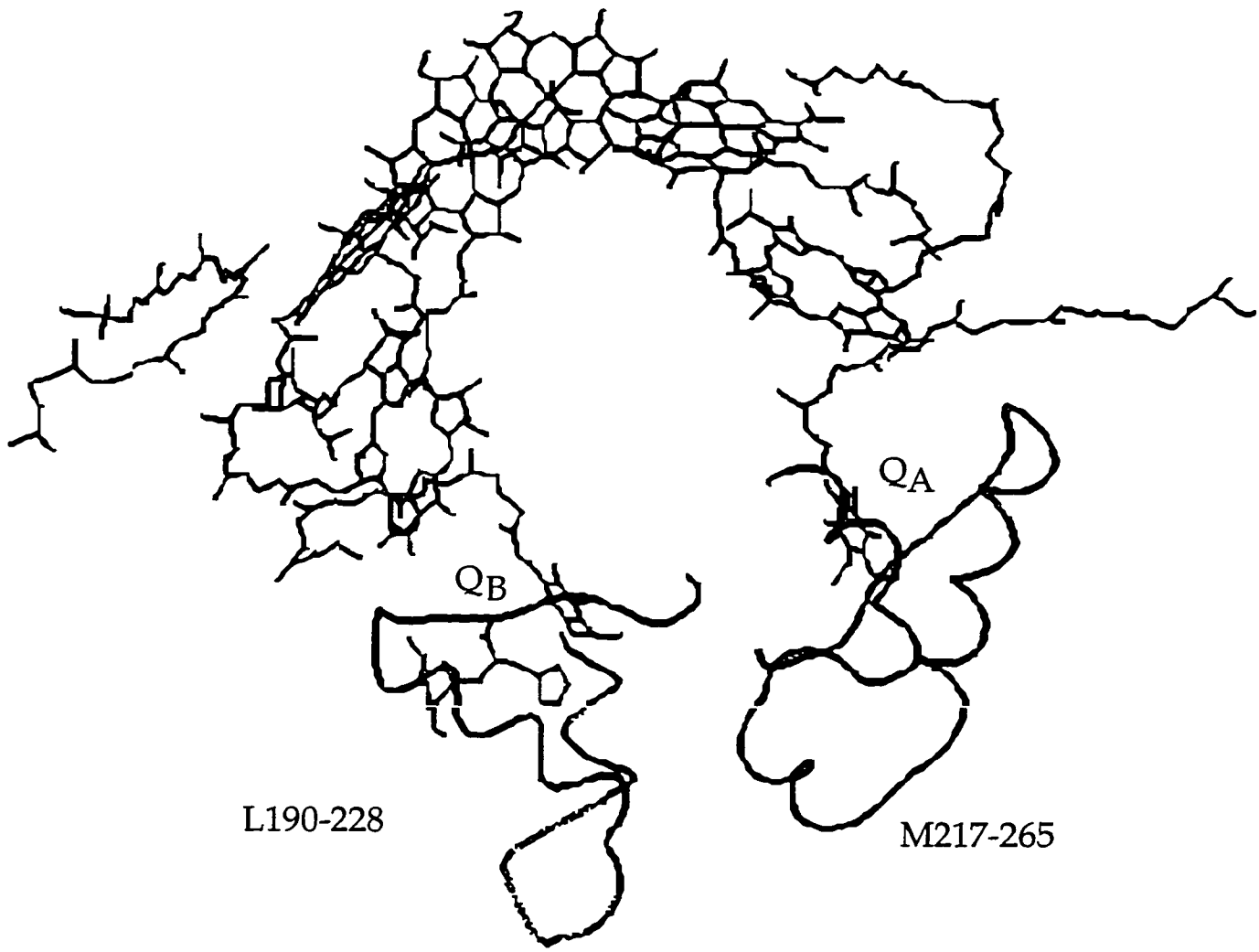

Figure 3.1. The Q_AQ_A mutant was generated by replacing the His^{L190}-Gly^{L228} Q_B segment with the His^{M217}-Gly^{M265} Q_A segment. The two compensatory mutations found in the photosynthetically competent revertent of Q_AQ_A (mutant A6D1) lie between Q_B and BPh_M (MetM144->Ile, AlaM145->Ser).

insert intact, but has the additional changes Met^{M144} -> Ile and Ala^{M145} -->Ser. This mutant RC provides a very good system to study how changing the Q_B site to be more like the Q_A site effects the photochemical cycle, the Q_B affinity and the Q_B dependent electron transfer rates.

In RCs, a special pair of BChls (P) is excited by absorption of a photon and an electron is transferred by way of BPh to the quinone Q_A to form a semiquinone(Q_A^-) and the state $P^+Q_A^-Q_B$. The Q_A^- then reduces the quinone at the Q_B site to form $P^+Q_AQ_B^-$. Figure 1.3 shows the charge recombination process in the absence of an exogenous donor. Scheme I shows the photochemical cycle of reaction centers in the presence of an electron donor to P: (in vivo the donor is cytchrome c)

Scheme I:

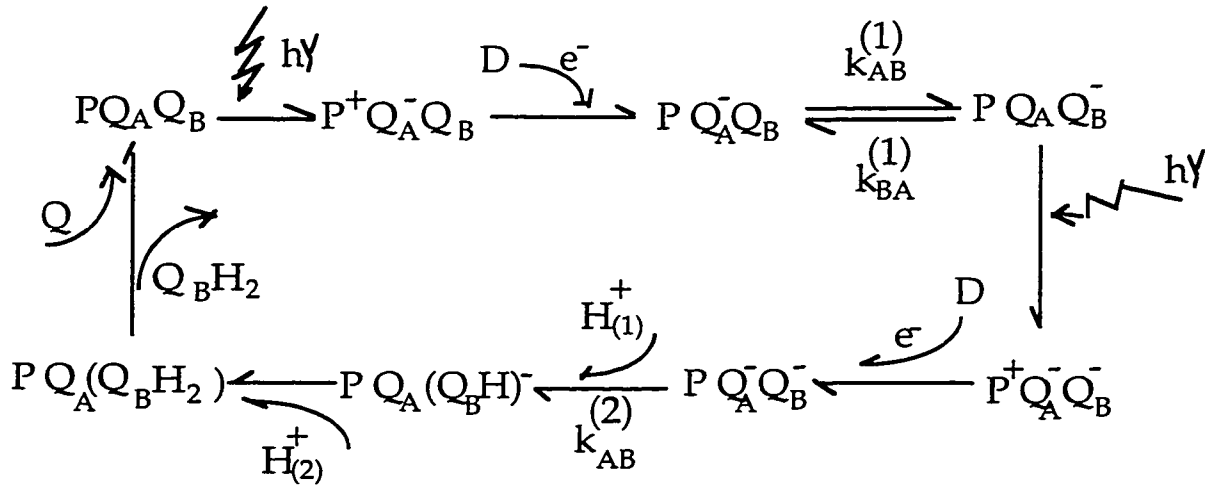

The mutant RC A6D1 provides a very good system to study how the more symmetrized Q_A and Q_B pockets will effect the whole photochemical cycle including the charge recombination process, the electron transfer and proton

uptake reactions. In this study, we compared the following properties of this mutant with wild type *Rb. capsulatus* (Wt), which shows how the changes in structure change:

1. The binding at the Q_B site.
2. The rate of electron transfer from Q_A^- to Q_B (k_{AB}).
3. The pH dependence of the back reaction rate.
4. The semiquinone oscillation and proton uptake.
5. The cytochrome c turn-over rate.

MATERIALS AND METHODS

Sample Preparation. Details of the techniques involved in generating A6D1 mutant of *Rb. capsulatus* have been described by Coleman and Youvan (1). The wild type and mutant cultures were grown in the dark. Reaction centers were isolated by the protocol of Prince and Youvan (2) with some modification. Lauryldimethylamine N-oxide(LDAO) was used to solubilize chromatophore membranes, followed by ion-exchange column on DEAE Biogel-A. For the A6D1 mutant, RCs were eluted from the column with 150mM KCl/0.05% LDAO/10mM Potassium Phosphate/pH=7.3. Purified wild type RCs had about 1.1-1.2 quinones/RC as indicated by slow back recovery kinetics (k_{BP}), but A6D1 RCs had no Q_B activity .

Spectroscopy. Mutant RCs were characterized by optical spectroscopy performed on a flash spectrometer designed by University of Pennsylvania Biomedical Instrumentation Group. The activation light was provided by a 10μs xenon flash lamp.

Methods. The kinetics of $P^+Q_A^-$ ->PQ_A and $P^+Q_AQ_B^-$ ->PQ_AQ_B charge recombination were measured at 425 nm where P^+-P has an absorption maximun. The semiquinone signals of Q_A^- and Q_B^- were monitored at 450 nm where Q^--Q has an absorption maximum, with 100μM ferrocene as the donor to P^+. Cytochrome c (cyt c) oxidation was monitored at 550 nm where cyt c^{2+}-cyt c^{3+} has an absorption maximum, with 20 μM horse heart cytochrome c.

Flash-induced proton uptake was measured spectroscopically using pH-indicator dyes (3, 4) at the $P^+Q_A^-$ isosbestic wavelength near 575 nm. The unbuffered assay solution contained 50mM KCl, 40μM pH indicator dye, 100μM Q4, 0.03% Triton x-100, 100μM ferrocene, and 1μM RC. Samples were degassed under nitrogen. Similar measurements were also made with 10mM buffers, and the net proton uptake was derived by subtracting the buffered traces from the unbuffered traces. Calibration was performed with standard HCl.

Theoretical model of distribution of reaction center states after successive flashes. In the presence of an exogenous electron donor (cyt c^{2+} for example), P^+ is reduced and the electron is trapped on the quinone acceptors following the first flash. With successive flashes electrons are added to the quinones as long as Q_A is unreduced. RCs in the state PQ_A^- are photochemically inactive on the time scale of the reaction with cyt c^{2+}. The mixture of states present after the first two flashes are shown below:

1st flash: $Q_AQ_B \xrightarrow{Cytc^{2+} \rightarrow Cytc^{3+}} Q_A^-Q_B \Leftrightarrow Q_AQ_B^-$

2nd flash: $\begin{cases} Q_A Q_B^- \xrightarrow{Cytc^{2+} \rightarrow Cytc^{3+}} Q_A^- Q_B^- \Leftrightarrow Q_A Q_B^{2-} \\ Q_A^- Q_B \Leftrightarrow Q_A Q_B^- \end{cases}$

Chemicals. UQ_4 was obtained from Sigma and was solubilized in alcohol. pH buffers used were Caps, Ches, Tris, phosphate, and Mes depending on the pH. Horse heart cytochrome c was from Sigma and was reduced by Sodium Borohydride (Sigma). Ferrocene (Aldrich) was diluted in alcohol. pH indicator dyes chlorophenol red and cresol red were from Sigma.

RESULTS and ANALYSIS

1. **The Rate of Charge Recombination from Q_A^- and Q_B^-.**

When quinone occupies only the Q_A site, charge recombination from $P^+Q_A^-$ to reform PQ_A occurs as a nearly single exponential process with a rate (k_{AP}) of 8 s^{-1} in both wild type and mutant RC (data not shown). Thus, the large scale modification of the Q_B site has little or no impact on the function of Q_A.

Charge recombination (Figure 3.2A) from $P^+Q_B^-$ to reform the ground state (k_{BP}) was determined in the presence of excess UQ4 (100-200 UQ4/RC). k_{BP} for the mutant is significantly slower ($\leq$0.05 s^{-1}) than for the wild type (0.85 s^{-1}). If charge recombination from $P^+Q_B^-$ occurs via $P^+Q_A^-$ then the difference between k_{AP} and k_{BP} can be used to derive the equilibrium constant between Q_A and Q_B (5). $K_{AB} = k_{AP}/k_{BP} - 1$, K_{AB} is $\approx$10 for the wild type and at least 200 for the mutant RCs. Thus, the Q_B^- state is stabilized by at least 80 meV in the mutant RC relative to the wild type protein. The removal of Glu L 212, and Asp L210 and L213 near Q_B may stabilize the

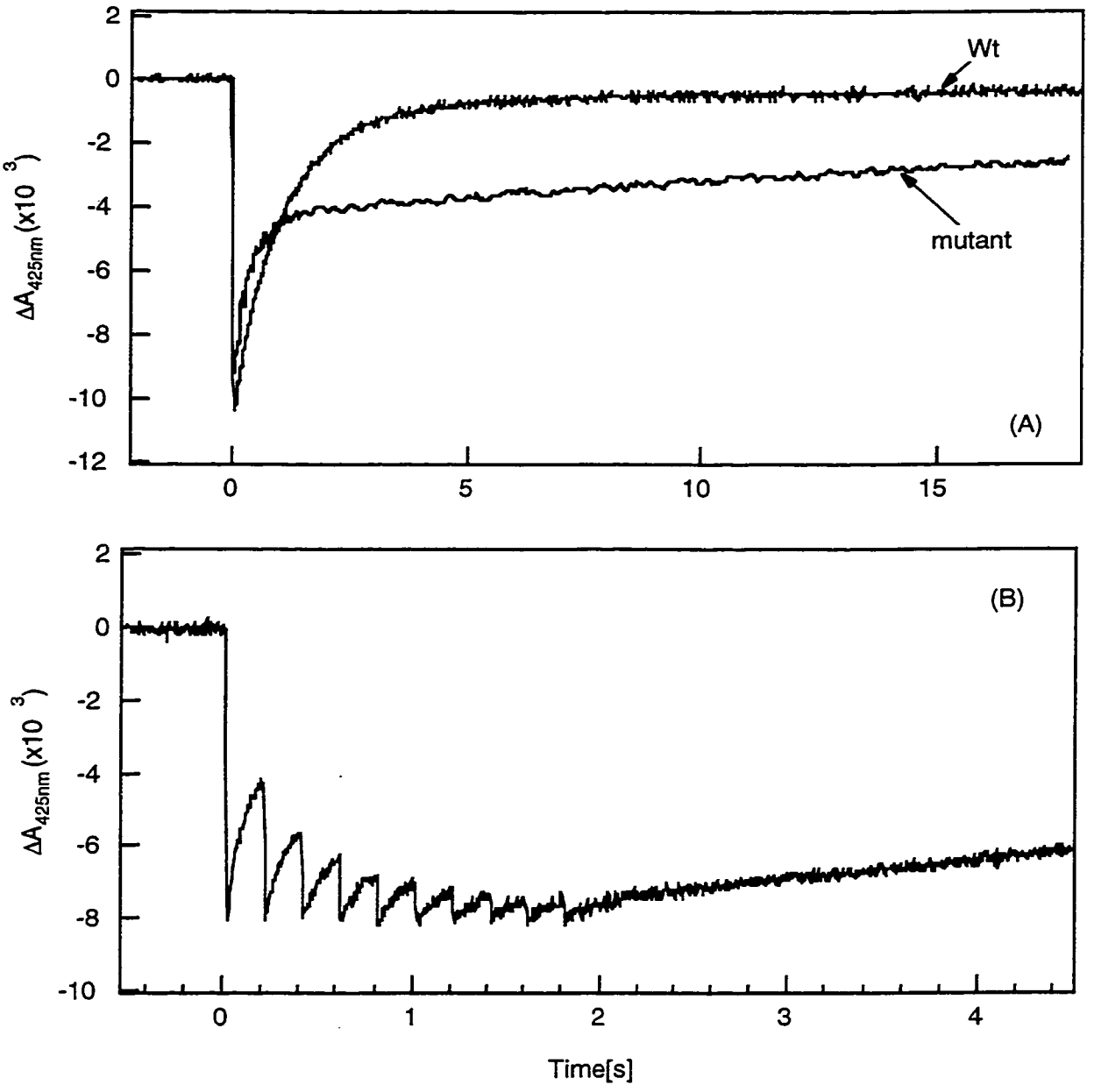

Figure 3.2. Charge separation and recombination monitored by the absorbance change at 425 nm as a function of time. pH=7.3, 0.04% LDAO, 0.5μM RCs, 100 μM UQ_4. The rate constants (1a): Wt, k_{AP}=7.6 s^{-1}, k_{BP}=0.85 s^{-1}; mutant, k_{AP}=7.4 s^{-1}, k_{BP}=0.027 s^{-1} . 1b. mutant RCs repetitively excited at an interval of 0.2 s.

negative charge on Q_B in the mutant. A slow rate of charge recombination from $P^+Q_B^-$ is also found in L212/L213 double mutants with *Rb. capsulatus* and *Rb. sphaeroides* (3, 6).

2. Q_B Reconstitution

When UQ_4 is added to RCs to reconstitute Q_B, charge recombination is seen to be biphasic with rates k_{AP} and k_{BP}. The reconstitution of UQ4 to the Q_B site can be determined by the fraction of the RCs that exhibit the slow rate k_{BP}. In addition, the ratio of cytochrome c oxidation on the first and second flashes can discriminate between RCs with and without Q_B. In the RCs without Q_B, if Q_A is oxidized by the first flash, no additional cytochrome c oxidation occurs on latter excitation (7).

Figure 3.3 shows the UQ_4 titration curves with wild type and mutant RCs. The dissociation constants (K_D) of the UQ_4 at Q_B site is calculated by

$$\%Q_B=\frac{[RC,QB]}{[RC]_{total}}=\frac{1}{2}\{(1+\frac{[Q_4]+Kd}{[RC]})-\sqrt{[(1+\frac{[Q_4]+Kd}{[RC]})\text{^}2-4\frac{[Q_4]}{[RC]}]}\}$$

Here the $\%Q_B$ is the percentage of RCs with quinone bound to the Q_B site. In order to fit the data in the Figure above, we have modified the equation by a factor that accounts for the asymptotic values of the $\%Q_B$ being less than 100% and some Q_B left after the protein purification for the wild type RCs. Using the fraction of slow back reaction as a monitor, the K_d value for the wild type is 4.4±0.5 μM and 11.9±0.6 μM for the mutant. When the RCs are saturated with UQ, 90% of the wild type and 50% of the mutant RCs

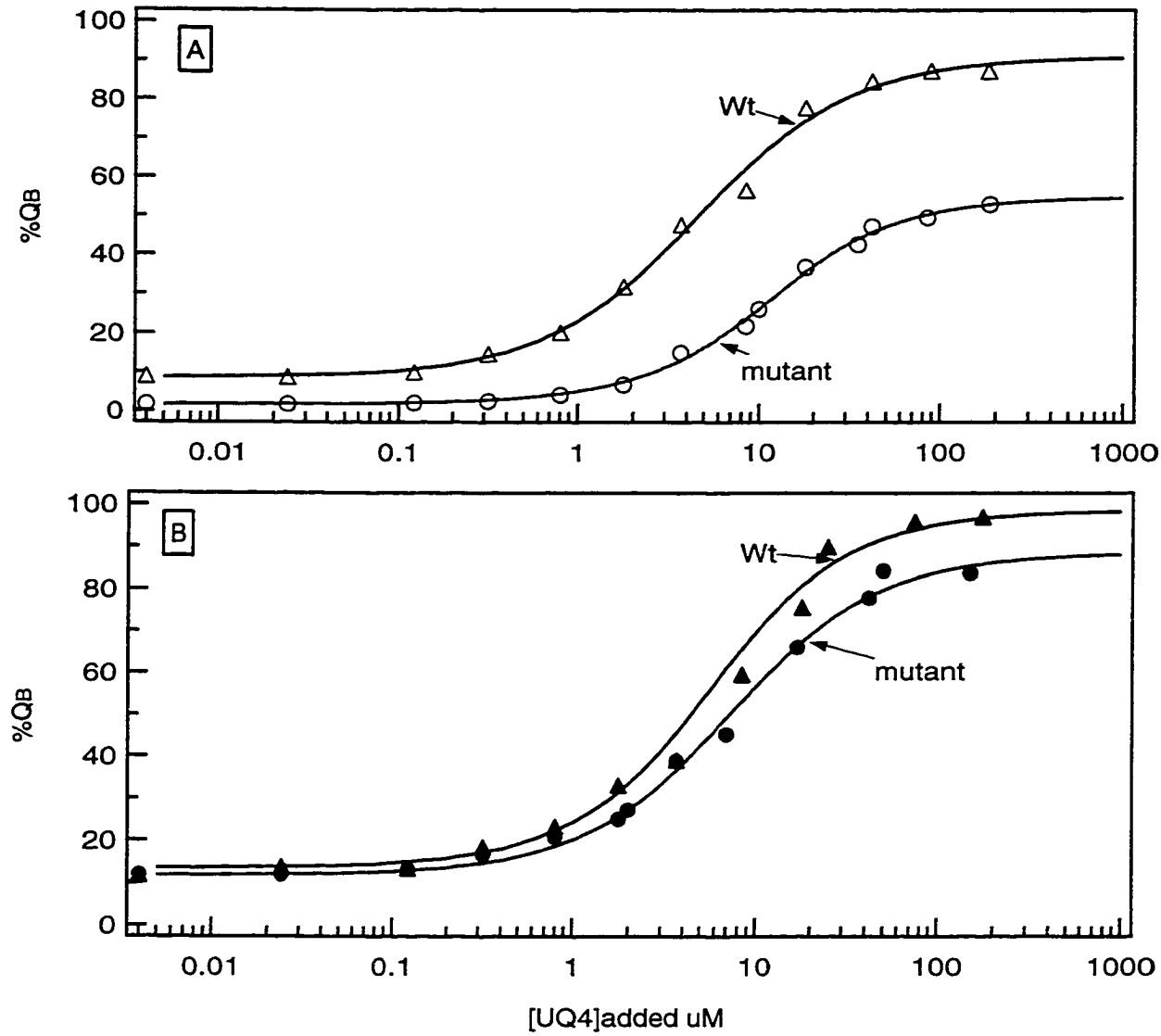

Figure 3.3. UQ_4 titration of the Q_B site of RCs from Wt (top curve) and mutant (bottom curve) RCs. Conditions were the same as Figure 1. (A). Using the fraction of slow back reaction as a monitor, the Kds for the Wt is 4.4±0.5μM and 11.9±0.6μM for the mutant. (B). Cytochrome c oxidation assay method, the Kd's are 7.8±0.9μM and 11±0.6μM respectively for wild type and mutant RCs when the flashes are spaced 0.5s apart.

show slow recombination kinetics followed one flash. With the cytochome c assay, with flashes spaced 0.5 s apart, the K_d's are 7.8±0.9 μM and 11±0.6 μM with an asymptote of 98% and 90% respectively for wild type and mutant RCs (Figure 3.3B). Thus, despite the large scale rearrangement of the Q_B site, the affinity of the binding site for UQ is weakened by less than a factor of three. However, the yield of $P^+Q_B^-$ is significantly smaller in the mutant RCs than in the wild type protein.

3. Cytochrome C Turn Over Rate.

The overall rate of the photocycle (Scheme II) was measured by monitoring the oxidation of cyt c at 550 nm (8, 9) in the presence of excess UQ_4 under continuous illumination ($I=300 mw.cm^{-2}$ with a long pass filter >700 nm).

RCs were illuminated from a direction perpendicular to the measuring beam. The rate of cyt c turn-over (Fig. 3.4) was determined from the absorption change at 550 nm normalized to the absorption change at 550 nm after a single flash (representing one cyt c oxidized per RC). Slowing any one of the electron and proton transfer can result in a decrease of the cyt c turn-over rate, The steady state turn- over rate will be limited by the rate of this step (Scheme I).

The measurent of the Wt RCs shows a fast cyt c turn over rate of 120 (cyt c/RC)/s, This is consistent with previous results (10) for the Wt *Rb. capsulatus* (Figure 3.4). The mutant shows a fast oxidation of about 0.8 cyt/RC followed by a slower steady-state turn-over rate of 24 cyt c/RC)/s. This suggests that the fast formation of the state $P^+Q_A^-$ oxidizing one cyt c

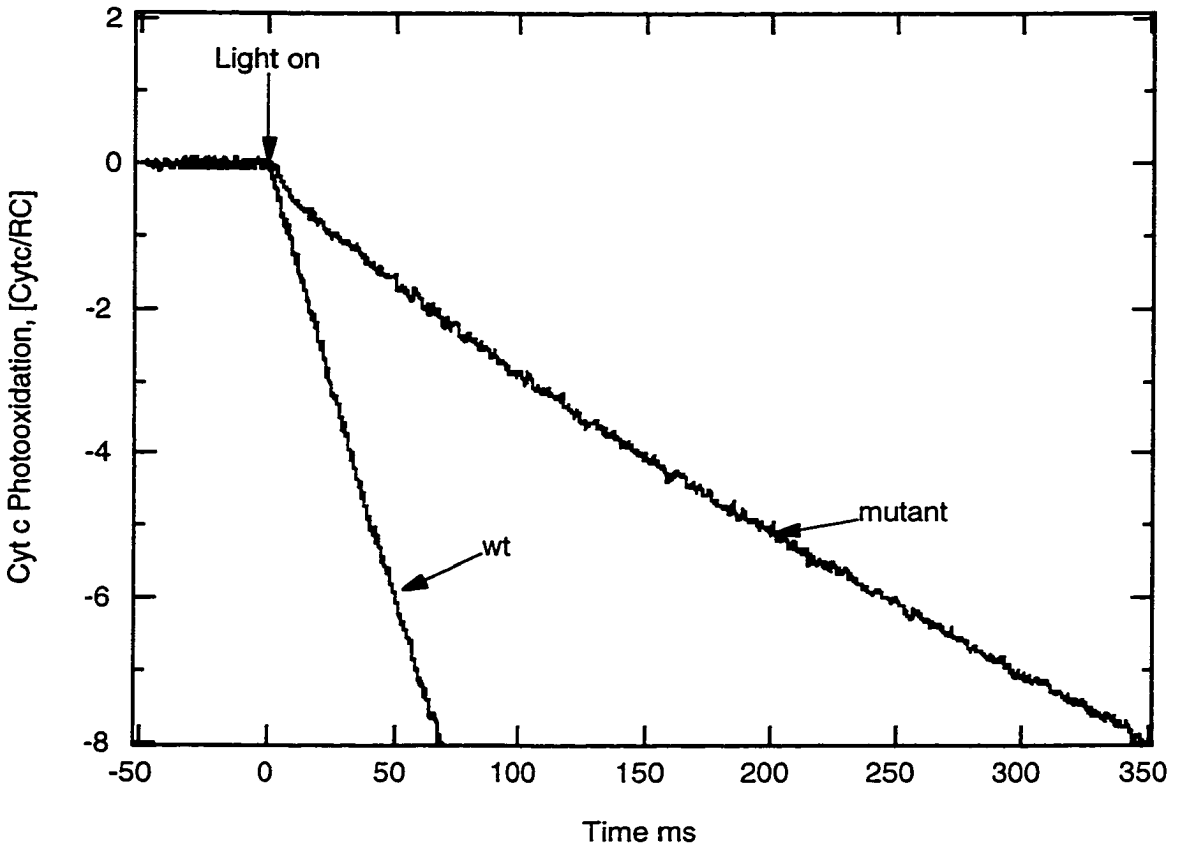

Figure 3.4. Cytchrome c (cyt c) photooxidation in the Wt and the mutant RCs. The measurement was monitored by the absorbance change at 550 nm in the presence of exogenous UQ_4 and cyt c under continuous illumination. Conditions: RC≈0.6μM, 0.04% LDAO, 20μM cyt c, I≈600 mW, 100μM UQ_4, at 24 °C.The normalization to (cyt/RC) was determined from the absorbance change at 550 nm after a single flash (representing 1 cyt/RC).

per RC is followed by a slow electron transfer process from $P^+Q_A^-Q_B$ to $P^+Q_AQ_B^-$ ($K_{AB}^{(1)}$).

4. The Forward Electron Transfer Rate.

The small yield of reaction centers in the $P^+Q_B^-$ state following a single flash appears to be due to a rate of electron transfer from Q_A^- to Q_B that is

comparable to the rate of electron transfer from Q_A^- to P^+. Figure 1b shows the result of repetitive excitation under conditions where the RCs are saturated with UQ_4. After the first flash approximately 50% of the charge recombination is at the faster rate (k_{AP}) and 50% at k_{BP}. On each additional flash half of the population that showed k_{AP} now shows the slower recombination rate characteristic of RCs in the state $P^+Q_B^-$. Thus, the low yield of $P^+Q_B^-$ after the first flash does not indicate that half the RCs have an incompetent Q_B site. Rather the quantum yield for formation of $P^+Q_B^-$ is 50% for all of the mutant RCs. If k_{AP} is 8 s^{-1}, a quantum yield of 50% suggests the rate of forward electron transfer k_{AB} is $\approx$8 s^{-1}.

To test this hypothesis, the effect of flash repetition on the oxidation of cyt c with the mutant and Wt RCs was measured (Figure 3.5). Since cytochrome c oxidation is not seen if Q_A is still reduced, the ratio of cytochrome c oxidized on the first and second flash can be used to assay the electron transfer rate from Q_A to Q_B. This was measured by the absorption change due to oxidation of cyt c after the 2nd and 3rd flash to the 1st one: $\Delta A_2/\Delta A_1$ and $\Delta A_3/\Delta A_1$. This reflects how fast the Q_B gets one and two electrons within the time between two flashes (Δt), which in turn depends on if Q_A is photoactive (with its electron already transferred to Q_B) with Δt, thus the electron transfer rate can be measured indirectly. In the presence of cyt c as an electron donor to P^+, the percentage of Q_A photoactive at time Δt after the first flash can be expressed:

$$\%\ Q_A \text{ available} = 1-\exp(-K_{AB}^{(1)} * \Delta t) = \Delta A_2/\Delta A_1 \text{ (after time } \Delta t)$$

Varying the time interval, Δt, between the first and second flashes, the observed rate of electron transfer from Q_A^- to Q_B ($k_{AB}+k_{BA}$) was

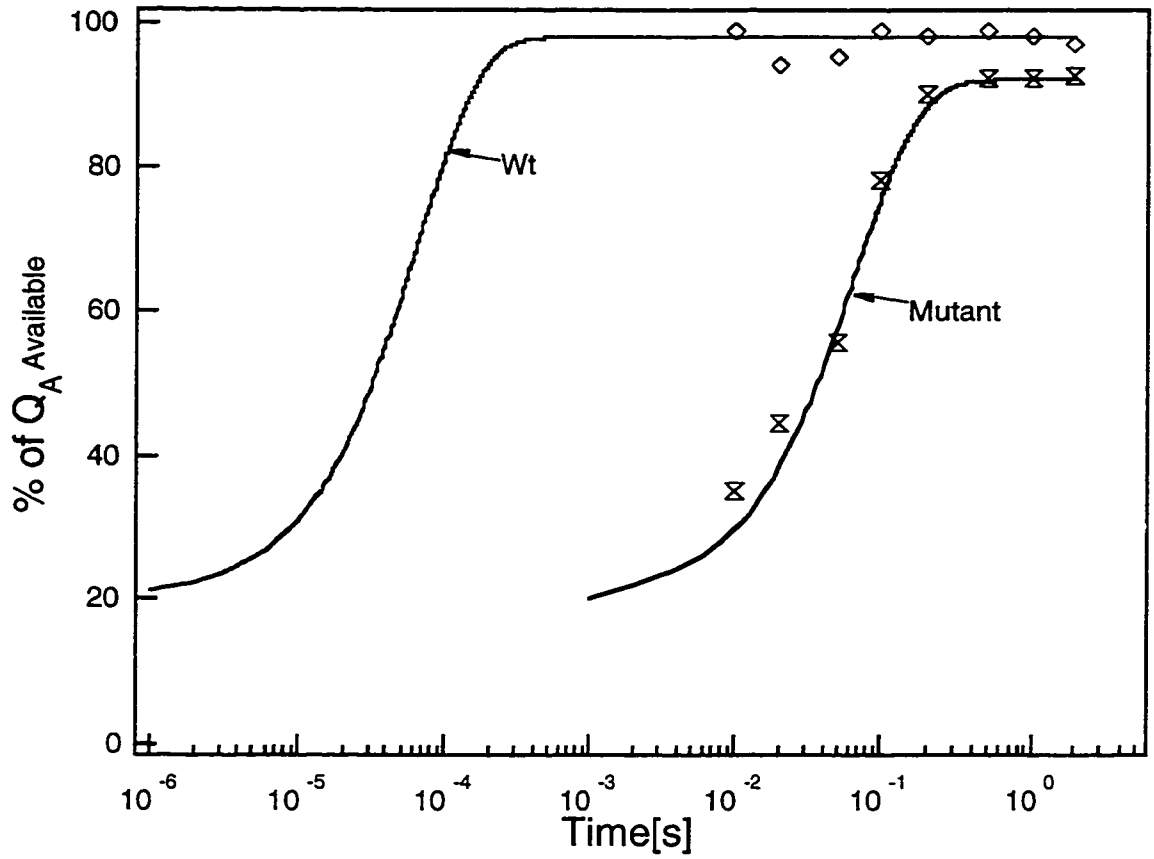

Figure 3.5. Electron transfer rate of the mutant calculated from the ratio $\Delta A_2/\Delta A_1$ of the absorption change of cyt c at 550 nm as a function of the repetition rate of the flash lamp. The electron transfer rate was calculated to be $k_{AB}^{(1)}$=14/s for the mutant. The curve for the Wt was simulated using the $k_{AB}^{(1)}$=15,400/s from Basiou et al (6).

determined to be 14 s^{-1}.

5. pH Dependence of the $P^+Q_AQ_B^-$ Decay Rate.

The pH dependence of the $P^+Q_AQ_B^-$ recovery rates k_{BP} for Wt and mutant RCs are shown in Figure 3.6. In the range of pH4-11, Wt RCs exhibited two regions of significant pH dependence of k_{BP}: below pH6 and above pH9.

This is consistent with the result measured by Maroti et al. for wild type capsulatus (11). In contrast, the charge recombination rate k_{BP} for A6D1 RCs is essentially pH independent from pH4.6-10.3, with a rate constant k_{BP} $\approx 0.02\ s^{-1}$. Similar results have been found both in the Ala-L212/Ala-L213 double mutant in *Rb. capsulatus* RC (11) and the L212EQ/L213DN double mutant in *Rb. sphaeroides* RC (3) where the electron transfer occurs by direct reduction of P^+.

For the Wt RCs, at pH<7, the slow phase in the presence of 100μM Q_4, in thoroughly dark-adapted fresh samples, the maximum amplitude of the slow Q_B phase reached about 90%. At high pH, the level of reconstitution appeared to fall. The relative amplitude of the slow phase decreased to 30% at pH 9 and above. However, for the mutant RCs, the relative amplitude of the slow phase was a constant at 50%.

6. Semiquinone Stability and Proton Binding.

In the presence of the exogenous donor Ferrocene, the oscillation of the RC semiquinone signal (12) was measured by monitoring the absorption change at 450 nm following multiple flashes. Typical absorption oscillation for every two flashes (Figure 3.7A) are seen for the wild type (6, 12): the first flash forms the semiquinone $Q_AQ_B^-$, the second flash form the dihydroquinone Q_BH_2 as seen from the disappearence of the semiquinone signal, was not observed in the mutant (Figure 3.7B) at pH 5.9 and 8.0. No stable semiquinone signal was observed, the semiquinone signal decayed with a rate about $7s^{-1}$ to the ground state after each flash in the mutant RCs.

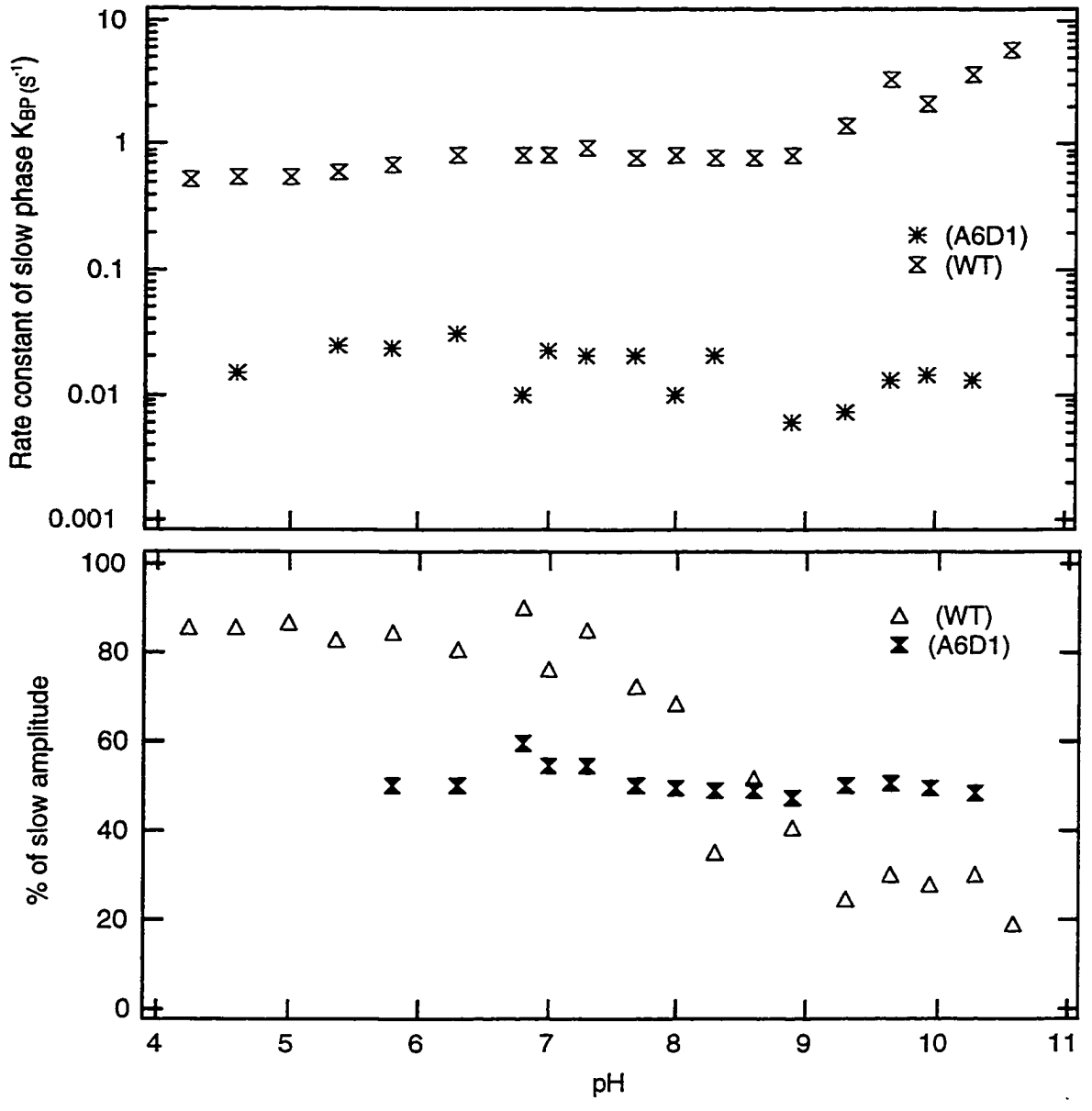

Figure 3.6. pH Dependence of the $P^+Q_AQ_B^-$ Decay Rate (top Figure). Conditions: RC=0.3 UM, UQ4=100 mM, 10 mM buffer. For the Wt RCs, at pH<7, the maximun amplitude of k_{BP} reached about 90% (bottom Figure). The relative amplitude of k_{BP} decreased to 30% at pH 9 and above. However, for the mutant RCs, the relative amplitude of k_{BP} was constant at ≈50%.

To better understand the reasons for the semiquinone signal disappearance, flash-induced proton binding by the mutant and the Wt RCs was measured optically using pH-sensitive dyes at 575 nm, pH6 and pH8 , as shown in Figure 3.8.

The proton uptake behavior in the Wt RCs (Fig. 3.8) is similar to the measurements in the native RCs of *Rb. sphaeroides* (3, 13, 14). For the mutant RC, both at pH6 and pH8, proton uptaken was very small compared to the Wt.

DISCUSSION

1. **The Pathway of $P^+Q_AQ_B^-$ Recombination**. The charge recombination rate of K_{BP} in the mutant RCs was slow ($K_{BP} \leq 0.05\ S^{-1}$) and essentially pH independent. The rate $K_{BP} \leq 0.05\ S^{-1}$ is smaller than the upper limit of 0.1 s^{-1} obtained by Kleinfield et al(15). These authors suggested that if the observed charge recombination rate is <0.1 s^{-1}, then the equilibrium constant between $Q_A^- \rightarrow Q_B$, $K_{eq}^{(1)} \approx (k_{AB} / k_{BA}) - 1 \geq \frac{1}{0.05} - 1 \approx 200$, thus the electron transfer from Q_B may go back to P^+ directly instead of via the $P^+Q_A^-Q_B$ state. The pH independence of the charge recombination reaction rate k_{BP} in $4.5 \leq pH \leq 10.6$ also supports this.

The very slow charge recombination rate k_{BP} was also found previously in the L212/L213 double mutants with *Rb. capsulatus* and *Rb. sphaeriodes* (3, 6). Takahashi et al. (3) indicated that although the decay rate in the mutant RCs was quite slow, adventitious donors to P^+ that could compete with

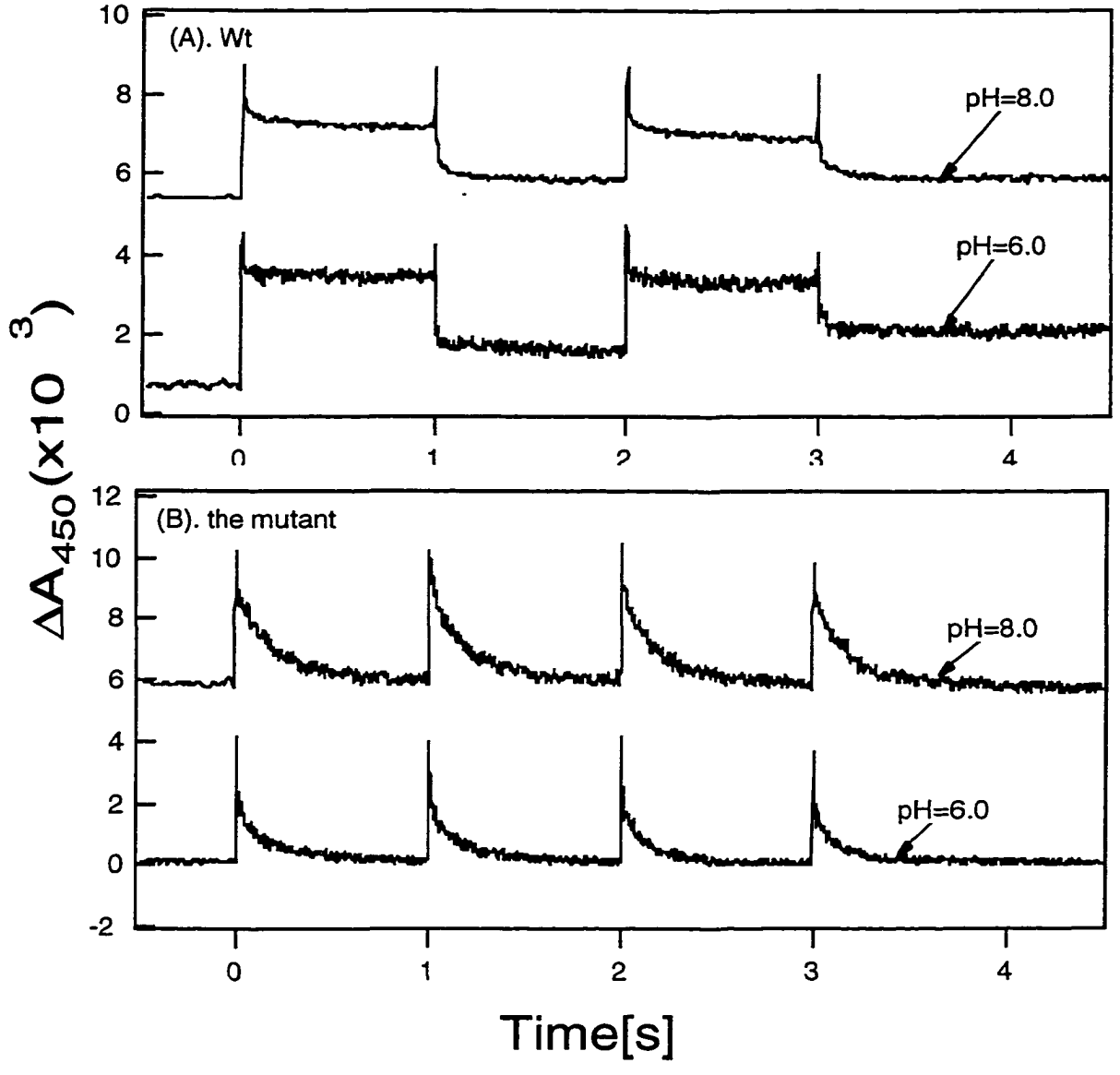

Figure 3.7. Changes in the optical absorption at 450 nm of semiquinone anion in response to a series of actinic flashes. Semiquinone oscillation in RCs (0.5μM) from Wt (A) and the mutant (B) at pH 6 and pH 8. Conditions: 0.04% LDAO, 100 μm Q4, and 100 μM ferrocene, 10 mM buffer. (See the Method section for the mixture of states present after the first two flashes.)

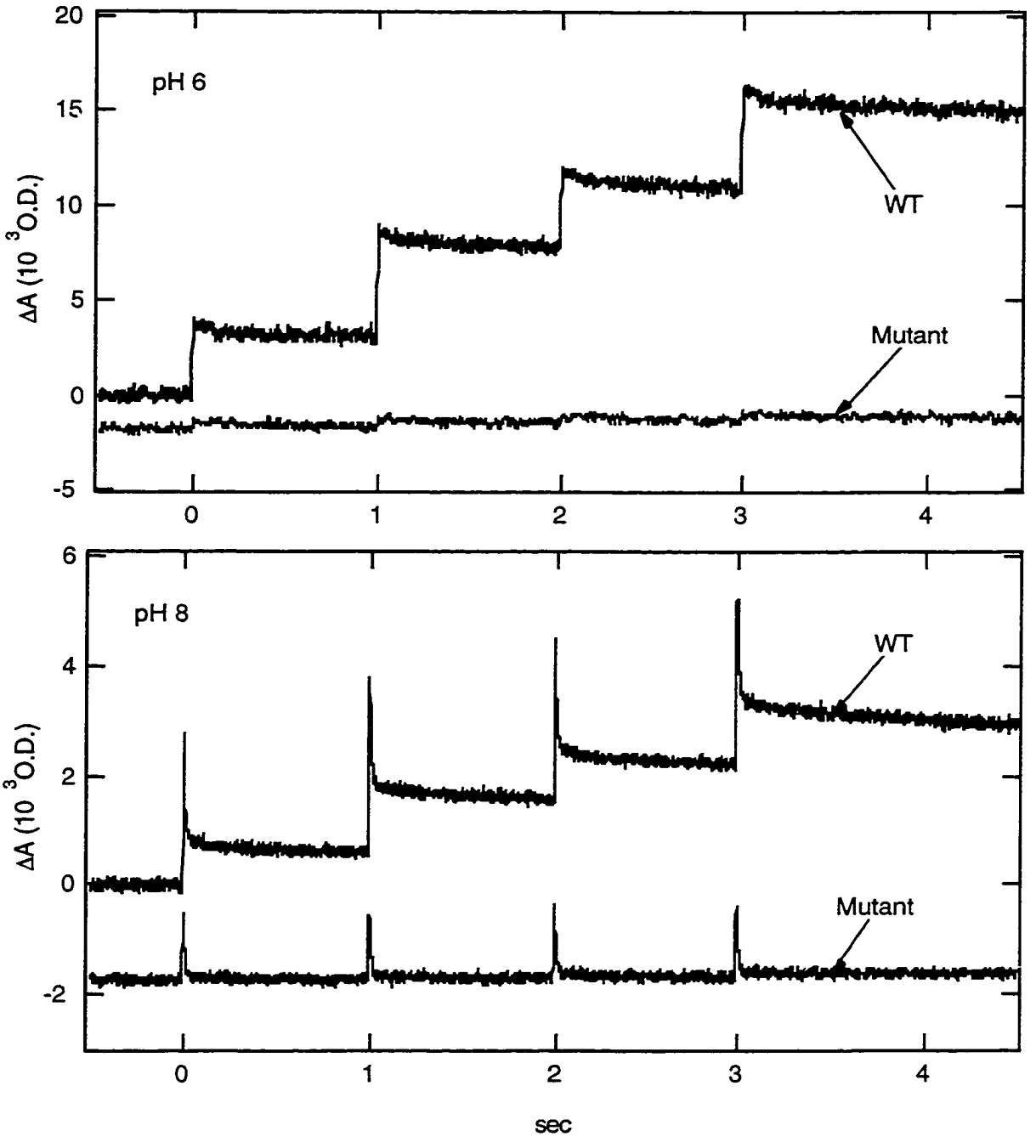

Figure 3.8. Proton uptake experiment for Wt and the mutant RCs. RC=1μM, 0.03% Triton, Q4=150 μm, 100 μM Ferrocene, 50 mM KCL. At pH 6, Chlorophenol red dye=50 μM, measured at 575 nm. At pH 8, Cresol red=50μM, measured at 555 nm.

recombination from Q_B^- only can contribute a minor part of the decay to P^+. The very slow rate k_{BP} was also found previously in the RCs without an H subunit in *Rb. sphaeriodes* (16). However a Protein Chip Array (Ciphergen Biosystems, Inc) assay has shown that all three subunits are present in the mutant RCs (data not shown). Another possibility was that Q_B^- escaped from the mutant RCs, leaving a long-lived P^+Q_A state, however this rate would be expected to be strongly pH dependent.

The direct electron transfer from Q_B^- to P^+ is the most likely path for charge recombination. The observation that the rate of k_{BP} is slower than the low-pH limit value of the Wt data supports this point. This would place a value on k_{BP} of about 0.05 s^{-1} in Fig. 1.3. The electron transfer equilibrium between Q_A and Q_B: $Keq(1)=k_{AB} / k_{BA} \approx 200$, also suggests that direct recombination route contributes significantly to the $P^+Q_B^-$. Assuming that the redox midpoint potential of Q_A/Q_A^- unchanged in the mutant, Application of the relationship $\Delta E_m = KT \ln K_{eq}$ yields a E_m for $Q_B/Q_B^- \geq 137$ mV in the mutant while for the Wt RCs, the $E_m(Q_B/Q_B^-) \approx 54$mV at pH close to 8 (11), So the Em for the mutant is at least 80 mV higher than in the Wt. This is consistent with the slow decay of a more stabile Q_B^-.

2. **The Electron Transfer Rate from $Q_A^- \rightarrow Q_B$.** The rate of the elelctron transfer is at least 10^4 s^{-1} in the Wt RCs (6). Several lines of evidence show that for the mutant the electron transfer rate is only ≈10/s. (1). The quantum yield for the charge recombination is about 50% even at high quinone concentration. Kleinfeld et al. predicted (15) if the parameters in Figure 1.3 have the relation: k_{AP}, $k_{AB} \gg k_{BA}$, k_{BP}; when the k_{AP} and k_{AB} are of the same order of magnitude, a charge recombination of the state $P^+Q_A^-Q_B$ occurs as the electron is transferred to Q_B. The ratio of the amplitudes of

the component with rate k_{AP} to the component with rate k_{BP} is about k_{AP}/k_{AB}, independent of the charge recombination pathway of $P^+Q_AQ_B^-$. Theoretical simulation of the electron transfer kinetics are in agreement with this (see Appendix 2).

(2). Cyt c Turn-over Rate. Based on Scheme I, Figure 3.5 shows the first electron transfer rate from Q_A^- to Q_B is the limiting step in the steady state turn over rate.

(3). Titration Curve. The 40% higher values of the $\%Q_B$ with the cyt c oxidation method than the dynamics analysis method (Fig. 3.3) can be explained by that the presence of cyt c as a electron donor to P^+ makes all electrons go forward. Thus makes charge recombination of $P^+Q_A^-$ can no longer compete with the forward electron transfer to Q_B.

Based on the above observations, the electron transfer rate of k_{AB} of 14 s^{-1} was measured indirectly by measuring the effect of flash repetition on the oxidation of cyt c. The relative amplitude of the slow phase doesn't change with pH, which indicates that the electron transfer rate of k_{AB} is pH independent.

3. **One Electron Gate Property**. For the Wt RCs, the semiquinone absorption change at 450 nm shows oscillations with a period of two flashes. This finding supports the two-electron gate hypotheses (12). Thus in Wt RCs Q_B leaves after taking two electrons and protons instead of one. The stable semiquinone signal after the first flash shows the Q_B^- stays inside the protein and the uptake protons H^+ go to the residues near Q_B instead of going to the

Q_B^- directly. The disappearance of the semiquinone signal after the second flash shows the Q_B^- takes another electron, and gets protonated (2 H^+), then leaves the RC in the form QH_2. In the mutant, there are two differences from the Wt: (a). the semiquinone signal behaves is the same after every flash at 450 nm and the proton binding to the RC for each flash is always very small. This suggests the semiquinone absorption oscillates with a period of one flash in the mutant instead of two flashes in the Wt RCs. This leads to a one-electron gate model. (b), the semiquinone signal decays with a slow rate of about 7 s^{-1} that is close to the rate of Q_A^- disappeareace. Since proton binding to the mutant RC is very small and the electron transfer from Q_A^- to Q_B is pH independent, this indicates the proton uptake from solution can not be the rate-limiting step. It appears that k_{AB} is close to the electron transfer rate from $Q_A^- \rightarrow Q_B$. This again supports the electron transfer from Q_A to Q_B as the rate limiting step. So if the semiquinone disappearance rate is the electron transfer rate from Q_A^- to Q_B, and the electron does go to the Q_B site based on the binding data (Fig. 3.2), then the electron on Q_B may be protonated quickly when there is a electron donor to P^+. This proton can not be from solution since proton uptake is very small. There are protons inside the protein near the Q_B can donate a proton to the Q_B and this proton tansfer could be fast or could be rate limiting.

A one-electron gate hypothesis as Scheme II can be proposed, that means the second quinone Q_B in the Q_A like pocket takes one electron, and gets protonated.

Scheme II.

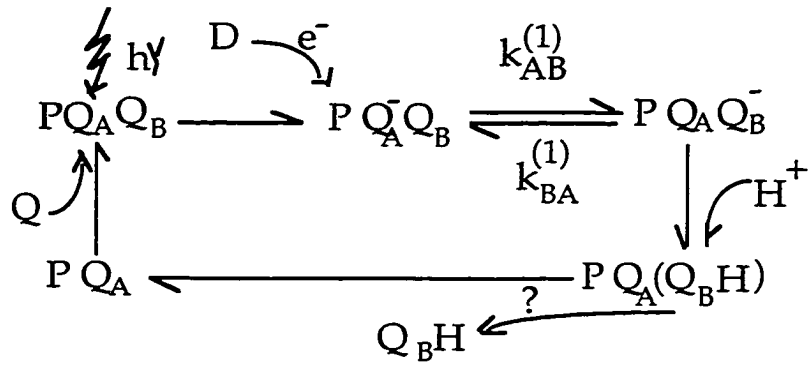

The pH independence of k_{BP} in the mutant is similar to that found in the double mutant L212/L213 (3, 11). This implies that the hydrogen bond from the protein to the quinone related to these two residues L212/L213 may not exist. So one of the carbonyls might be "suspended" in the Q_B site and this might be related to the : one-electron gate" system. Comparing the structure of Q_A pocket and Q_B pocket of the Wt RCs, there is a cluster of acid residues close to the Q_B which form a buffer to transfer protons in response to electron transfer to Q_B in Wt RCs (17). but the Q_A site doesn't have this buffer capability. This may be the case in the Q_B site in the mutant and might be responsible forthe first proton could go to Q_B directly instead of going to the buffer residues.

4. **Why is k_{AB} so slow?**

The mutant RCs described here represent a large scale rearrangement of the Q_B site. The affinity of Q_B is surprisingly unchanged. The $P^+Q_B^-$ state in the mutant appears to be at least 80 meV more stable than in the wild type protein, a result also found in a number of mutants that change only selected residues in the Q_B site (18). Thus, this mutant and the other L212/l213 double mutants show comparable results. However, the largest change in the

mutant is to slow the electron transfer from Q_A to Q_B. In the wild type this reaction occurs in a multiphase process with rates from 10^3 to 10^4 (6, 19). In contrast, in this mutant the reaction occurs at 14 s^{-1}, 100 to 1000 times slower.

It is not clear why the electron transfer rate is so much slower in the mutant than the wild type RCs. The reaction has a larger, favorable ΔG than in the wild type protein. An increased electron transfer distance between Q_A and Q_B because the quinone is bound at an alternate site could contribute to the slower rate (20, 21). In addition, the large change in rate points to some required change in protein conformation or proton transfer that is more difficult to accomplish in the mutant RCs.

REFERENCES

1. Coleman, W. J., and Youvan, D. C. (1993) *Nature 366*, 517-518.
2. Prince, R. C., and Youvan, D. C. (1987) *Biochim. Biophys. Acta 890*, 286-291.
3. Takahashi, E., and Wraight, C. A. (1992) *Biochemistry 31*, 855-866.
4. Paddock, M. L., Rongey, S. H., McPherson, P. H., Juth, A., Feher, G., and Okamura, M. Y. (1994) *Biochemistry 33*, 734-745.
5. Mancino, L. J., Dean, D. P., and Blankenship, R. E. (1984) *Biochim. Biophys. Acta 764*, 46-54.
6. Baciou, L., Bylina, E. J., and Sebban, P. (1993) *Bipphysical J. 65*, 652-660.
7. Giangiacomo, K. M., and Dutton, P. L. (1989) *Proc. Natl. Acad. Sci. USA 86*, 2658-2662.

8. Paddock, M. L., Rongey, S. H., Feher, G., and Okamura, M. Y. (1989) *Proc. Natl. Acad. Sci. USA 86*, 6602-6606.

9. Paddock, M. L., McPherson, P. H., Feher, G., and Okamura, M. Y. (1990) *Proc. Natl. Acad. Sci. 87*, 6803-6807.

10. Bylina, E. J., and Youvan, D. C. (1987) *Z. Naturforsch. 42c*, 769-774.

11. Maroti, P., Hanson, D. K., Baciou, L., Marianne, S., and Sebban, P. (1994) *Proc. Natl. Acac. Sci. 91*, 5617-5621.

12. Wraight, C. A. (1977) *Biochim. Biophys. Acta 495*, 525-531.

13. Maroti, P., and Wraight, C. A. (1988) *Biochim. Biophys. Acta 934*, 329-347.

14. McPherson, P. H., Okamura, M. Y., and Feher, G. (1993) *Biochim. Biophys. Acta 1144*, 309-324.

15. Kleinfeld, D., Okamura, M. Y., and Feher, G. (1984) *Biochim. Biophys. Acta 766*, 126-140.

16. Debus, R. J., Feher, G., and Okamura, M. Y. (1985) *Biochemistry 24*, 2488-2500.

17. Gunner, M. R., and Honig, B. (1992) in *The Photosynthetic Bacterial Reaction Center: Structure, Spectroscopy and Dynamics II* (Breton, J., and Vermeglio, A., Eds.) pp 403-410, Plenum, New York.

18. Takahashi, E., and Wraight, C. A. (1994) *Advances in Molecular and Cell Biology 10*, 197-251.

19. Okamura, M. Y., and Feher, G. (1992) *Annu. Rev. Biochem. 61*, 861-896.

20. Moser, C. C., Keske, J. M., Warncke, K., Farid, R., and Dutton, P. L. (1992) *Nature 355*, 796-802.

21. Deisenhofer, J., and Michel, H. (1989) *The EMBO Journal 8*, 2149-2170.

Chapter 4

Kinetic Phases in the Electron Transfer from $P^+Q_A^-Q_B$ to $P^+Q_AQ_B^-$ and the Associated Processes in *Rhodobacter sphaeroides* R-26 Reaction Centers

ABSTRACT: Electron transfer from $P^+Q_A^-Q_B$ to form $P^+Q_AQ_B^-$ was measured in *Rb. sphaeroides* R-26 reaction centers (RCs) where the native primary quinone, ubiquinone-10 (UQ_A), was replaced by 2-methyl-3-phytyl-1,4-naphthoquinone (MQ_A). The native secondary quinone, UQ-10, was retained as UQ_B. The difference spectrum of the semiquinone MQ_A^- minus UQ_B^- absorption is very similar to that of MQ^- minus UQ^- in solution (398-480 nm). Thus, the absorption change provides a direct monitor of the electron transfer from MQ_A^- to UQ_B. In contrast, when both Q_A and Q_B are UQ-10 the spectral difference between UQ_A^- and UQ_B^- arises from electrochromic responses of RC chromophores. Three kinetic processes are seen in the near UV (390-480 nm) and near IR (740-820 nm). Analysis of the time correlated spectra support the conclusion that the changes at $\tau_1 \approx 3$ μs are mostly due to electron transfer, electron transfer and charge compensation are mixed in $\tau_2 \approx 80$ μs, while little or no electron transfer occurs at 200-600 μs (τ_3) in MQ_AUQ_B RCs. The 80 μs rate has been previously observed, while the fast component has not. The fast phase represents 60% of the electron transfer reaction (398 nm). The activation energy for electron transfer is $\Delta G \approx 3.5$ kcal/Mol for both τ_1 and τ_2 between 0-30° C. In isolated RCs with UQ_A, if

there is any fast component, it appears to be faster and less important than in the MQ_A reconstituted RCs.

INTRODUCTION

Reaction centers (RCs) of purple non-sulfur photosynthetic bacteria store the energy of a photon by a series of electron transfer reactions (1, 2, 3). Following absorption of a photon by a dimer of bacteriochlorophylls (P), the primary quinone (Q_A) is reduced in 200 ps forming $P^+Q_A^-$. Electron transfer from Q_A to the secondary quinone Q_B has been measured to occur within 200 microseconds yielding $P^+Q_B^-$. Sub-stoichiometric proton uptake by the protein occurs at this step (4, 5). When there is an available electron donor to P^+ such as cytochrome c the absorption of a second photon yields a dihydroquinone at the Q_B site as Q_B^- accepts a second electron with the concomitant binding of 2 protons onto the quinone. It appears that proton transfer precedes the second reduction of Q_B (6). The final product of two cycles of electron transfer *in vivo* are two oxidized cytochromes in the cell periplasm and reduced dihydro-ubiquinone in the cell membrane. Thus, RCs use the quinones in the Q_A and Q_B sites to create a 2 electron gate where the single electron donors and acceptors cytochrome c, P and Q_A yield a doubly reduced, protonated product Q_BH_2 (7, 8).

The electron transfers from Q_A to Q_B have been the subject of much study (9, 10). This reaction starts the process of coupling electron and proton transfer in RCs and has been used as a model of this crucial step in the vectorial energy transfer and storage process (11, 12). RCs are one of the few energy-coupling, intrinsic membrane proteins where the atomic resolution

structure is known. In addition, as this is a photosynthetic protein, single turnover reactions can be measured. The reaction has been studied by site directed mutagenesis (10, 13), by a variety of spectroscopic techniques (14), and by theoretical analysis (15, 16). It is well established that the first electron transfer does not involve proton binding by Q_B^- as indicated by optical (17), EPR (18), and ENDOR (19) measurements. The reaction does result in sub-stoichiometric proton uptake from the surroundings and proton rearrangement within the protein (4, 5, 20-23). The electron transfer from Q_A to Q_B is the only intra-RC electron transfer that shows significant temperature and pH dependence (2, 24). In this it is different from the other intra-RC reactions that proceed with less than a five fold change in rate from room temperature to 1K. Thus, analysis of the quinone dependent reactions must consider that protein or proton motions may control the electron transfer rate.

The basic problem with studying the electron transfer from Q_A to Q_B in RCs from *Rb. sphaeroides* is that the same quinone, Ubiquinone-10, is found in both quinone binding sites. In the near-UV region of the spectra, the light-induced absorbance changes are almost identical for the reduction of UQ_A or UQ_B and are similar to that obtained for ubisemiquinone in alcoholic solution (17, 25). Therefore, there is no primary optical marker to distinguish between the semiquinone states UQ_A^- and UQ_B^-. Instead, secondary signals have been used including: (1) changes in the spectrum of the bacteriopheophytins adjacent to the quinones at 750 or 770 nm (17, 26); (2) small differences in the absorbance of UQ_A^- and UQ_B^- at 397 nm (7, 17, 27, 28); (3) changes in the protein and quinone vibrations monitored at 1430-1780 cm^{-1} (20, 21); and (4) the recovery of P's competence to initiate a second turnover of electron transfer, a process which cannot occur until Q_A^- has been oxidized by Q_B (29,

30). All measurements show a process with a lifetime between 100 and 300 μs (3300 to 10000 s^{-1}) at room temperature and pH 7-8 in native RCs of *Rb. sphaeroides* that has been assigned to the first electron transfer from Q_A^- to Q_B (7, 17, 30). Recent measurements have shown that the reaction has other phases, with both faster (26) and slower (27) components. Unfortunately, the secondary, electrochromic markers which monitor the charge distribution can not easily distinguish between electron transfer or secondary processes such as proton transfer or protein rearrangement. However, the direct optical observation of electron transfer from Q_A^- to Q_B in *Rb. sphaeroides* RCs can be made if the ubiquinone-10 (UQ_{10}) in the Q_A site is substituted by 2-methyl-3-phytyl-1,4-naphthoquinone (MQ_A), while UQ_{10} is retained as Q_B. The spectrum of menasemiquinone (MQ^-, λ_{max} at 400 nm) is different from ubisemiquinone (UQ^-, λ_{max} at 450 nm) (31-33) providing a direct monitor of the electron transfer from MQ_A^- to UQ_B.

The replacement of UQ_A by MQ_A is expected to modify the Q_A^- to Q_B electron transfer very little. Although MQ is 140 meV harder to reduce in aqueous solution than UQ, in the *Rb. sphaeroides* Q_A site MQ_A and UQ_A have reduction potentials that differ by only 30 meV (34). In addition, crystallographic structures (35) and FTIR measurements (36) show MQ_A and UQ_A have very similar interactions with the protein. The use of MQ_A and UQ_B mimics the native quinone complement in *Rps. viridis* RCs (33). Specific quinone substitution succeeds because the Q_A site in *Rps. sphaeroides* RCs has a preference for MQ over UQ (37). In addition menaquinone will not function as Q_B when Q_A is UQ or MQ, so only electron transfer from MQ_A^- to UQ_B occurs (38).

MATERIALS AND METHODS

Protein Isolation. Rb. sphaeroides R-26 reaction centers were isolated following standard procedures using Lauryldimethylamine-N-oxide (LDAO, Calbiochem) detergent extraction followed by purification using ammonium sulfate and DEAE chromatography (39). Q_A and Q_B were removed with orthophenathroline using the method of Okamura (40), with minor modifications (34). This typically yields RCs with no Q_B and ≈5% Q_A. The RC concentration was measured at 802 nm or 865 nm given the extinction coefficients: $\varepsilon_{802}=0.288\mu M^{-1}cm^{-1}$ or $\varepsilon_{865}=0.135\mu M^{-1}cm^{-1}$.

Quinone Reconstitution. The long tailed quinones are effectively insoluble in water, but become soluble when detergent is added. However, detergent weakens the affinity of quinone for the binding sites. The method of Wraight (41) using quinone dissolved in Triton X-100 was the basis of the most effective and reproducible method of reconstitution. Quinone solutions of 1 mM MQ (2-methyl-3-phytyl-1,4-naphthoquinone, Vitamin K1, Fluka) or 10 mM UQ_{10} (Sigma or Fluka) were heated for 5-10 seconds in a microwave oven to dissolve the quinone. The MQ used here is a close analog to MQ_4 or UQ_4, however, the tail has one isoprenyl unit and three isopranyl (saturated isoprenyl) units on the end of the tail. A final concentration of 1.2-1.6 MQ/RC was added to a 4-5 μM RC solution with 0.02% Triton X-100 at room temperature. Complete MQ_A reconstitution was verified by comparing RC light initiated electron transfer at 430 nm before and after addition of 2-Methyl-1,4-naphthoquinone (MQ_0). The water soluble MQ_0 rapidly fills any empty Q_A sites, increasing the activity. Samples were also checked for

recovery of the ground state from the $P^+Q_A^-$ state with $\tau_{AP}\approx 75$ ms, characteristic of electron transfer from MQ_A^- to P^+. If UQ is Q_A, τ_{AP} is 100 ms. Following complete reconstitution of the Q_A site, the Q_B site was reconstituted with UQ_{10} at ≈15 UQ/RC. The final UQ_B occupancy was above 95%.

Due to the competition between MQ_3 and UQ_{10} for the Q_A site, a small fraction of the Q_A sites were occupied by a UQ_{10}. The fraction of MQ_3 as Q_A was determined from the charge recombination kinetics given the different k_{BP}'s in $P^+UQ_AUQ_B^-$ and in $P^+MQ_AUQ_B^-$ RCs. Approximately 85% of the Q_A binding sites contain MQ_3 with 15% UQ_{10} occupancy. The different k_{BP} rate constants were fixed during the 2 exponential fitting.

Charge recombination kinetics were measured at 430 nm, pH8.0, room temperature (22±2°C), 10 mM Tris, 4-5 μM RC, with 0.02-0.03% Triton X-100 for 4 types of RCs. Without Q_B τ_{AP} is 75 ms (k_{AP}=(13.3±0.6/sec) from $P^+MQ_A^-$; 108 ms (9.3±0.2/sec) from $P^+UQ_A^-$ (1.5 stigmatellin/RC added to remove any UQ_B (Fluka)). When Q_B is present, charge recombination at τ_{BP} is 2.8s (k_{BP}=0.36±0.4/sec) from $P^+MQ_AUQ_B^-$; 1.19s (0.84±0.01/sec) from $P^+UQ_AUQ_B^-$. The driving force (ΔG) for electron transfer from Q_A^- to Q_B can be calculated from the charge recombination rates k_{AP} and k_{BP} (30, 42). The pathway for charge recombination in $P^+Q_B^-$ RCs is via Q_A^- (at k_{AP}) so that $P^+Q_A^-Q_B$ and $P^+Q_AQ_B^-$ come to equilibrium (K_{AB}) and then return to the ground state at

$$k_{BP}=k_{AP}/(K_{AB}+1) \qquad (4.1)$$

In UQ_AUQ_B RCs the reaction ΔG is 60 meV; in MQ_AUQ_B RCs it is 93 meV.

Optical Measurements. Light-induced absorbance changes were measured using a flash spectrophotometer designed by the University of Pennsylvania Biomedical Instrumentation Group. Actinic light was provided by a 5 ns, 532 nm pulsed YAG laser pumping the fluorescent dye LDS 751 (Exciton). The peak of the fluorescence was at 750 nm. The laser intensity was adjusted to provide 80-90% saturation of the P^+ signal. The measuring light, placed perpendicular to the excitation light, was from a 100W quartz-halogen-tungsten lamp (ORIEL) with appropriate neutral density and interference filters and was controlled by a shutter placed before the RC sample which was only opened during measurement. For kinetic measurement of Q_A to Q_B, the shutter was opened for less than 10 ms. The transmitted light was detected using a Thorn EMI 9798QB photomultiplier. The output from the photomultiplier was amplified by a Stanford Research System model SR445 or Comlinear Model E103 fast amplifiers. For measurement of the $P^+Q_A^-Q_B$ to $P^+Q_AQ_B^-$ electron transfer, the amplified signal was sent to 2 LeCroy (model 9310M 300 MHz and 9304A 250 MHz) digital storage oscilloscopes recording and averaging different time scales. The time resolution of the measuring system was limited by the 80 ns rise time of the photomultiplier tube. The time between flashes was 1 to 4 minutes and 50-60 kinetic traces were averaged.

Semiquinone spectra were measured 25 ms after a single saturating flash, in the presence of 200 ferrocene/RC. Ferrocene (Aldrich) was diluted in alcohol. With ferrocene as an electron donor to the bacteriochlorophyll dimer, charge recombination from $P^+Q_A^-$ or $P^+Q_AQ_B^-$ was prevented. Instead, a stable PQ_A^- or $PQ_AQ_B^-$ state is created which decays slowly allowing clear observation of the semiquinone signal (43, 44). The time between flashes was 10 minutes. 3-5 kinetic traces were averaged.

The measurements of time-resolved electrochromism associated with the formation of quinone anions at 760 nm were performed as described by Tiede et al. (26).

Data Analysis. The Levenberg-Marquardt algorithm, a non-linear least-squares fitting in IGOR Pro (WaveMetrics) was used to analyze the kinetic traces by fitting to 2 or 3 exponentials plus a constant using the standard expression:

$$A(t)=A_0+A_1*Exp(-t/\tau_1)+A_2*Exp(-t/\tau_2)+A_3*Exp(-t/\tau_3) \quad (4.2)$$

Two sets of data were recorded simultaneously by the two digitizing oscilloscopes. In the time range 0-20 μs, 2000 data points were collected. This kinetic trace was fit to a single exponential. In the time range 0-2 ms, 20,000 data points were collected. This data was averaged nonlinearly so that each kinetic component has similar data density to provide a total of 2700 data points. Thus, more data points were retained at early times. The fitting of the longer time scale data depended on the results of fitting the fast trace. If a fast component was seen in the 20 μs data, the longer data set was fit with 3 exponentials. The fastest rate was fixed from the early time data. If there was no fast phase, the longer data set was fit to 2 exponentials. The following fitting methods were used for the different spectral components.

1. $P^+MQ_A^-$ or $P^+UQ_A^-$ show no changes at 398 nm for at least 1 ms. At times greater than 1.5 ms, the charge recombination of P^+Q^- begins to be observed. Analysis of the changes that depend on the presence of Q_B at this wavelength is carried out on the raw data.

2. At wavelengths other than 398 nm, the kinetic signal associated with Q_A^- to Q_B electron transfer is very small compared to the difference between the P^+ and P signal. In addition, the large ΔA from the flash induced oxidation of P produces a small reproducible hysteresis in the PMT tube ($\tau \approx 200$ μs). Therefore, analysis of the kinetic processes associated with Q_B^- requires subtraction of $P^+Q_A^-$ kinetic traces from those obtained with a matched $P^+Q_AQ_B^-$ sample. The samples, with Q_A alone and both Q_A and Q_B present were reconstituted with Q_A in the same tube and then split. UQ_B was added to one sample. The concentration difference between the two samples is less than 1%.

RESULTS

The spectrum of $P^+Q_A^-$, Q_A^-, and Q_B^- in the near UV. From 398 to 480 nm the change in absorbance going from the ground state (PQ_AQ_B) to the $P^+Q_A^-$ state (denoted the $P^+Q_A^-$ spectrum) or to the $P^+Q_B^-$ state (the $P^+Q_B^-$ spectrum) is dominated by the changes in absorbance of P as it is oxidized. Replacing the native ubiquinone by menaquinone has little effect on the $P^+Q_A^-$ spectrum (Fig.4.1). The small increase in absorbance below 435 nm in the $P^+MQ_A^-$ spectrum arises because MQ^- absorbs more than UQ^- in this region (Fig. 4.3a). The contribution of Q_A^- or Q_B^- to the spectra can only be seen clearly by the addition of an electron donor to P^+, such as ferrocene. The semiquinone minus quinone difference spectra of UQ_A^-, $UQ_AUQ_B^-$ (Fig. 4.2a) and $MQ_AUQ_B^-$ (Fig. 4.2c) are very similar. Each of these intra-RC UQ species bears a strong resemblance to the UQ^- spectrum in solution (Fig. 4.3a) (31).

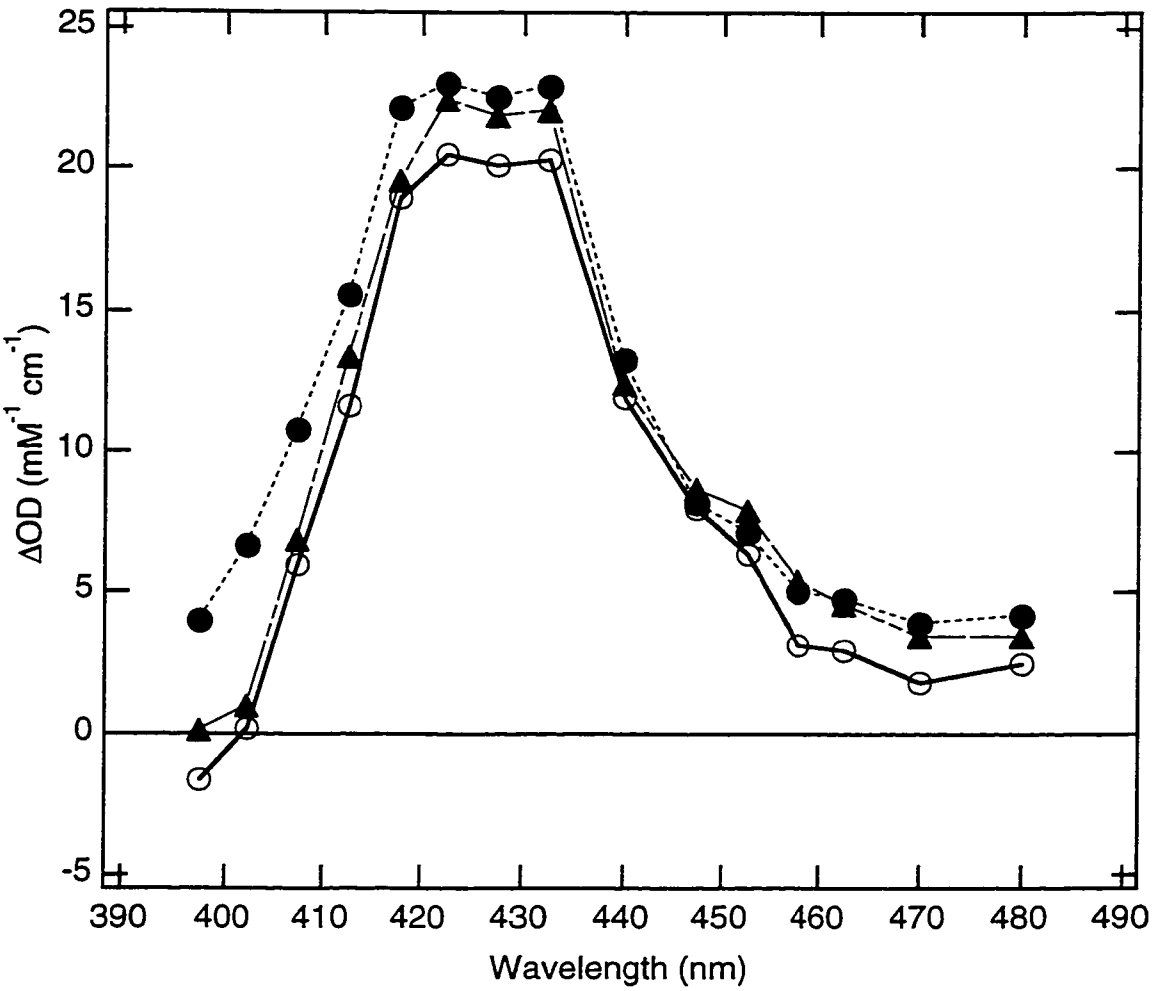

FIGURE 4.1. Light minus dark absorbance spectra of RCs without Q_B where Q_A is UQ_{10} (▲) or MQ_3 (●), RCs with MQ_AUQ_B (○). Change in optical density (ΔOD) measured 10 μs after the flash, with 4 μM RCs in 0.02% Triton, 10mM Tris, 2.5 mM KCl at 22 °C, pH 8.0. The RC concentration was determined from the static extinction coefficients at 802 and 865 nm: $\varepsilon_{802}=0.288\mu M^{-1}cm^{-1}$ or $\varepsilon_{865}=0.135\mu M^{-1}cm^{-1}$.

The peak of the UQ^- spectrum at 445 nm in solution (Fig. 4.3a) is red shifted by 5 nm when it is UQ_A^- and by only 2 nm as UQ_B^- (Fig. 4.2a). The

main features of the UQ_B^- spectrum is independent of which quinone is in the Q_A site (Fig. 4.2a and 4.2c). Thus, the peaks at 420, 445 and 460 nm in the (UQ_A^-)-$(UQ_AUQ_B^-)$ difference spectrum (Fig. 4.2b) can be obtained simply by subtracting a solution spectrum shifted by 5 nm from one shifted by only 2 nm and multiplied by ≈1.2. The only significant difference between the solution spectrum and the intra-RC UQ_A^- and UQ_B^- spectra is the peak in the UQ_A^- spectrum at 398 nm, which is not found in the UQ_B^- spectra. The amplitude of the absorbance difference between UQ_A^- and UQ_B^- (Fig. 4.2b) is small compared to the changes associated with the oxidation of P (see Fig. 4.1). The UQ_A^- peak at the P^+ minus P isobestic point near 400 nm provides the best window to follow Q_A to Q_B electron transfer coupled processes. Unfortunately, this peak represents a still unassigned electrochromic shift of the quinone or other protein cofactor. It will be seen that this wavelength monitors later events as well as the electron transfer itself.

While in the native *Rb. sphaeroides* RCs, Q_A and Q_B are the same compound so there is no primary difference in their spectra, there is a significance difference in the semiquinone spectra of UQ and MQ. The maximum MQ^- absorbance is at 400 nm in RCs and in solution, while the maximum for UQ in solution, or in the Q_A or Q_B sites is near 450 nm. The absorbance difference of (MQ_A^-) minus $(MQ_AUQ_B^-)$ in MQ_A reconstituted RCs (Fig. 4.2d) looks very much like the difference between MQ^- and UQ^- in aqueous solution (Fig. 3b) with the same peaks, and troughs. There are additional features near 400, 420 and 465 nm. These peaks are found in the UQ_A^- - UQ_B^- spectrum. However, the ≈15% of the RCs with UQ_A does not

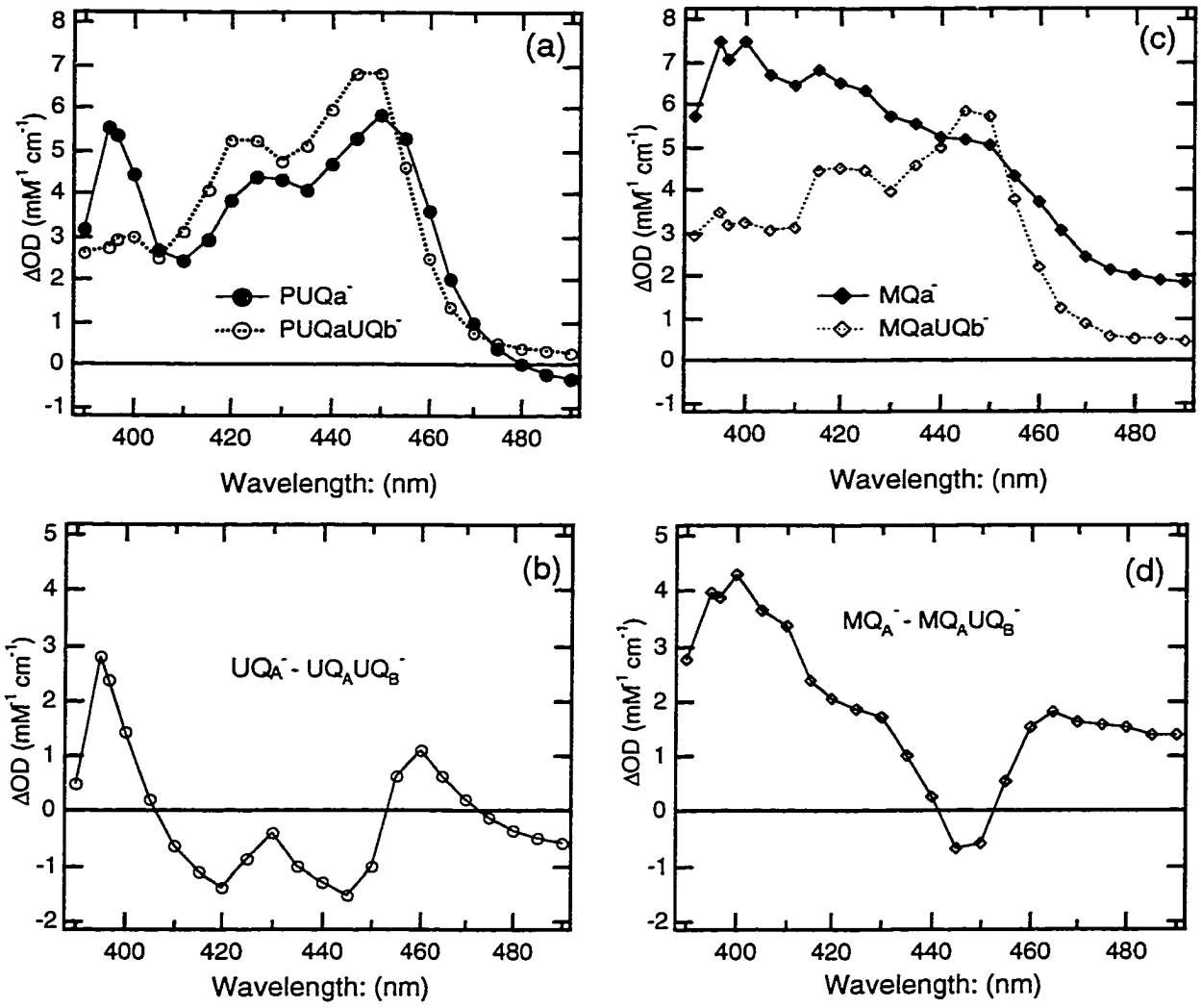

FIGURE 4.2. Light minus dark difference spectrum of 1 μM RCs with 200μM Ferrocene measured 25 ms after excitation flash. This provides the (semiquinone) -(quinone) spectra for: (a) PUQ_A^-(●), $PUQ_AUQ_B^-$(○); (c) PMQ_A^-(◆), $PMQ_AUQ_B^-$ (◇). Double difference spectrum of (b) PUQ_A^- minus $PUQ_AUQ_B^-$; (d) PMQ_A^- minus $PMQ_AUQ_B^-$. The Q_B occupancy was normalized to 100%. 3-5 measurements were averaged. Buffer conditions are the same as in Fig. 4.1.

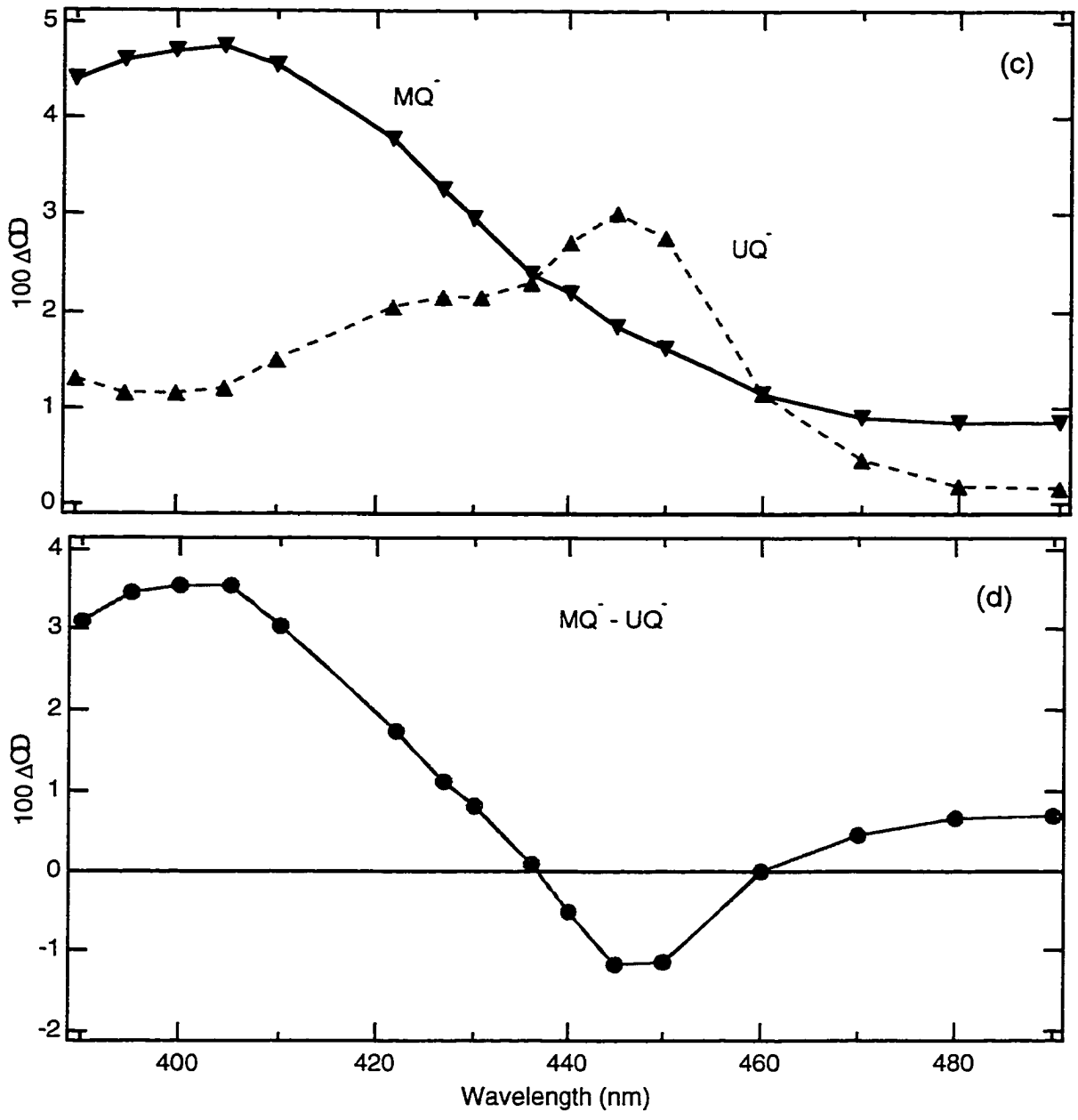

FIGURE 4.3. Semiquinone - quinone difference spectra in solution measured by pulse radiolysis in aqueous solution. (a) 100 μM MQ^- (solid line) 5 M isopropyl alcohol pH=6.4; 100 μM UQ^- (dotted line) 7M isopropyl alcohol, pH=8. (b) Double difference spectrum of MQ^- minus UQ^-. Data taken from Patel and Willson (31).

fully account for the magnitude of the changes indicating small shifts of the MQ^- spectrum as it binds to the protein, or changes in the protein spectrum in response to formation of Q_A^-.

Absorption Changes Associated with $Q_A^-Q_B$ to $Q_AQ_B^-$ Electron transfer. When RCs were reconstituted with MQ at the Q_A site and UQ at the Q_B site, at 398 nm three kinetic components were observed following formation of $P^+MQ_A^-UQ_B$ (Fig. 4.4, summarized in Fig. 9a). A fast absorbance change: τ_1=3.5 ± 0.9 μs ($3.3x10^5$ s^{-1}) with A_1≈45%, an intermediate phase, τ_2=80±15 μs (12,500/sec) with A_2≈25%, and a slow phase, τ_3=260±50 μs (3800/sec) with A_3≈30%. These transients depend on the presence of UQ_B. With MQ at the Q_A site and no Q_B, there is no change in the optical absorption for 1 ms. In $P^+MQ_A^-$ RCs only charge recombination to the ground state at τ_{AP}= 75 ms is seen. Stigmatellin, a competitive inhibitor of Q_B, removes all sub-millisecond components in MQ_AUQ_B RCs. Thus, these three components are associated with electron transfer from MQ_A^- to UQ_B^-.

The two slower rates, τ_2≈80 μs and τ_3≈260 μs, have been previously reported in UQ_AUQ_B RCs (26, 27) (Fig. 4.9). τ_1 is faster than previously reported in isolated RCs. However, as seen in Figure 4 the fast phase is a significant fraction of the processes that occur on electron transfer from Q_A^- to Q_B. The fast phase is clearly part of this reaction since the initial absorbance amplitude for $P^+Q_A^-$ to $P^+Q_B^-$ electron transfer kinetics must equal the absorbance of the starting state which is $P^+Q_A^-$. Having the same initial amplitude in a closely matched pair of samples with and without Q_B is the best way to check that none of the Q_A^- to Q_B reaction occurs faster than the time

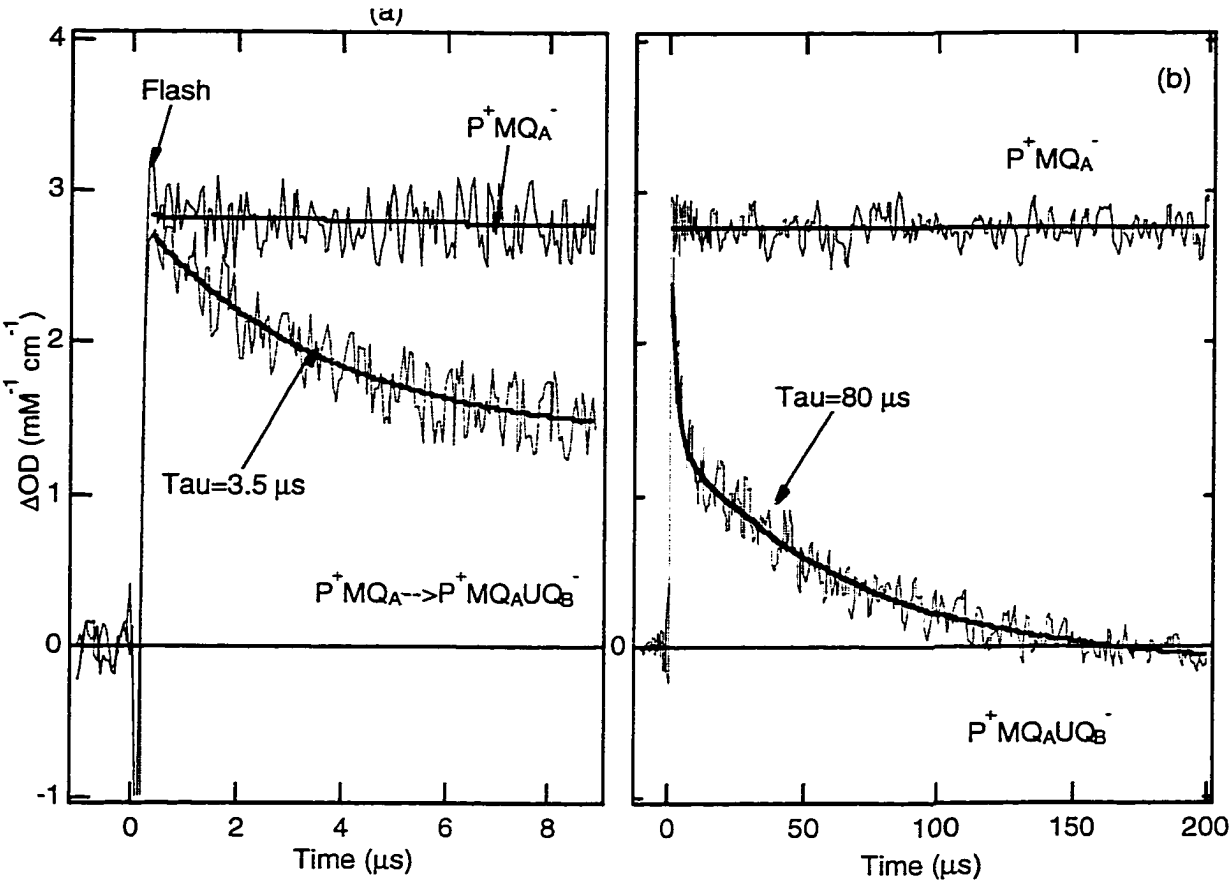

FIGURE 4.4. The kinetics of light-induced absorbance changes at 398 nm, pH=8. (a) First 10 μs: RCs reconstituted with MQ_A only (top), with both MQ_A and UQ_B (bottom). τ_1 of 3.5 μs was obtained by single exponential fitting to the bottom trace. (b) The same transient monitored for 200 μs. τ_2 is 87 μs obtained when τ_1 is fixed at 3.5 μs. Measurement conditions as in Fig.4.1.

resolution of the measurements. When only the slower components are analyzed ≈50% of the absorbance change at 398 nm occurs as a burst phase (Fig 4.4b). A predicted absorbance change on reaction can also be derived from the difference in the absorbance of ferrocene trapped MQ_A^- and UQ_B^- (Fig. 4.2) which is 4.0±0.4 ΔOD/mM at 400 nm (normalized to 100% Q_B

reconstituted) . The sum of the initial amplitudes of the τ_2 and τ_3 components is only 60% of the predicted value. Adding the τ_1 contribution, the value is within 90% of that expected.

The transient absorbance difference in MQ_AUQ_B RCs was also measured at 757 nm at 6°C (Fig. 4.5). Three phases are seen: τ_1=6.3 ±1.2 μs, τ_2=205 ±55 μs and τ_3=950 ±180 μs with relative amplitudes of 0.53, 0.39 and 0.08, respectively. These rates are similar to the rates observed at 398 nm at 5.2°C where τ_1=6.6 ±0.5 μs, τ_2=120 ±12 μs and τ_3=1.1 ±0.1 ms with relative amplitudes of 0.41, 0.27 and 0.32, respectively (see Fig. 4.6 and 4.9b).

The time course of the absorbance changes associated with the UQ_A^- to UQ_B electron transfer reaction were also measured at 398 nm. At this wavelength, the two slower rates τ_2=65±25 μs and τ_3=260±50 μs seen in MQ_AUQ_B RCs are clearly observed. A fast absorption change at < 1 μs, representing approximately 15% of the total amplitude may also be seen. Unfortunately, this fast rate is at the limit of the instrument response time. No absorption changes are seen at 398 nm from 2-40 μs following the formation of $P^+Q_A^-$ in UQ_AUQ_B RCs. The same results are found in RCs where both Q_A and Q_B are reconstituted with UQ_{10} as well as in RCs when UQ_A is retained duing the purification procedure. Thus, the quinone extraction and replacement is not the cause of the difference between the MQ_A and UQ_A RCs. *2 or 3 Exponential Curve Fitting.* The rate constants obtained by fitting kinetic transients depend to some degree on the analysis method. The fast component τ_1 is 23 times faster than τ_2 so it is clearly seen in MQ_AUQ_B RCs. In contrast the 2 slower components differ by only 3 fold so are harder to resolve. Fitting a kinetic trace obtained at room temperature, 398 nm, and pH8, (Fig. 4.6) to 3 exponentials yields τ's of 3.5, 78, and 260 μs. Fitting the

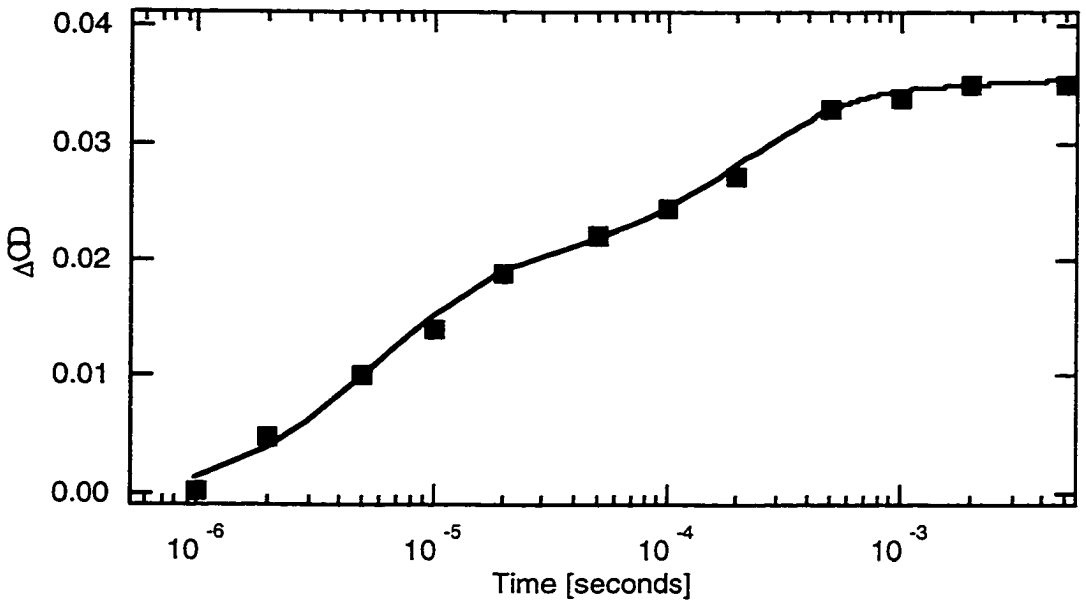

FIGURE 4.5. Absorbance changes in MQ_AUQ_B RCs at 757 nm and 6°C. Amplitude normalized to ΔOD(865 nm, 0 μs) = 1. Solid line fit to 3 exponentials: τ_1=6.3 ±1.2 μs, τ_2=205 ±55 μs and τ_3=950 ±180 μs with relative amplitudes of 0.53, 0.39 and 0.08.

same date with 2 exponentials, gives τ's of 3.5 and 130 μs. The improvement with the third component is small (see residuals in Fig. 4.6). However, at lower temperature (5.2°C) (Fig. 4.6-bottom), τ_2 and τ_3 are better separated. Here a 2 exponential fit shows substantially more error than when 3 exponentials are used. The results at both low temperature and high pH (data not shown) where the second (τ_2) and third (τ_3) components are better separated demonstrate that there are at least 3 phases of absorbance changes. In addition, as will be seen below τ_2 and τ_3 have different spectra. Therefore, all kinetic traces with Q_B were fitted to 3 exponentials.

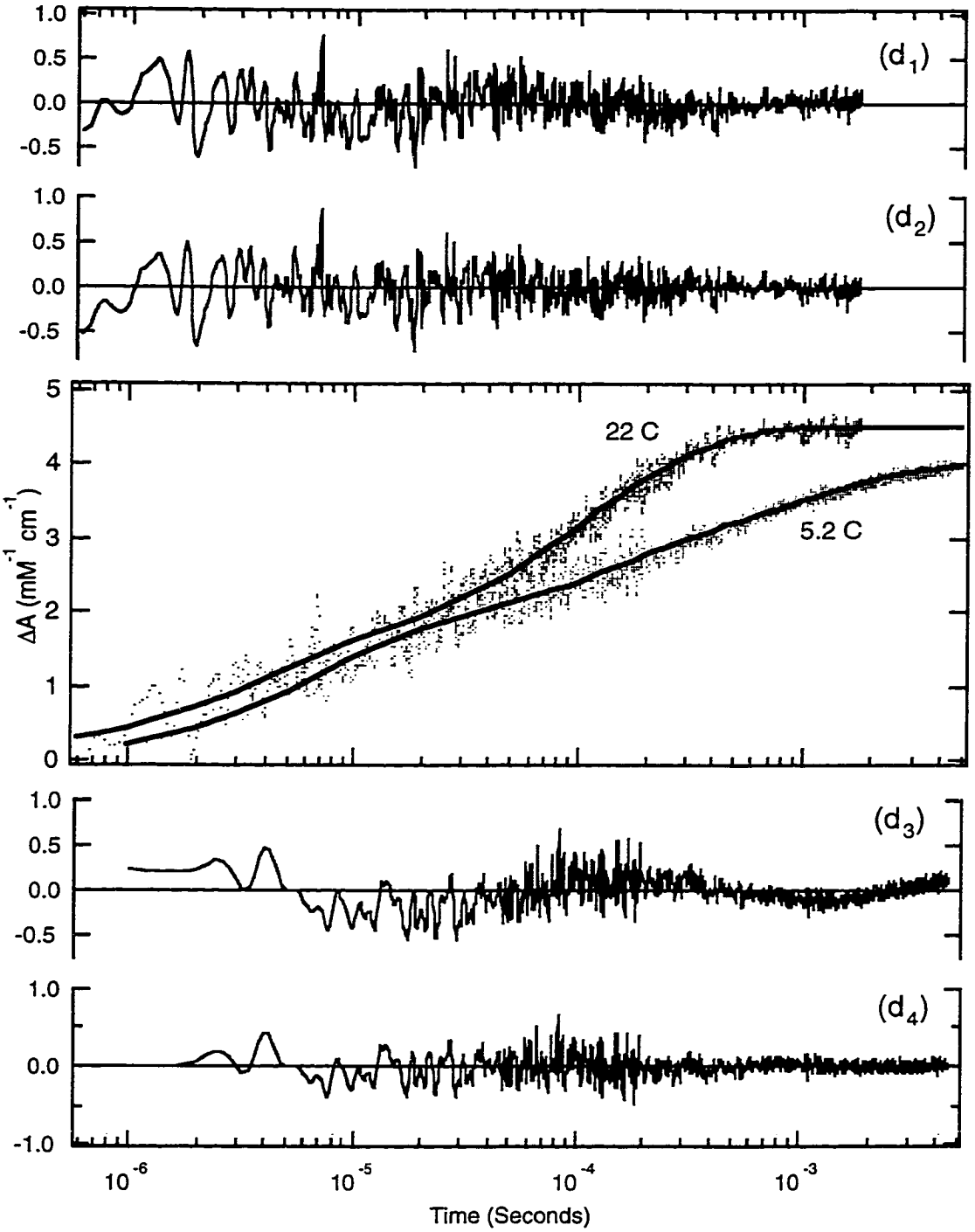

FIGURE 6. Kinetics of absorption change at 398 nm at 22 °C and 5.2 °C. Residuals of fitting 22 °C data with (d_1) 2 exponentials (3.5, and 130 μs) or (d_2) 3 exponentials (3.5, 78, and 260 μs) and 5.2 °C data with (d_3) 2 exponentials (7, and 490 μs) or (d_4) 3 exponentials (7, 120 and 1100 μs). 3 exponential fitting on data.

The Spectra of the Three Kinetic Components. The wavelength dependence of each kinetic component (the transient absorption difference spectrum) can provide the information to identify the reaction occurring at this rate. In MQ_AUQ_B RCs, the shape of the transient absorption spectra with lifetimes of 3 μs and 80 μs (Fig. 4.7a) largely matches the shape of the MQ^- minus UQ^- spectra in solution (Fig. 3b). Thus, 60% of the electron transfer from MQ_A^- to UQ_B occurs with a lifetime of 3 μs while the remaining 40% of the MQ_A^- transfers its electron to UQ_B in 80 μs. In contrast, τ_3 (200 -600 μs) is only measurable near 400 or 450 nm. Thus, the slow rate monitors other changes in the protein occurring after electron transfer. This slow phase accounts for 30% of the total change at 398 nm in MQ_AUQ_B RCs.

The sum of the three components are in reasonable agreement with the difference spectrum predicted from ferrocene trapped MQ_A^- minus UQ_B^- (Fig. 4.7c), especially around 400 nm and 450 nm. At other wavelengths, while the shape of the spectrum matches qualitatively, there are differences between the amplitudes of the two curves (Fig. 4.7c). The reason for the mismatch is unknown. One explanation for the static difference of MQ_A^- minus UQ_B^- being bigger than the amplitude change obtained from the kinetic results (Fig. 4.7c) is that the trapped semiquinone spectrum was measured 25 ms after the flash rather than being limited to the 2 ms observed in the kinetic measurements. Thus, the static states of MQ_A^- and UQ_B^- in RCs where charge recombination is blocked may include additional proton uptake or protein conformational changes that add to the difference spectra.

In UQ_AUQ_B RCs, the only evidence for the fast component τ_1 is found near 400 nm where the expected absorbance changes are the largest. The shape of the 65 μs (τ_2) component (Fig. 4.7b) is very close to the spectrum

predicted from the ferrocene trapped semiquinone spectrum (Fig. 4.2b). While the amplitude at τ_3 has a spectrum similar to τ_2 in the 398-435 nm range, its amplitude is close to zero at wavelengths longer than 450 nm (Fig. 4.7b). The 398 nm peak in the τ_2 and τ_3 difference spectra do show the oxidation state change of UQ_A^- (Fig. 4.7b). However, the lifetime correlated spectra shows that these kinetic components show different shifts in the free-radical anion or protein spectra near 450 nm. The sum of the amplitudes at τ_2 and τ_3 qualitatively matches the spectrum predicted from the static Q_A^- and Q_B^- spectra (Fig. 4.7d).

The Temperature Dependence of Processes Associated with the Electron Transfer from Q_A to Q_B. The temperature dependence of the kinetic components was measured between 0 and 27°C in both MQ_AUQ_B and UQ_AUQ_B RCs (Fig. 8 and table 1). The pH of Tris buffer changes from pH 8 to 8.6 over the temperature range 22 to 5 °C. However, measurement of the rate as a function of pH shows that this should have negligible effect. In MQ_AUQ_B RCs the proportion of the electron transfer that occurs at τ_1 does not change with temperature (Fig. 8b). The activation energy of τ_1 is 3.8±1.1 kcal/mole (Fig. 8a) with a pre-exponential factor of $(2.2\pm0.3)\times10^8$ s^{-1}. The activation energy of τ_2 is 3.4±0.6 kcal/mole with a pre-exponential factor of $(5.0\pm0.3)\times10^6$ s^{-1} (Table 4.1). The activation energy of τ_3 is 7.1±1.3 kcal/mole.

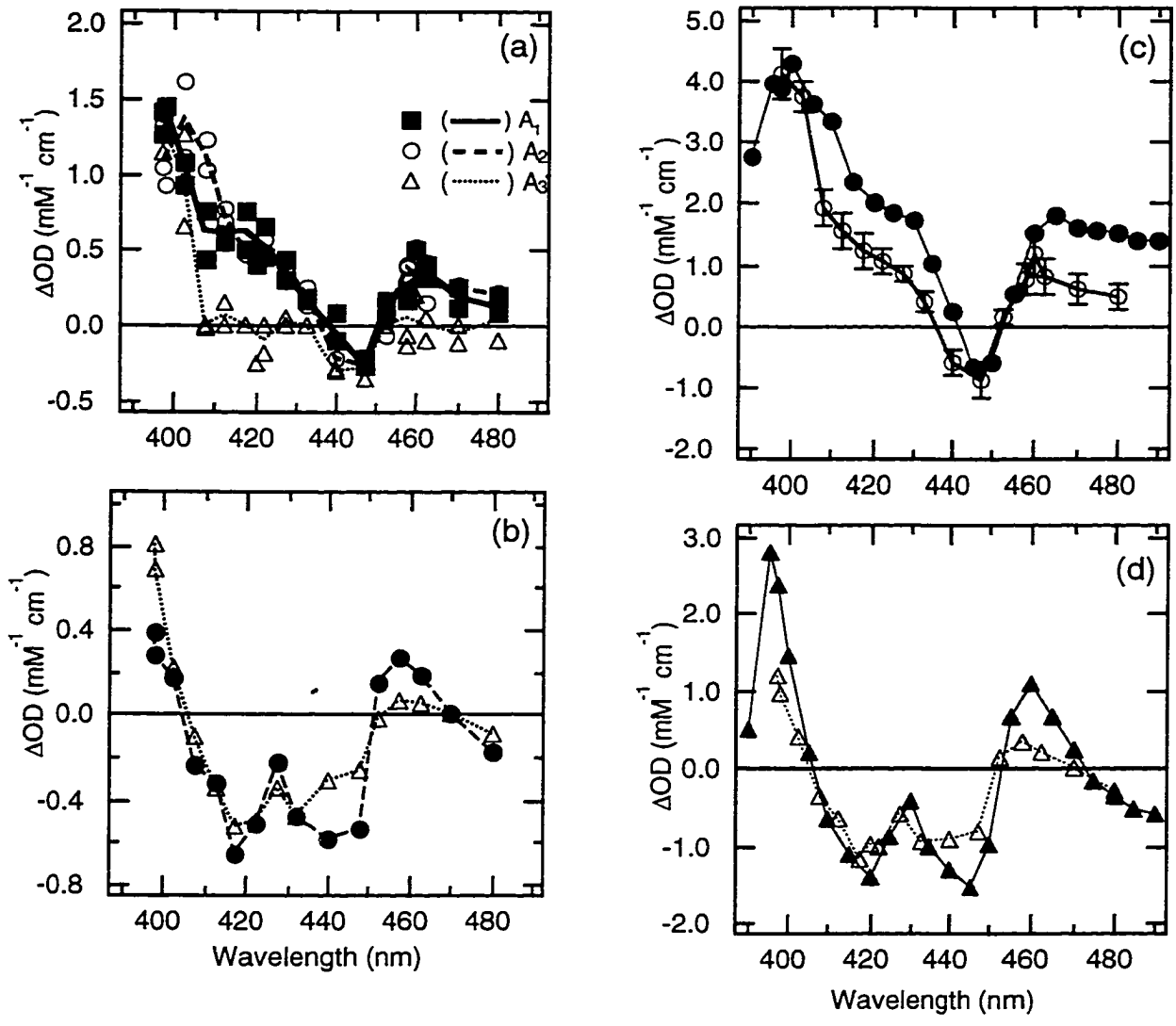

FIGURE 4.7. The spectra of each kinetic component. (a) MQ_AUQ_B RCs: A_1 (■), A_2 (○), A_3 (△). (b) UQ_AUQ_B RCs: A_2 (●), A_3 (△). (c). MQ_AUQ_B RCs: $A_1+A_2+A_3$ (○); double difference spectrum measured with ferrocene as an electron donor from Fig. 4b (●). (d). UQ_AUQ_B RCs: A_2+A_3 (△) double difference spectrum from Fig. 2b (▲). Results in c and d normalized to 100% UQ_B.

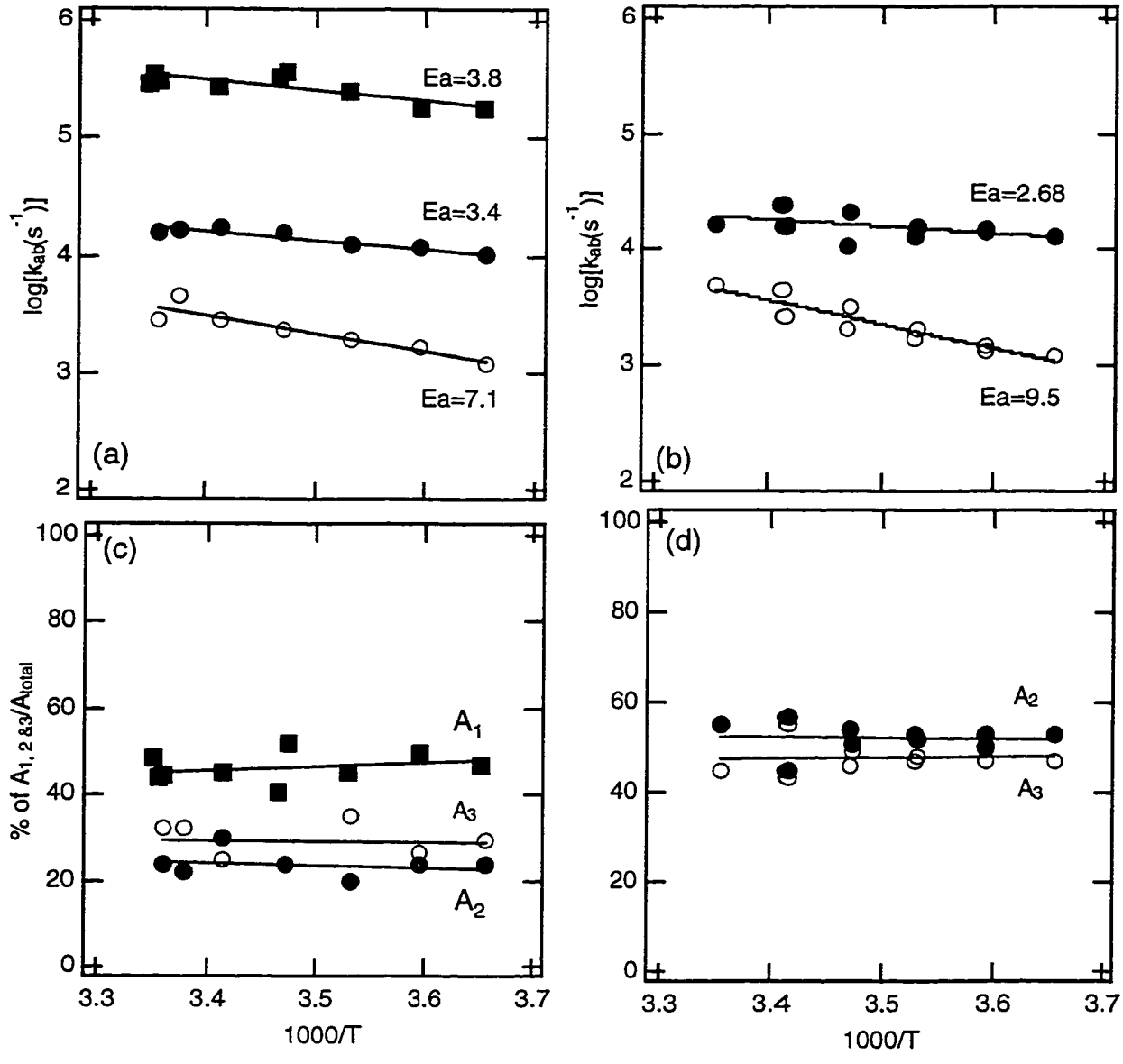

FIGURE 4.8. Temperature dependence of each kinetic component. The activation energies (E_a) are in Kcal/Mol. MQ_AUQ_B RCs: (a) Arrhenius plot for $k_1=1/\tau_1$ (■), $k_2=1/\tau_2$ (●) and $k_3=1/\tau_3$ (○). (c) Percentage of the total ΔA ($=A_1+A_2+A_3$) at A_1 (■), A_2 (●) and A_3 (○). UQ_AUQ_B RCs: (b) Arrhenius plot for $k_2=1/\tau_2$ (●) and $k_3=1/\tau_3$ (○). (d) Percentage of the total ΔA ($=A_2+A_3$) at A_2 (●) and A_3 (○). The conditions were the same as in Figure 3 and all data were measured at 398 nm.

Table 1. Summary of Activation Energies (Ea)			
RC\Time constant at 22 °C	τ_1 (3.5 μs)	τ_2 (80 μs)	τ_3 (200-600μs)
MQ_AUQ_B (kcal/mole)	3.8±1.1	3.4±0.6	7.1±1.3
UQ_AUQ_B (kcal/mole)		2.7±1.2	9.5±1.4

DISCUSSION

Biphasicity of $Q_A^-Q_B$ -> $Q_AQ_B^-$ Electron Transfer

Electron Transfer from Q_A^- to Q_B when Q_A is MQ. The analysis of the kinetic components of the spectral changes in the 398 to 480 nm region reveals 3 time scales for events connected to the electron transfer from MQ_A^- to UQ_B (Fig. 4.9). Electron transfer in MQ_A RCs occurs in the 2 faster phases, with lifetimes of 3.5±0.9 μs (τ_1) and 80±15 μs (τ_2) at 22°C. The lifetime correlated difference spectra in RCs (Fig. 7a) look like the static MQ^- minus UQ^- spectrum in solution (Fig. 4.3b) (31). This clearly identifies these components as individual phases of electron transfer[2]. The rate and pH dependence (not shown) of the 80 μs component is close to the traditionally assigned single lifetime for the electron transfer from UQ_A^- to UQ_B of 100 to 300 μs (7, 17, 30). However, the 3 μs phase is faster than has been previously described in isolated UQ_A containing *Rb. sphaeroides* RCs (Fig. 4.9), although similar rates and amplitudes for biphasic UQ_A^- to UQ_B electron transfer have been seen in chromatophores (45, 46). Similar fast rates have been reported for native *Rps. viridis* RCs, with electron transfer from MQ_A^- to UQ_B, occurring with lifetimes of 6 μs at pH7 and 30 μs at pH8 in membrane fragments (47) and 18

μs in whole cells (48) at pH 7. Possible mechanisms that can yield these distinct rates will be considered below.

Both τ_1 and τ_2 are also seen in the electrochromic response of the BPh, measured at 757nm in MQ_A RCs. This wavelength is near the isobestic point for the $P^+Q_A^-$ spectrum, and as discussed previously (26, 45, 46), it monitors the electrostatic perturbation of the BPh optical absorption associated with the

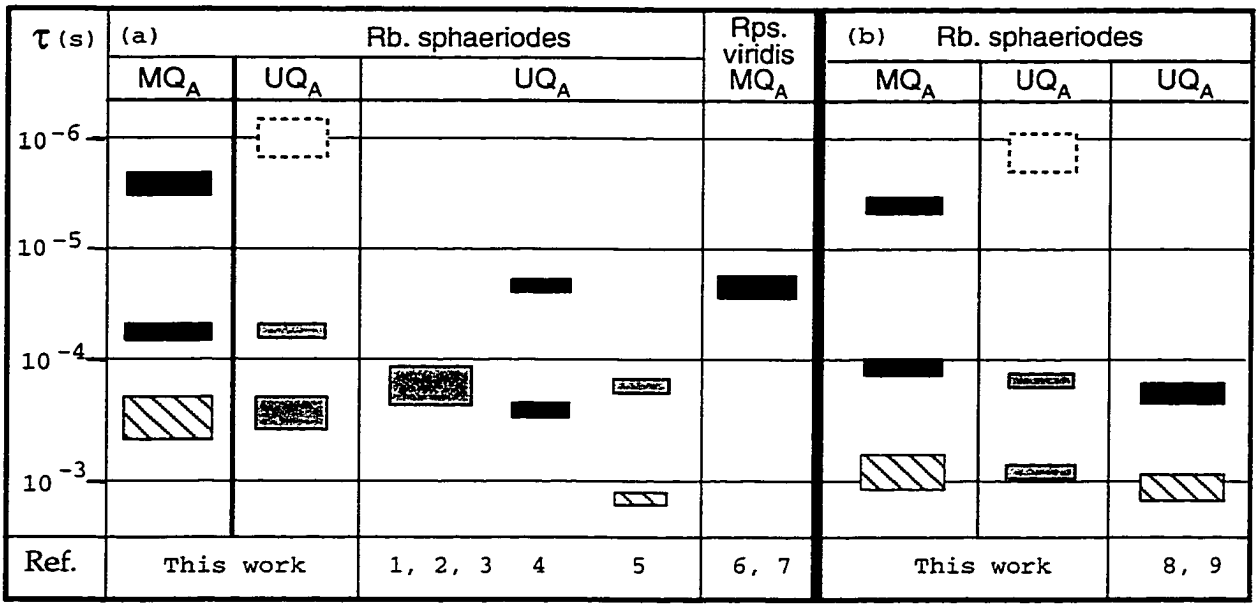

FIGURE 4.9. Summary of measured time constants of electron transfer from Q_A^- to Q_B and associated processes: (A) at room temperature; (B) at 4-6 °C. Black boxes are assigned to electron transfer and hatched boxes are assigned to proton uptake or protein rearrangement. The possibility of a fast τ_1 in UQ_A RCs is shown by the dashed border. The grey boxes are from measurements where the process monitored by a kinetic transient has not be assigned. Single exponential fit to data at 750 nm: 1. Verméglio and Clayton (17); 2. Wraight (7); 3. Kleinfeld et al. (30). Double exponential fit of data at 757 nm: 4. Tiede et al. (26). at 397 nm: 5. Takahashi et al. (27). Double flash method: 6. Leibl et al. (48); 7. Mathis et al. (82). FTIR measurements at 1725 cm^{-1}: 8. Hienerwadel et al. (20); 9. Hienerwadel et al. (21).

formation of the Q_B^- state. Charge compensating events will attenuate this signal, and differences between the electron transfer and charge compensating events will add kinetic complexity. However, the close correspondence between the lifetimes determined in the near UV and at 757 nm supports the interpretation that changes at this near IR wavelength primarily detect electron transfer. The relative amplitudes of the kinetic components in the near UV and at 757 nm need not be the same, since the near UV and 757 nm signals need not have the same dependence on dielectric and protonation state changes in the cofactor surroundings.

There is a third kinetic component present near 398 nm, τ_3= 200-600 μs (22 °C), which also depends on the presence of a functional Q_B. The spectrum of the absorbance changes associated with τ_3 shows clearly that this is not electron transfer (Fig. 7a). Thus, electron transfer and slower protein responses are kinetically well-separated in MQ_A containing RCs. A kinetic separation is also seen in the near IR transient spectra. Measurements at 770 nm (data not shown) with lifetimes at 6° C of approximately 60 μs and 2 ms show a distinct lag compared to those at 757 nm where the lifetimes are 6.6 μs, 205 μs, and 950 μs. Previous measurements in chromatophores have shown that the 770 nm transients reflect quenching of the electrochromism associated with the Q_B^- state, while transients at 757 nm monitor both electron transfer and charge-compensating events (45, 46). Hence, measurements in the near UV and near IR both support the conclusion that the changes at τ_1 are mostly due to electron transfer, electron transfer and charge compensation are mixed in τ_2, while little or no electron transfer occurs at τ_3 in MQ_AUQ_B RCs.

Electron Transfer from Q_A^- to Q_B when Q_A is UQ. Measurement and assignment of Q_A^- to Q_B^- electron transfer and accompanying non-electron transfer events is significantly more difficult with RCs containing UQ_AUQ_B than those containing MQ_AUQ_B. Rather than a change in the primary optical signal the UQ_A^- absorbance is simply red shifted 3 nm relative to UQ_B^-. UQ_A^- is also associated with an absorption peak near 398 nm, which is an isobestic point of the P^+-P signal. The origin of this peak is unknown, but it appears not to be a property of the UQ^- itself, and hence apparently arises from an electrochromic response of another RC cofactor to the oxidation state of Q_A. In addition, the assignment of changes at 398 to processes occurring after electron transfer must be considered in UQ_AUQ_B RCs since this wavelength is seen to report non-electron tranfer events in the MQ_AUQ_B RCs.

Optical transients in RCs with UQ_AUQ_B show kinetic components comparable to τ_2 and τ_3 in MQ_AUQ_B RCs(Fig. 7b). In contrast, to the results in MQ_AUQ_B RCs, there is less distinction between the spectra of τ_2 and τ_3 (Fig. 7). The coincidence of the kinetics of electron transfer and charge compensating events in UQ_AUQ_B RCs is also supported by measurements in the near IR. These show equivalent, complex kinetics occurring on the time scales of τ_2 and τ_3 throughout the near IR region, including measurements at 757 nm monitoring both electron transfer and charge compensation, and at 770 nm which responds selectively to charge compensation events (45, 46). A small fraction of the changes at 398 and 757 may occur faster than can be measured (<1 μs). However, any burst phase accounts for at most 15% of the signal.

Non-electron Transfer Events occurring at τ_2 and τ_3. It is not possible to assign the source of the non-electron transfer components from the near IR or near UV spectra. However, previous studies have identified processes such as proton transfer and protein relaxation occurring with lifetimes similar to τ_3 which may underlie the spectral changes observed here. Thus, Hienerwadel et al. (20, 21) have made time-resolved IR measurements in native *Rb. sphaeroides* RCs (4 °C, pH 7-7.5) under conditions where τ_2 here is 120±15 μs and τ_3 is ≈1 ms (Fig. 9b). Several peaks between 1780-1430 cm^{-1} change with life-times of ≈170 μs ($\tau_{1/2}$ = 120 μs). The carboxylic acid group of Glu L212 (1725 cm^{-1}) was protonated in 260 μs (25%) and 1.4 ms (75%) (21). The 170-260 μs component, comparable to τ_2 here, was assigned to events that occur with the electron transfer itself and the slow component (τ_3 here) represents later proton transfers or conformational changes. In addition, pH indicator dye shows H^+ uptake at 10^4-10^3 s^{-1} following $P^+Q_A^-$formation (49). Other methods also show transients on the time scale of τ_3 that appear to be protein relaxation following electron transfer. The electrochromic shift of the BPh absorbance that monitors Q_B^- formation is diminished at 100-300 μs (≈20°C). This is indicative of protein relaxation screening BPh_M from Q_B^- (45). Brzezinski et al. observed a voltage change with τ≈200 μs (at 20°C) following formation of $P^+Q_A^-$ or $P^+Q_B^-$ (50). This component diminished the total voltage change for formation of $P^+Q_A^-$ (a 23 Å distance) by about 10%.

The Activation Energy of the Events Associated with Electron Transfer from Q_A^- to Q_B. Both phases of the electron transfer reaction have relatively small activation energies of 3 to 4 kcal/Mol while E_a is significantly larger for τ_3 (Table 1). There are few earlier published values for the activation energy of

the electron transfer from Q_A^- to Q_B. Mancino et al. (42) measured a value of 14.3 kcal/Mol (τ_{AB}=200 μs at 750 nm), significantly larger than the E_a for τ_2. Their measurements were modeled by a single exponential, mixing τ_2 and τ_3. A single component fit of the data reported here from 0-2 ms yields a value of 8.1 kcal/Mol. Recent measurements at 757 nm in UQ_A RCs are in better agreement with the results reported here, with an E_a=4.5 kcal/Mol (τ=25-40 μs at 20°C) and E_a=11 kcal/Mol (τ=210-240 μs at 20°C) (26), identified with τ_2 and τ_3 respectively.

Kinetic Models That Yield 2 Rates for Electron Transfer from Q_A^- to Q_B

The electron transfer in MQ_A RCs has two distinct, temporally well separated, kinetic components: 3.5 ± 0.9 μs (60%) and 80 ± 15 μs (40%) Two different kinetic schemes can account for the observed rates each of which requires two populations of RCs. In a series or gated mechanism (Scheme 1), the 80 μs phase represents transformation from an inactive (RC_2) to an active (RC_1) state which then undergoes electron transfer in 3 μs. Initially 60% of the RCs are in the active state. In a parallel mechanism (scheme II), both populations undergo electron transfer at 3 μs (RC_1) and 80 μs (RC_2) respectively. The equilibration of the two forms of RCs would occur on a time scale much longer than 80 μs. While the data appears to favors a gated mechanism, we cannot yet rule out the parallel scheme.

Data supporting the gated mechanism. Here electron transfer occurs in 3 μs, while changes in the inactive fraction of protein required for electron transfer determine the τ_2 lifetime. As described above while spectral changes

in the near UV show electron transfer occurs at both τ_1 and τ_2 there are no changes at τ_1 at 770 nm, a wavelength which only monitors protein relaxation but does not respond directly to electron transfer. However, changes at 770 do occur at τ_2. Thus,

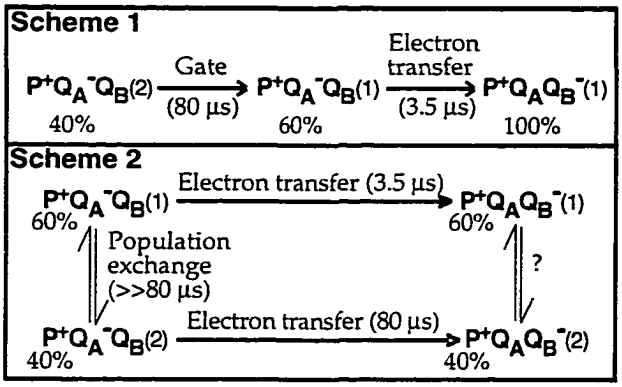

changes such as proton distribution or protein conformation occur in the second phase of electron transfer. In the gated model these changes are required and determine the rate for electron transfer in RC_2 RCs.

Data opposing the parallel mechanism. Charge recombination from the $P^+Q_AQ_B^-$ state (k_{BP}) can measure K_{AB}, the equilibrium constant between $Q_A^-Q_B$ and $Q_AQ_B^-$ (Eqn. 1). k_{BP} in the MQ_AUQ_B RCs is close to a single exponential, so there is little difference between K_{AB} in the populations of RCs that react at τ_1 and t_2. The most straightforward explanation is that there is only one $P^+Q_AQ_B^-$ state, supporting the gated mechanism. The parallel mechanism requires either similar K_{AB}'s in RC_1 and RC_2 or a conformation change after formation of Q_B^- but before charge recombination (<1 s) yielding one $P^+Q_AQ_B^-$ state. The 60:40 population of RC_2 and RC_1 would need to be restored during the 2 minutes between flashes.

Data opposing the gated mechanism. Much of the data supports a mechanism where the electron transfer occurs from one population of RCs. However, two pieces of data are difficult to accommodate in this mechanism. The E_a for the 80 μs component is only 3.4 kcal/Mol, the same as for the 3 μs phase. Thus, whatever changes occur at τ_2 to transform RC_2 to RC_1 must be accomplished with only a small activation energy although there may still be a substantial entropy of activation. Also, the relative amplitude of the 2 phases does not change with temperature (Fig. 8). This requires a negligible enthalpy difference between RC_1 and RC_2 to maintain the temperature independent equilibrium constant.

Variation in the kinetic parameters that distinguish RC_1 and RC_2. If electron transfer is rate limiting for τ_1 then electron transfer theory can provide a rough estimate of the differences between RC_1 and RC_2 that could yield a 20 fold slower τ_2. In the simplest formation of the theory by Marcus $k_{AB} = Ce^{-\beta R} \exp(-(\Delta G-\lambda)^2/4\lambda k_B T))$, where $C \approx 10^{13}$/s, ΔG is the free energy difference between reactants and products; λ the reorganization energy; r the distance between the electron donor (Q_A) and acceptor (Q_B); β the fall off of the rate with distance; T the temperature and k_B Boltzman's constant (51-54). For this reaction the $-\Delta G$ of 60-90 meV is much less than λ which is estimated to be 700-1300 eV (53, 55). The rate will increase as $-\Delta G$ approaches λ. A reduction in λ of ≈300 meV or increase in exothermicity of ≈200 meV could increase the rate by 20 fold. Alternatively if β is 1.4 $Å^{-1}$ (53), a 2.7 Å change in distance from Q_A to Q_B could account for the difference in rates extrapolated to $-\Delta G=\lambda$ of 2.2×10^8 s^{-1} (for τ_1) and 5.0×10^6 s^{-1} (for τ_2) (see results). The rates

extrapolated to infinite temperature provide the estimates of the rates at $-\Delta G=\lambda$ (Fig. 8).

What Might Yield RCs with Different Electron Transfer Rates

Electron transfer from Q_A^- to Q_B occurs at more than a single rate in all RCs. The rates vary by at least 20 fold. If electron transfer is mixed into the processes occurring at τ_3 the rate would vary by more than 100 fold. We do not yet know what causes RCs to switch from one rate to another. However, a number of perturbations have been found to change the distribution of rates. In UQ_AUQ_B RCs the electron transfer rate changes from faster and clearly biexponential in chromatophores, to slower, more nearly single exponential in purified UQ_A RCs (26, 45, 46). At room temperature electron transfer and relaxation events are mixed in this single phase. Since relaxation processes have a larger activation energy on cooling electron transfer becomes more clearly separated from other events (Fig. 6) (26, 45). Dehydration of isolated UQ_A RCs by increasing the solution osmotic strength shifts the electron transfer towards the more native faster τ_1 and τ_2 lifetimes (26). These are global changes to the protein surroundings and so do not point to a specific molecular switch between the RC forms where electron transfer is at τ_1 and τ_2 or those where it is at τ_2 and τ_3. For reasons that are not yet understood, reconstitution of MQ into the Q_A site in isolated RCs yields electron transfer kinetics that appear to be closer to the *in vivo* reaction than found in isolated UQ_A RCs. The similarity of the kinetics could be fortuitous, or it could be a reflection of the preference of the site for MQ. MQ binds more tightly than UQ to the Q_A site in isolated RCs (37). and is preferred at this site in bacteria

such as *Rps. viridis*, which synthesize both quinones (33). Alternately, reconstitution with the larger MQ_A may remove bound water producing effects similar to that seen in isolated RCs at high osmolarily where τ_1 is seen (26). The ability to switch the proportion of fast and slow reacting RCs by quinone replacement will provide an opportunity to characterize the changes in the RCs that yield the different rates in future experiments.

Differences between RCs with MQ_A and UQ_A The distinctly different patterns of transient near UV and near IR spectra for UQ_AUQ_B RCs and MQ_AUQ_B RCs suggest that these RCs differ in the rate-determining steps for electron transfer from Q_A^- to Q_B^-. In isolated UQ_AUQ_B RCs at room temperature both electron and non-electron transfer events are distributed over the τ_2 and τ_3 lifetimes, while in MQ_AUQ_B RCs electron transfer occurs at τ_1 and τ_2, while non-electron transfer events occur at τ_2 and τ_3. This difference is unexpected. Many previous experiments have shown that MQ_A RCs behave similarly to UQ_A RCs. Structural comparisons show: (1) similar interactions between Q_A and the protein in the crystal structures of *Rps. viridis* RCs where MQ is the native Q_A and in *Rb. sphaeroides* RCs with UQ_A (35); (2) the same hydrogen bonding pattern and cofactor orientation in *Rb. spheroides* RCs with native UQ_A or reconstituted MQ_A (personal communication, Guenter Fritzsch); and (3) similar protein changes for both UQ_A and MQ_A in Q_A^- minus Q_A FTIR difference spectra in *Rb. sphaeroides* RCs (56). In addition, functional studies show: (1) the free energy for electron transfer from MQ_A^- to UQ_B is only 30 meV more favorable then with UQ_A; (2) the quantum yield for electron transfer from BPh^- to MQ_A is 100% even at cryogenic temperature where the quinone must be rigidly held in the binding site (57);

and (3) electron transfer from MQ_A^- to P^+ is as well characterized by a single exponential as in native RCs even at cryogenic temperatures (58). FTIR measurements of the hydrogen bonding of MQ_A and UQ_A show the clearest differences between the quinones. One of the UQ carbonyls shifts by >30 cm^{-1} and the other by < 5cm^{-1} when it is bound to the Q_A site. Thus, UQ_A^- appears to make only one, strong hydrogen bond, probably with the proximal carbonyl (O_4) (59, 60). In contrast, MQ_A^- carbonyls each shift by ≈10-20 cm^{-1} so it appears to make two hydrogen bonds (56). This raises the possibility that the second hydrogen bond could fix Q_A firmly in the correct position for rapid electron transfer.

Possible Sources of Heterogeneity in the Q_A Pocket. Measurements of the electron transfer between P and Q_A suggest there is only small functional heterogeneity for Q_A (61-64). Extensive analysis of the charge recombination to the ground state in $P^+UQ_A^-$ RCs at room temperature shows the kinetics for this reaction can be fit with two rates that vary by at most a factor of 3 (62, 65, 66). The free energy of the Q_A^- state can be estimated from the rate of the charge recombination in $P^+Q_A^-$ RCs reaction when Q_A is replaced with quinones ≈150 meV lower in potential than UQ_A (34, 65-69). Heterogeneity in the Q_A^- free energy of ≈ 20 meV in *Rb. sphaeroides* (65) and ≈ 30 meV in *Rps, viridis* RCs (66, 70) have been found. It seems unlikely that this small difference in reaction free energy is sufficient to account for the 20 fold difference between τ_1 and τ_2.

Differences in hydrogen bonding of the quinones could change the electron transfer rates. Only one of the two Q_A carbonyls is needed for function (57, 58, 71, 72). A Q_A^- with stronger hydrogen bonds will be more

rigidly held in the site, which may reduce λ, facilitating faster electron transfer. His M219, the proximal hydrogen bond donor is a ligand of the non-heme iron connecting the Q_A and Q_B sites (35, 54, 73). Differences in this bridge for electron transfer, in RC_1 and RC_2 could modify the rate by changing $e^{-\beta R}$ (53, 54).

Possible Sources of Heterogeneity in the Q_B Pocket. Two electron transfer rates, each with ≈50% of the total amplitude could result from two Q_B binding sites with similar quinone affinities. In the parallel mechanism both sites would be active, in the gated mechanism movement from inactive to active site occurs at τ_2. Several distinct binding sites have been shown. FTIR measurements in *Rb. sphaeroides* RCs suggest 25% of Q_Bs have weak interactions between the protein and quinone carbonyls, while 75% have strong interactions (74). X-ray crystal structures of *Rps. viridis* RCs show two sites for the competitive inhibitor o-phenanthroline, and 7 sites for ubiquinone-1 (75) (for review see (35)). For *Rb. sphaeroides* RCs Allen et al. (76) and El-Kabbani et al. (77) located Q_B at a position close to where it is found in *Rps. viridis* RCs (35) in an inner binding site. In contrast Ermler et al. (78) and Stowell et al. (79, 80) have found Q_B ≈3.5 Å further away from Q_A in the hydrophobic entrance of the Q_B binding pocket. The quinone is in the inner site in light activated RCs and the outer site in dark adapted protein.

In the gated mechanism the quinone must move between the binding sites that distinguish RC_1 from RC_2 in 80 μs with an E_a of only 3.5 kcal/Mol. There are negligible differences in the protein in structures with and without Q_B (35) or with the quinone in different locations (80). This is consistent with a low barrier for quinone relocation. However, the position of the tail in the

'light' and 'dark' adapted structures shows the quinone flipped by 180° along an axis between the quinone C_2 and C_3 (35, 80). In the inner site O_4 is hydrogen bonded to His L190, while O_1 is closer to the His in the outer site. For this rearrangement to convert RC_2 into RC_1 it needs to occur in 80 μs with a 3-4 kcal enthalpy of activation. The large difference between the quinone orientations in the light and dark structures may make this difficult. In the parallel mechanism both binding sites would be active. However, K_{AB} must be similar at each active sites to maintain a single rate for charge recombination from $P^+Q_B^-$ (k_{BP}). This seems unlikely since there are two possible hydrogen bonds to Q_B in the inner site, and one in the outer site (78, 79, 80). The electron transfer could occur to both locations, with the semiquinone moving to occupy one site. This also requires release of Q_B^- from the pocket so that it can flip over.

Possible Sources of Heterogeneity in the Protein. The complexity of the electron transfer kinetics from Q_A^- to Q_B may reflect heterogeneity of the electrostatic environment of Q_B. This region of the protein is characterized by an interconnected group of acidic residues including Glu L212, AspL213, and GluH173 (15, 16, 22). Calculations of the proton occupancy of these residues show several protonation states with similar energies indicating RCs may exist in a variety of sub-states. Glu L212 is the nearest acid in the cluster to Q_B and its ionization is predicted to destabilize Q_B^- disallowing electron transfer (15, 22). Calculations predicted a role for this acid in the formation of Q_B^- (22), subsequently confirmed by FTIR and time resolved IR measurements showing the acid undergoing sub-stoichiometric protonation (0.3-0.6 H^+/RC) at $\approx\tau_2$ (21, 23). These measurements could support a role for

GluL212 in a gated mechanism where protonation of this site controls the rate of the electron transfer at τ_2. The remaining fraction, if it is protonated in the ground state, could react at τ_1 (15, 16). In addition, τ_2 depends on pH, slowing above pH 9. Thus, proton uptake is important in this phase of electron transfer (7, 27, 30, 81). In contrast, no significant pH dependence at τ_1 is observed from pH 6 to 11 (data not shown). Interestingly, the fast, μs electron transfer from MQ_A to UQ_B in native *Rps. viridis* RCs also shows only a weak pH dependence (48, 82).

REFERENCES

1. Feher, G., Allen, J. P., Okamura, M. Y., and Rees, D. C. (1989) *Nature 339*, 111-116.
2. Gunner, M. R. (1991) *Current Topics in Bioenergetics 16*, 319-367.
3. Blankenship, R. E., Madigan, M. T., and Bauer, C. E. (1995) *Anoxygenic Photosynthetic Bacteria*, Vol. 2, Kluwer Academic Publishers.
4. Maroti, P., and Wraight, C. A. (1988) *Biochim. Biophys. Acta 934*, 314-328.
5. McPherson, P. H., Okamura, M. Y., and Feher, G. (1988) *Biochim. Biophys. Acta 934*, 348-368.
6. Graige, M. S., Paddock, M. L., Bruce, J. M., Feher, G., and Okamura, M. Y. (1996) *J. Am. Chem. Soc. 118*, 9005-9016.
7. Wraight, C. A. (1979) *Biochim. Biophys. Acta 548*, 309-327.
8. Wraight, C. A. (1977) *Biochim. Biophys. Acta 495*, 525-531.

9. Kleinfeld, D., Okamura, M. Y., and Feher, G. (1985) *Biochim. Biophys. Acta 809*, 291-310.

10. Okamura, M. Y., and Feher, G. (1995) in *Anoxygenic Photosynthetic Bacteria* (Blankenship, R. E., Madigan, M. T., and Bauer, C. E., Eds.) pp 231-257, Kluwer Academic Publishers.

11. Cramer, W. A., and Knaff, D. B. (1991) *Energy Transduction in Biological Membranes: A Textbook of Bioenergetics*, Springer-Verlag, New York.

12. Nicholls, D. G., and Ferguson, J. S. (1992) *Bioenergetics 2*, Academic Press Limited, London.

13. Takahashi, E., and Wraight, C. A. (1994) *Advances in Molecular and Cell Biology 10*, 197-251.

14. Breton, J., and Verméglio, A. (1988) *The Photosynthetic Bacterial Reaction Center: Structure and Dynamics*, Plenum Press, New York.

15. Beroza, P., Fredkin, D. R., Okamura, M. Y., and Feher, G. (1995) *Biophys. J. 68*, 2233-2250.

16. Lancaster, C. R. D., Michel, H., Honig, B., and Gunner, M. R. (1996) *Biophys. J. 70*, 2469-2492.

17. Verméglio, A., and Clayton, R. K. (1977) *Biochim. Biophys. Acta 461*, 159-165.

18. Hales, B. J., and Case, E. E. (1981) *Biochim. Biophys. Acta 637*, 291-302.

19. Lubitz, W., Abresch, E. C., Debus, R. J., Isaacson, R. A., Okamura, M. Y., and Feher, G. (1985) *Biochim. Biophys. Acta 808*, 464-469.

20. Hienerwadel, R., Thibodeau, D., Lenz, F., Nabedryk, E., Breton, J., Kreutz, W., and Mantele, W. (1992) *Biochemistry 31*, 5799-5808.

21. Hienerwadel, R., Grzybek, S., Fogel, C., Kreutz, W., Okamura, M. Y., Paddock, M. L., and Breton, J. (1995) *Biochemistry 34*, 2832-2843.

22. Gunner, M. R., and Honig, B. (1992) in *The Photosynthetic Bacterial Reaction Center: Structure, Spectroscopy and Dynamics II* (Breton, J., and Vermeglio, A., Eds.) pp 403-410, Plenum, New York.

23. Nabedryk, E., Brenton, J., Hienderwadel, R., Fogel, C., Mantele, W., Paddock, M. L., and Okamura, M. Y. (1995) *Biochemistry 34*, 14722-14732.

24. Okamura, M. Y., and Feher, G. (1992) *Annu. Rev. Biochem. 61*, 861-896.

25. Bensasson, R., and Land, E. J. (1973) *Biochim. Biophys. Acta*, 176-181.

26. Tiede, D. M., Vazquez, J., Cordova, J., and Marone, P. A. (1996) *Biochemistry 35*, 10763-10775.

27. Takahashi, E., Maroti, P., and Wraight, C. A. (1992) in *Electron and Proton Transfer in Chemistry and Biology* (Muller, A., Ed.) pp pgs. 219-236, Elsevier.

28. Tiede, D. M., and Hanson, D. K. (1992) in *The Photosynthetic Reaction Center II* (Breton, J., and Vermeglio, A., Eds.) pp 341-350, Plenum Press, New York.

29. Parson, W. W. (1969) *Biochim. Biophys. Acta 189*, 384-396.

30. Kleinfeld, D., Okamura, M. Y., and Feher, G. (1984) *Biochim. Biophys. Acta 766*, 126-140.

31. Patel, K. B., and Willson, R. L. (1973) *J. Chem. Soc. 69*, 814-825.

32. Swallow, A. J. (1982) in *Function of Quinones in Energy Conserving Systems* (Trumpower, B. L., Ed.) pp 59-72, Academic Press, New York.

33. Shopes, R. J., and Wraight, C. A. (1985) *Biochim. Biophys. Acta 806*, 348-356.

34. Woodbury, N. W., Parson, W. W., Gunner, M. R., Prince, R. C., and Dutton, P. L. (1986) *Biochim. Biophys. Acta. 851*, 6-22.

35. Lancaster, C. R. D., Ermler, U., and Michel, H. (1995) in *Anoxygenic Photosynthetic Bacteria* (Blankenship, R. E., Madigan, M. T., and Bauer, C. E., Eds.) pp 503-526, Kluwer, Dordrecht.

36. Breton, J., and Nabedryk, E. (1996) *Biochim. Biophys. Acta 1275*, 84-90.

37. Warncke, K., Gunner, M. R., Braun, B. S., Gu, L., Yu, C., Bruce, J. M., and Dutton, P. L. (1994) *Biochemistry 33*, 7830-7841.

38. Giangiacomo, K. M., and Dutton, P. L. (1989) *Proc. Natl. Acad. Sci. USA 86*, 2658-2662.

39. Clayton, R. K., and Wang, R. T. (1971) *Methods Enzymol 23*, 696-704.

40. Okamura, M. Y., Isaacson, R. A., and Feher, G. (1975) *Proc. Natl. Acad. Sci, USA 72*, 3492-3496.

41. McComb, J. C., Stein, R. R., and Wraight, C. A. (1990) *Biochim. Biophys. Acta 1015*, 156-171.

42. Mancino, L. J., Dean, D. P., and Blankenship, R. E. (1984) *Biochim. Biophys. Acta 764*, 46-54.

43. Slooten, L. (1972) *Biochim. Biophys. Acta 275*, 208-218.

44. Clayton, R. K., and Straley, S. C. (1972) *Biophys. J 12*, 1221-1234.

45. Tiede, D. M., Gallo, D. M., and Hanson, D. K. (1997) *Biophys. J. 72*, A248.

46. Tiede, D. M., Utschig, L., Hanson, D. K., and Gallo, D. M. (1997) *submitted to Photosynthesis Research.*

47. Carithers, R. P., and Parson, W. W. (1975) *Biochim. Biophys. Acta 387*, 194-211.

48. Leibl, W., Sinning, I., Ewald, G., Michel, H., and Breton, J. (1993) *Biochemistry 32*, 1958-1964.

49. Maróti, P., and Wraight, C. A. (1997) *Biophys. J. 73*, 367-381.

50. Brzezinski, P., Okamura, M. Y., and Feher, G. (1992) in *The Photosynthetic Bacterial Research Center II* (Brenton, J., and Vermeglio, A., Eds.) pp 321-330, Plenum Press, New York.

51. Devault, D. (1980) *Q. Rev. Biophys. 13*, 387-564.

52. Marcus, R. A., and Sutin, N. (1985) *Biochim. Biophys. Acta 811*, 265-322.

53. Moser, C. C., Keske, J. M., Warncke, K., Farid, R., and Dutton, P. L. (1992) *Nature 355*, 796-802.

54. Onuchic, J. N., Beratan, D. N., Winkler, J. R., and Gray, H. B. (1992) *Ann. Rev. Biophys. Biomol. Struct. 21*, 349-377.

55. Labahn, A., Paddock, M. L., McPherson, P. H., Okamura, M. Y., and Feher, G. (1994) *J. Phys. Chem. 98*, 3417-3423.

56. Breton, J., Burie, J., Berthomieu, C., Berger, G., and Nabedryk, E. (1994) *Biochemistry 33*, 4953-4965.

57. Gunner, M. R., and Dutton, P. L. (1989) *J. Am. Chem. Soc. 111*, 3400-3412.

58. Gunner, M. R., Robertson, D. E., and Dutton, P. L. (1986) *J. Phys. Chem. 90*, 3783-3795.

59. Brudler, R., de Groot, J. M., van Liemt, W. B. S., Steggerda, W. F., Esmeijer, R., Gast, P., Hoff, A. J., Lugtenburg, J., and Gerwert, K. (1994) *EMBO J. 13*, 5523-5530.

60. Breton, J., Claude, B., Burie, J., Nabedryk, E., and Mioskowski, C. (1994) *Biochemistry 33*, 14378-14386.

61. Morrison, L. E., and Loach, P. A. (1978) *Photochem. Photobiol. 27*, 751-757.

62. Parot, P., Thiery, J., and Vermèglio, A. (1987) *Biochim. Biophys. Acta 893*, 534-543.

63. Gao, J., Shopes, R. J., and Wraight, C. A. (1991) *Biochim. Biophys. Acta. 1056*, 259-272.

64. Baciou, L., and Sebban, P. (1995) *Photochem. and Photobiol. 62*, 271-278.

65. Sebban, P. (1988) *Biochim. Biophys. Acta 936*, 124-132.

66. Sebban, P., and Wraight, C. A. (1989) *Biochim. Biophys. Acta 974*, 54-65.

67. Gunner, M. R., Tiede, D. M., Prince, R. C., and Dutton, P. L. (1982) in *Function of Quinones in Energy Conserving Systems* (Trumpower, B. L., Ed.) pp 265-269, Academic Press, New York.

68. Kleinfeld, D., Okamura, M. Y., and Feher, G. (1985) *Biophys. J. 48*, 849-852.

69. Franzen, S., Goldstein, R. F., and Boxer, S. G. (1990) *J. Phys. Chem. 94*, 5135-5149.

70. Shopes, R. J., and Wraight, C. A. (1987) *Biochim. Biophys. Acta 893*, 409-425.

71. Gunner, M. R., Braun, B. S., Bruce, J. M., and Dutton, P. L. (1985) in *Antennas and Reaction Centers of Photosynthetic Bacteria* (Michel-Beyerle, M. E., Ed.) pp 298-305, Springer-Verlag, Berlin.

72. Warncke, K., and Dutton, P. L. (1993) *Biochemistry 32*, 4769-4779.

73. Moser, C. C., Page, C. C., Chen, X., and Dutton, P. L. (1997) *Journal of Biological Inorganic Chemistry*, in press.

74. Brudler, R., de Groot, H. J. M., van Liemt, W. B. S., Hoff, A. J., Lugtenburg, J. L., and Gerwert, K. (1995) *FEBS letter*, 2-14.

75. Deisenhofer, J., Epp, O., Miki, R., and Michel, H. (1985) *Nature 318*, 618-624.

76. Allen, J. P., Feher, G., Yeates, T. O., Komiya, H., and Rees, D. C. (1988) *Proc. Natl. Acad. Sci. USA 85*, 8487-8491.

77. El-Kabbani, O., Chang, C.-H., Tiede, D., Norris, J., and Schiffer, M. (1990) *Biochemistry 30*, 5361-5369.

78. Ermler, U., Fritzsch, G., Buchanan, S. K., and Michel, H. (1994) *Structure 2*, 925-936.

79. Abresch, E. C., Stowell, M. H. B., McPhillips, T. M., Rees, D. C., Soltis, S. M., and Feher, G. (1997) *Biophysical Journal 72*, A8.

80. Stowell, M. H. B., McPhillips, T. M., Rees, D. C., Soltis, S. M., Abresch, E. C., and Feher, G. (1997) *Science 276*, 812-816.

81. Paddock, M. L., Rongey, S. H., Feher, G., and Okamura, M. Y. (1989) *Proc. Natl. Acad. Sci. USA 86*, 6602-6606.

82. Mathis, P., Sinning, I., and Michel, H. (1992) *Biochim. Biophys. Acta 1098*, 151-158.

Chapter 5

ΔG^0_{AB} and pH Dependence of the Electron Transfer from $P^+Q_A^-Q_B$ to $P^+Q_AQ_B^-$ in *Rhodobacter sphaeroides* Reaction Centers

ABSTRACT

Electron transfer from $P^+Q_A^-Q_B$ to $P^+Q_AQ_B^-$ was measured between 390 and 500 nm in R-26 RCs where Q_A was substituted with several different naphthoquinones, Q_B was ubiquinone (UQ_B) in all cases. These substitutions change the redox midpoint potential of Q_A and therefore change the driving force for electron transfer. The electron transfer rate is heterogeneous. In RCs with 2-methyl-3-phytyl-1,4-naphthoquinone (MQ) substituted at Q_A (MQ_A), three rates are observed: $\tau_1 \approx 3\mu s \pm 0.9\mu s$, $\tau_2 = 80 \pm 20\mu s$, and $\tau_3 = 0.4 \pm 0.2ms$ at pH=8 and 22°C. In the MQ_A RCs, no significant pH dependence of the fast kinetic phase τ_1 is observed from pH 6-11. In contrast, τ_2 slows above pH 9. Measured at 400 nm, 406 and 470 nm, τ_1 is found to be free energy dependent and changes by a factor of 10 as the free energy difference for electron transfer from Q_A^- to Q_B is varied by 100 meV. The free energy dependence of the rate provides a reorganization energy of 850±100 meV. The slower phase τ_2 is free energy independent. When the isoprene tail length is increased from 2 to 10 isoprene units for the naphthoquinones at the Q_A site (NQ_A), the fraction of τ_1 decreases.

INTRODUCTION

The electron transfers between Q_A and Q_B have been the subject of much investigation which has begun to shown how proton and protein motions can control electron transfer reactions. The electron transfer from Q_A^- to the secondary quinone, Q_B, has been measured to occur within 3-200 microseconds yielding $P^+Q_B^-$ (1, 2, 3, 4, 5, 6). It is this reaction that will be the subject of the work reported here.

If there is no exogenous donor to donate an electron to P^+, the electron on the acceptors will go back to P^+ in a charge recombining, back reaction. The back reactions from Q_A^- or Q_B^- to P^+ each have two pathways: k_{BP} or k_{AP} where the electron goes back directly to P^+; and k_{BAP} or k_{BHP} where the electrons go back indirectly to P^+ via a higher energy state(Fig. 1.2). In the thermally activated, uphill reactions, the reaction rates are proportional to the free energy difference between the initial and intermediate states. Therefore these rates can provide a measure of the relative free energy of different states.

The early, fast electron transfer reactions show little temperature or pH dependence indicating that these reactions can occur in a relatively rigid protein. In contrast, the slower electron transfer from Q_A^- to Q_B have significant temperature and pH dependence (7, 8), suggesting that protein and proton motions may be important for this reaction. While recent studies provide evidence for direct protonation of the semiquinone state Q_B^- in

chromatophores at low pH, in isolated RCs at physiological pH's neither the semiquinone Q_A^- or Q_B^- binds a proton(9, 10).

An electron transfer from Q_A^- to Q_B that occurs at ≈100 μs has been studied intensively. The reaction is pH independent from pH 6 to 9 and is faster at lower and slower at higher pH. In the intermediate pH range there is sub-stoichiometric proton binding on formation of $P^+Q_A^-$, but little proton uptake from solution is required on electron transfer from Q_A^- to Q_B (11, 12, 13, 14, 15, 16). Studies of the 100 μs reaction shows that this electron transfer rate constant $k_{AB}^{(1)}$ does not change with ΔG_{AB}^0. This finding provides strong evidence that the electron transfer itself does not control $k_{AB}^{(1)}$; rather some other process provides a conformation gate determines the rate (3). The enthalpy of these electron transfer has been shown recently to be ≈3.5 kcal (4, 5, 6); although earlier measurements had provided larger values. Thus, the conformational gate appears to have a modest enthalpy barrier.

When the ubiquinone-10 (UQ_{10}) in the Q_A site is substituted by 2-methyl-3-phytyl-1,4-naphthoquinone (MQ_A), while UQ_{10} is retained as Q_B, the electron transfer from Q_A^- to Q_B is heterogeneous with time constants of τ_1≈3μs±0.9μs (60% of $\tau_1+\tau_2$), τ_2 =80±20μs, and τ_3 =0.4±0.2ms at pH=8 and 22 °C (6). Since the spectrum of menasemiquinone (MQ^-, λ_{max} at 400 nm) is different from ubisemiquinone (UQ^-, λ_{max} at 450 nm) (17, 18, 19), these measurements can provide a direct monitor of the transfer of the electron from MQ_A^- to UQ_B. Analysis of the time resolved near UV spectra and the electrochromic response of BPh in IR suggests that the changes at τ_1 are mostly due to electron transfer, electron transfer and charge compensation are

mixed in τ_2, while little or no electron transfer occurs at τ_3 in MQ_AUQ_B RCs. Similar rates of electron transfer are found in UQ_AUQ_B chromatophores (5), but no fast electron transfer rate is found in isolated RCs with UQA and UQB. Since the well studied τ_2 is a gated electron transfer reaction, the charactersicts of the electron transfer reaction itself have not been studied. In this work, the driving force ΔG^0_{AB}, pH, and isoprenal tail length dependence of the faster reaction (τ_1) were determined and compared with the process at τ_2. The free energy was changed by substituting quinones with different redox potentials for ubiquinone at Q_A in R-26 RCs and in a Q_A site mutant M265IT. The $-\Delta G^0_{AB}$ is varied by more than 200 meV.

MATERIALS AND METHODS

Protein Isolation. *Rb. sphaeroides* R-26 reaction centers were isolated by standard procedures as described before. Q_A and Q_B were removed and the RC concentration was determined at 802 nm or 865 nm using the extinction coefficients: $\varepsilon_{802}=0.288\mu M^{-1}cm^{-1}$ or $\varepsilon_{865}=0.135\mu M^{-1}cm^{-1}$.

M265 mutant: The mutant RCs with isoleucine at M265 replaced by threonine (M265IT) were prepared in a carotonoid containing *Rb. sphaeroides*, background. The mutation lowers the in situ E_m of Q_A by about 120 meV, increasing the free energy of electron transfer from Q_A to Q_B (ΔG^0_{AB}). The isolated protein was a gift of E. Takahashi and C.A. Wraight.

Estimation of $-\Delta G^0_{AB}$ for $P^+XQ_A^-UQ_B$ to $P^+XQ_AUQ_B^-$.

The $-\Delta G^0_{AB}$ can be estimated by two methods: (1). determine $-\Delta G^0_{AB}$ by the back reaction from Q_B^- if the pathway is via Q_A^-. (2). determine the <u>in situ</u> redox potentials $Em(Q_A)$ of different quinones in the Q_A site, then the $-\Delta G^0_{AB}$ in the $P^+XQ_A^-UQ_B$ to $P^+XQ_AUQ_B^-$ reaction can be calculated as $\Delta G^0_{AB}=E_m(Q_A^-/Q_A)- E_m(Q_B^-/Q_B)$ assuming $E_m(Q_B^-/Q_B)$ is a constant of -50±10 mV.

(1). Determine $-\Delta G^0_{AB}$ when the back reaction from Q_B^- is via Q_A^- . The driving force (ΔG) for electron transfer from Q_A^- to Q_B can be calculated from the charge recombination rates k_{AP} and k_{BAP} (22, 23). The pathway for charge recombination in $P^+Q_B^-$ is via Q_A^- (at k_{AP}) with $P^+Q_A^-Q_B$ and $P^+Q_AQ_B^-$ remaining at equilibrium (K_{AB}). The observed rate will be:

$$k_{BAP}=k_{AP}/(K_{AB}+1) \qquad (5.2)$$

Then $\Delta G=\exp(-K_{AB}/kT)$. In $UQ_{10}UQ_{10}$ RCs the reaction $-\Delta G$ is 60 meV; in MQ_AUQ_{10} RCs it is 93 meV, in NK2, NQ4 and NQ10 RCs, the $-\Delta G$ is 86, 94 and 94 meV respectively.

(2) Determine the <u>in situ</u> redox potentials $Em(Q_A)$ of different quinones in the Q_A site which takes advantage of reactions where $P^+Q_A^-$ equilibrates with a higher energy state P^+BPhe^- of the protein. $Em(Q_A)$ can be obtained by two different measurements.

A. Delayed Fluorescence. $P^+Q_A^-$ and P* are at equilibrium during the lifetime of $P^+Q_A^-$. Single photon counting can monitor the concentration of P* from the amplitude of the fluorescence that has the same lifetime as $P^+Q_A^-$

. This provided the energy of DMNQ and TMNQ relative to P^* in the Q_A site which were compared with values in UQ_{10} as Q_A RCs (20).

B. Charge recombination, k_{AHP}. There are two routes for charge recombination from the $P^+Q_A^-$state. A direct tunneling reaction at k_{AP} and an uphill reaction where $P^+Q_A^-$ preequilibrates with P^+H^- which decays in a quinone independent reaction. The observed reaction will occur at the sum of the 2 rates. The relative proportion of the direct and uphill reactions depend on the energy levels of $P^+Q_A^-$ states. The tunneling rate has only a weak dependence on the free energy of the reaction. However, the rate of the indirect path increases by a factor 10 for each increase in the energy of the $P^+Q_A^-$ by -58 meV. The uphill reaction is slower than the direct route for the native quinone, but becomes increasingly important as the Q_A Em is lowered. The XQ_A midpoint relative to that of the native RC UQ_{10} was calculated by (21)

$$Em(XQ)-Em(UQ_{10})=-58\ \log(k_{AP}-7.0)-53.3\ meV,\ (pH=7.3) \quad (5.1)$$

A value of Em (TEMNQ)-Em(UQ10)=-120 meV was calculated from the eq.5.1 using observed value, $k_{AHP}=21.1\ s^{-1}$.

When $-\Delta G_{AB}$ is greater than 100 meV the indirect route for charge recombination via Q_A becomes slower than the direct tunneling reaction at k_{BP}. The direct route is relatively insensitive to ΔG_{AB}, so no longer provides a monitor of the free energy of the $P^+Q_B^-$ state. This is found when the Q_A site in native RCs in reconstituted with low potential quinones and with the

M265IT mutant with UQ in the Q_A site. The free energy of the $P^+Q_B^-$ state was assumed to be unchanged from the wild type in these mutants. The free energy of the $P^+Q_A^-$ state was obtained from the rate of charge recombination at k_{AHP} as described above.

Quinone Reconstitution. The long tailed quinones are effectively insoluble in water, but become soluble when detergent is added. However, detergent weakens the affinity of quinone for the binding sites. The method of Wraight (24) using quinone dissolved in Triton X-100 was the basis of the most effective and reproducible method of reconstitution for long tailed quinones. All other quinones were solubilized in ethanol before use. Quinones were obtained from the following sources: MQ (2-methyl-3-phytyl-1,4-naphthoquinone, Vitamin K1) was from Fluka, UQ0, UQ1, UQ2, UQ4 and UQ_{10} were from Sigma , MQ2, MQ4, MQ10, and TEMNQ were gifts from C.C. Moser and P.L. Dutton. TMNQ and some TEMNQ were gifts from M.S. Graige and M.Y. Okamura.

The assay solution contained 4-5 μM RCs with 0.02% Triton X-100, 2.5 mM KCl, 10 mM Tris buffer at pH7.8-8.0. The lifetime for recovery of the ground state from the $P^+Q_A^-$ state (τ_{AP}), is monitored at 430 nm. If UQ is Q_A, τ_{AP} is 100 ms.

Following complete reconstitution of the Q_A site with the replacement quinone, the sample solution is split to provide 2 matched samples for the purpose of comparison and obtaining the difference signal of Q_A and Q_AQ_B containing RCs. Q_B was reconstituted in one of the samples with UQ (UQ_B).

UQ_B was either UQ_{10} reconstituted with ≈12-15 UQ_{10}/RC if a MQ or a tightly bound NQ was at Q_A (tightly than UQ_{10}); or UQ_1 using 2-6 UQ_1/RC if other losely bound NQs were at Q_A. The final UQ_B occupancy was about 95% for UQ_{10}, and more than 80% for UQ_1.

The different quinones XQ and UQ compete for the Q_A site, In addition, UQ binds more tightly to the Q_A site than to the Q_B site and binds more tightly then XQ to the Q_A site. Thus, a fraction of the Q_A site was occupied by a UQ. The goal is to prepare samples with the maximum fraction of RCs with XQ_A and UQ_B. Too much UQ_B will displace XQ_A, too little will leave a large fraction of RCs without Q_B. The optimal concentration of UQ to be added was calculated given a concentration of XQ near the solubility limit of the exogenous quinone using the known dissociate constant for the quinones for the Q_A and QB sites (25) (appendix 1). As described in the results section, the kinetics of charge recombination was used to determine the relative occupancy of each quinone in each binding site.

Optical Measurements. Transient absorption kinetics were measured and the data were analyzed as described previously (chapter 4). For higher time resolution, a 10 μs (full width at half-maximum) Xenon flash provides a more intense short time measuring light. The absorption change is then calculated by $\Delta A(t) = \log(I_0(t)/I_x(t))$ where I_0 and I_x represent transmitted light through the RC sample without or with an activating laser flash.

RESULTS

Determination of Quinone Occupancy of Q_A and Q_B Site. Because of the competition of UQ_A with XQ_A, it is not possible to get complete reconstitution of UQ_B without having some UQ_A as well (see appendix 1). When XQ and UQ are added, a mixture of RCs results which contains: XQ_AUQ_B, UQ_AUQ_B, and when the Q_B site is empty, XQ_A and UQ_A. RCs with XQ_B are considered to be unimportant for several reasons. The occupancy of the Q_B site by XQ is considered to be negligible given the concentration of XQ. In addition, studies with any other naphthoquinones added have shown that there is never electron transfer from NQ_A to NQ_B. Lastly, the reaction from UQ_A to XQ_B would be uphill and so will not contribute to the results.

The kinetics of P^+ reduction is used to determine the distribution of quinones in the Q_A and Q_B site. RCs with each quinone configuration have a different, well defined rate constant of charge recombination at 430 nm, a maximum for the P^+-->P signal in the near UV region (see Fig 5.1). The kinetics can be fit by a single exponential only when a single type of quinone is added. Adding 2 quinones produces 4 reactions: $P^+UQ_A^-$ --> PUQ_A, $P^+XQ_A^-$-->PXQ_A, $P^+UQ_AUQ_B^-$ -->PUQ_AUQ_B and $P^+XQ_AUQ_B^-$ --> PXQ_AUQ_B. The first 3 rates can be measured in samples with only UQ or XQ added. In analyses of mixtures of quinones, these pre-established rate constants are fixed with only the rate constant of the last process unassigned. The kinetics of UQ_AUQ_B, MQ_AUQ_B, $TMNQ_AUQ_B$ in R-26 RCs and MQ_AUQ_B in M265IT mutant RCs are shown in Figure 5.1. Rates for the different quinones for k_{AP} range from 6

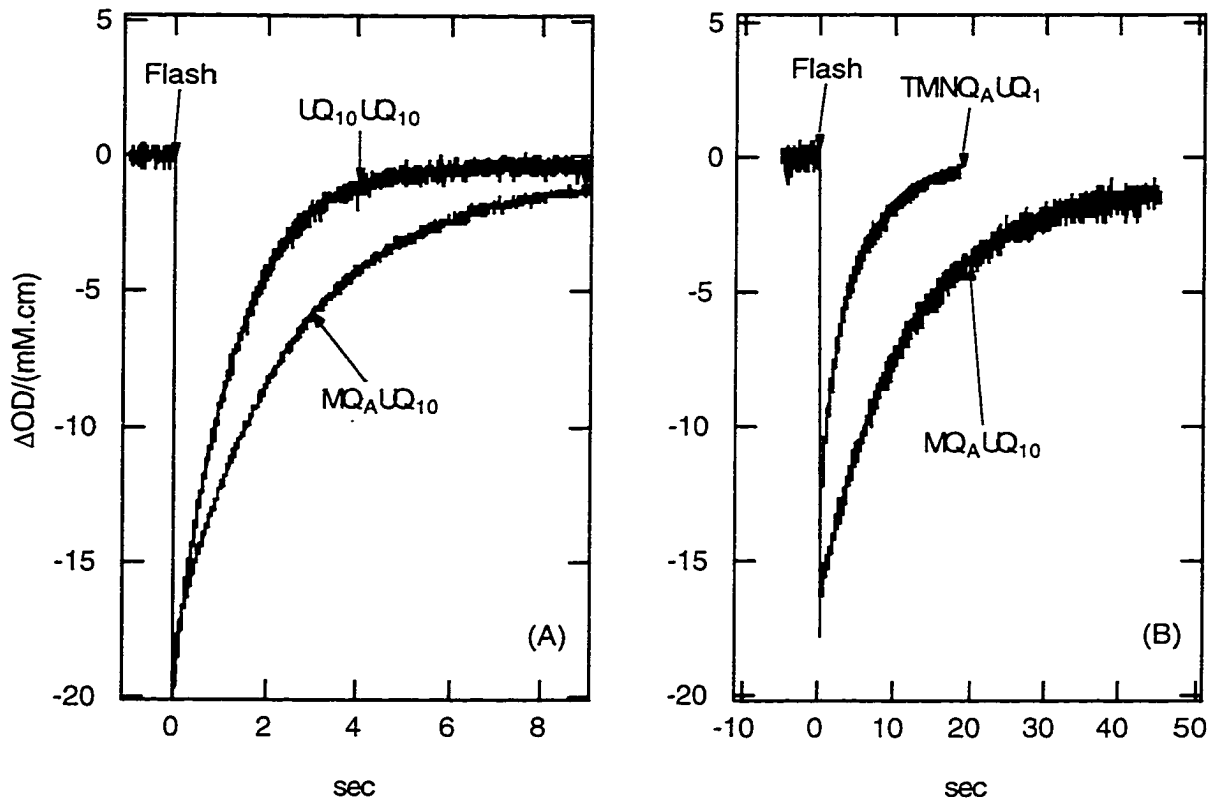

FIGURE 5.1. Charge recombination kinetics $k_{P^+\to P}$ monitored by light minus dark absorbance change of the donor (P) recovery at 430 nm. (A). Indirect charge recombination $P^+Q_AQ_B^- \leftrightarrow P^+Q_A^-Q_B \rightarrow PQ_AQ_B$ at 0.85 s^{-1} in RCs with UQ_{10} in both binding sites (top curve), at 0.36 s^{-1} in RCs with MQ in Q_A and UQ_{10} in Q_B binding sites (80% MQ_AUQ_B) (bottom curve). (B). In the sample with TMNQ and UQ_1 in R-26 RCs, the charge recombination is multiphases and can be fitted with rates of 6.9 s^{-1} for UQ_1 at Q_A with no Q_B (10%), 16 s^{-1} for TMNQ at Q_A with no Q_B (15%), 1.7 s^1 for UQ_1 at both binding sites (14%) and 0.19 s^{-1} for $TMNQ_A$ UQ_B RCs (61%) (top curve). The rate constants for the analysis of TMNQ and UQ_1 at Q_A with no Q_B and $(UQ_1)_A(UQ_1)_B$ were determined in seperate samples and then fixed for curve fitting here. In the sample with MQ and UQ_{10} in M265IT RCs (the binding of MQ at Q_A is much tighter than UQ_{10} and MQ does not bind to Q_B site) , the charge recombination rate is 0.1 s^{-1} in 95% RCs (bottom curve). Conditions in all samples: ≈4 μM RCs in 0.02% Triton, 10mM Tris, 2.5 mM KCl at 22 °C, pH 8.0.

to 400 s^{-1}, for k_{BP} from 2 to 0.1 s^{-1} (Table 5.1). From the ratio of the amplitude of each component, the fraction of RCs with XQ_AUQ_B was estimated for R-26 RCs to range from 45% to 80% (Table 5.1).

For the mutant M265IT RCs, it is impossible to determine the fraction of XQ_AUQ_B and UQ_AUQ_B RCs from the kinetics of charge recombination. When both Q_A and Q_B site is occupied by UQ_{10}, the estimated free energy for $-\Delta G^0_{AB}$ is greater than 160 meV so that charge recombination occurs at by direct electron transfer to P^+ at k_{BP} rather than indirectly via Q_A^-. Substitution by XQ_A now does not change the charge recombination rate.

2. **Determination of $k^{(1)}_{AB}$ in XQ_AUQ_B RCs.** Time resolved absorption difference spectra of $P^+XQ_A^-UQ_B$ --$P^+XQ_AUQ_B^-$ in the R-26 and M265 mutant RCs were measured at 400, 406 and 470 nm after a laser flash. Thus, the initial state immediately after the flash is $P^+XQ_A^-UQ_B$. This state either evolves into $P^+XQ_AUQ_B^-$ (at k_{AB}) or returns to the ground state (at k_{AP}) The rate k_{AP} is determined in matched samples without UQ added. The isobestic point for UQ_A^- minus $UQ_AUQ_B^-$ are at 406 and 470 nm. Thus, at these wavelengths only the desired reaction in the XQ_AUQ_B RCs will be seen. The semiquinone difference spectra of XQ_A^- - UQ^- has its maximum at 400nm. However there is also a significant contribution from the UQ_A^- to UQ_B reaction at this wavelength.

The absorption change in the RCs containing TMNQ as Q_A with UQ_1 as Q_B (Fig.5.2a &b), shows a fast absorption change with τ_1=0.39 μs (k_1=2.6x10^6 s^{-1}).

Q_A	k_{AP} (s^{-1})	Q_B	k_{AP} (s^{-1})	RC type	ΔG_{AB} meV	Rate (S^{-1}) (A1) constant
DMNQ	8.2±0.1	UQ1	0.88	R-26	60	0.103e+06 (0.3)
UQ_{10}	9.3±0.2	UQ_{10}	0.85	R-26	60	
MQ	13.6±0.6	UQ1	0.81	R-26	72	0.098e+06(0.27)
MQ	13.6±0.6	UQ2	0.77	R-26	73	0.173e+06(0.46)
NQ2	15.5±0.8	UQ10	0.50	R-26	86	0.114e+06(0.45)
MQ	13.6±0.6	UQ4	0.47	R-26	87	0.094e+06
MQ	13.6±0.6	UQ10	0.38	R-26	93	0.286e+06(0.6)
NQ4	15±1.0	UQ10	0.45	R-26	94	0.159e+06 (0.4)
TMNQ	15.5±0.9	UQ1	0.16	R-26	130	2.3e+06 (0.75)
TEMNQ	25±0.2	UQ1	0.19	R-26	160	1.7e+06 (1)
DMNQ	29±1	UQ1	0.37	M265IT	180	4.9e+06
MQ	38±3	UQ10	0.1	M265IT	213	3.3e+06
TMNQ	400±10	UQ1	0.48	M265IT	250	1.3e+06

Table 5.1. Summary of dependence of $k_{AB}^{(1)}$ on - ΔG_{AB}^{0} with Napthoquinones as Q_A and Ubiquinones as Q_B RCs.

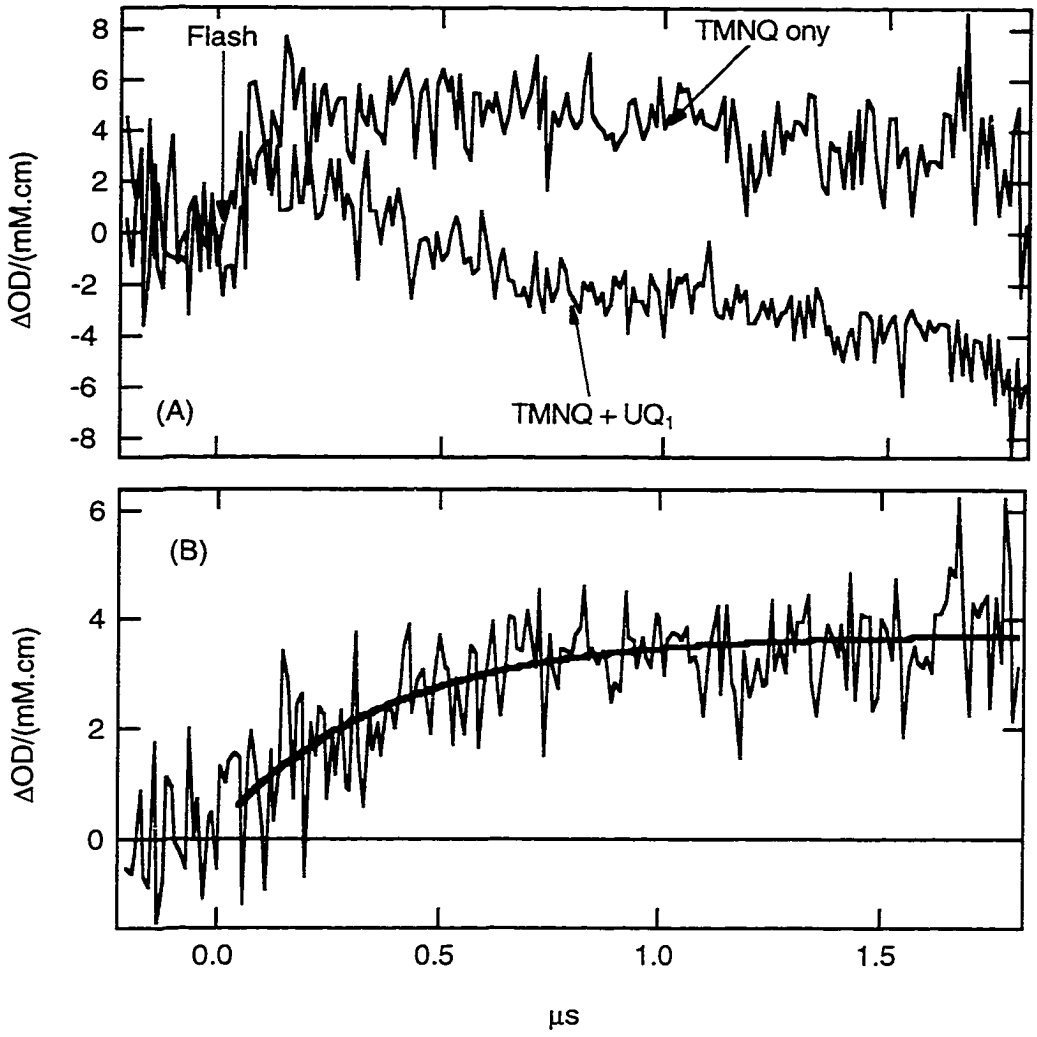

FIGURE 5.2. Optical absorbance changes associated with electron transfer from XQ_A to UQ_B with TMNQ at Q_A and UQ_1 at Q_B in R-26 RC at 400nm. The kinetic traces were measured with a 2 μs (at 400 nm) flash lamp as measuring light. (A) Change in optical absorption after formation of $P^+(TMNQ)_A^-$, This sample contains TMNQ only (top curve); change in $TMNQ_AUQ_{1B}$ RC (bottom curve). (B) Double difference of $P^+(TMNQ)_A^-$ minus $P^+(TMNQ)_A^-UQ_{1B}$ --> $P^+(TMNQ)_AUQ_{1B}^-$; the data is fit to a single exponential (solid line) with τ_1=0.39 μs (k_1=2.6x10^{-6} s^{-1}). This set of data was measured by using a 3 μs flash lamp as measuring light.

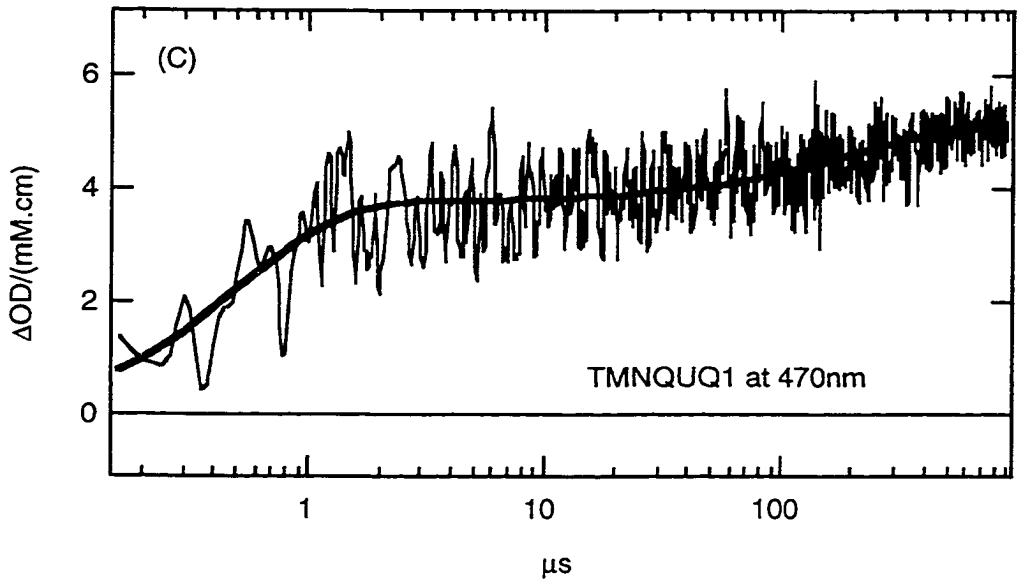

Figure 5.2 (C). At 470 nm which is the isobestic point of UQ_A^- and UQ_B^-, the double difference of $P^+(TMNQ)_A^-$ minus $P^+(TMNQ)_A^-UQ_{1B}$ --> $P^+(TMNQ)_AUQ_{1B}^-$ can be fitted with two exponential with τ_1 =0.52 μs or $k_1=(1.94\pm0.22)\times10^{-6}$ s^{-1} (75%), τ_2 =199 μs (25%). A CW lamp was used as the measuring light in this case. 60 measurements were averaged. Buffer conditions are the same as in Fig. 1.

This transient depends on the presence of UQ_1 in the Q_B site. With TMNQ alone at Q_A site and no Q_B, there is no change in the optical absorption for 1 ms at 400 and 470 nm (data not shown). At 470 nm, the isobestic point for UQ_A^- and UQ_B^-, two kinetic components were observed following the formation of $P^+(TMNQ)_A^-(UQ_1)_B$ (Fig.5.2c): a fast component, $k_1=(1.94\pm0.23)\times10^6$ s^{-1}(τ_1=0.52μs), A_1=75%; $k_2=(5.03\pm0.44)\times10^3$ s^{-1} τ_2=199μs, A_2=25%. Thus, there is a fast optical transient (τ_1=0.45μs) following a laser flash that can be assigned to the XQ_A^- to UQ_B electron

transfer. The rate constant k_{AB}'s and the fraction of each the reaction at each rate are listed in table 5.1 for RCs with different XQ_As.

Effects of the free energy ΔG^0_{AB} on the electron transfer kinetics. The rate of the fastest phase (k_1) is compared for RCs with $-\Delta G_{AB}$ from 60 to 250 meV. The variation in ΔG_{AB} is obtained by use of different NQs as Q_A. This rate is dependent on $-\Delta G^0_{AB}$, increasing by a factor of 10 for each 100 meV (Fig.5.3). As found previously (3) the rate constant k_2 was independent of the electron transfer driving force ΔG^0_{AB}. It has an average value of $k_2=(9.1\pm2.6)\times10^3\ s^{-1}$ ($\approx$110μs). The reactions were determined at the UQ_A^- to UQ_B isobestic point (406 or 470 nm) where the slow component k_3 is not seen (6).

Effects of the free energy ΔG^0_{AB} on the amplitude of the fast phase. The fraction of the reaction occurring in the fast phase is found to increase with the reaction's driving force ΔG^0_{AB} (Fig.5.4) in R-26 RCs. No fast component (τ_1) was observed when UQ_{10} was both Q_A and Q_B. This may be consistent with the relatively small driving force for the reaction. However, no fast component is found from UQ_A to UQ_B in the M265IT mutant which should have appropriate driving force.

The influence of the number of menaquinone isoprene units at the Q_A site. There is little or no variation in the midpoint potential of menaquinones with different tail lengths. Thus, with menaquinone 2, 4 and 10 at Q_A k_{AP} are the same. In addition, when these RCs are reconstituted with UQ_{10} at Q_B, the

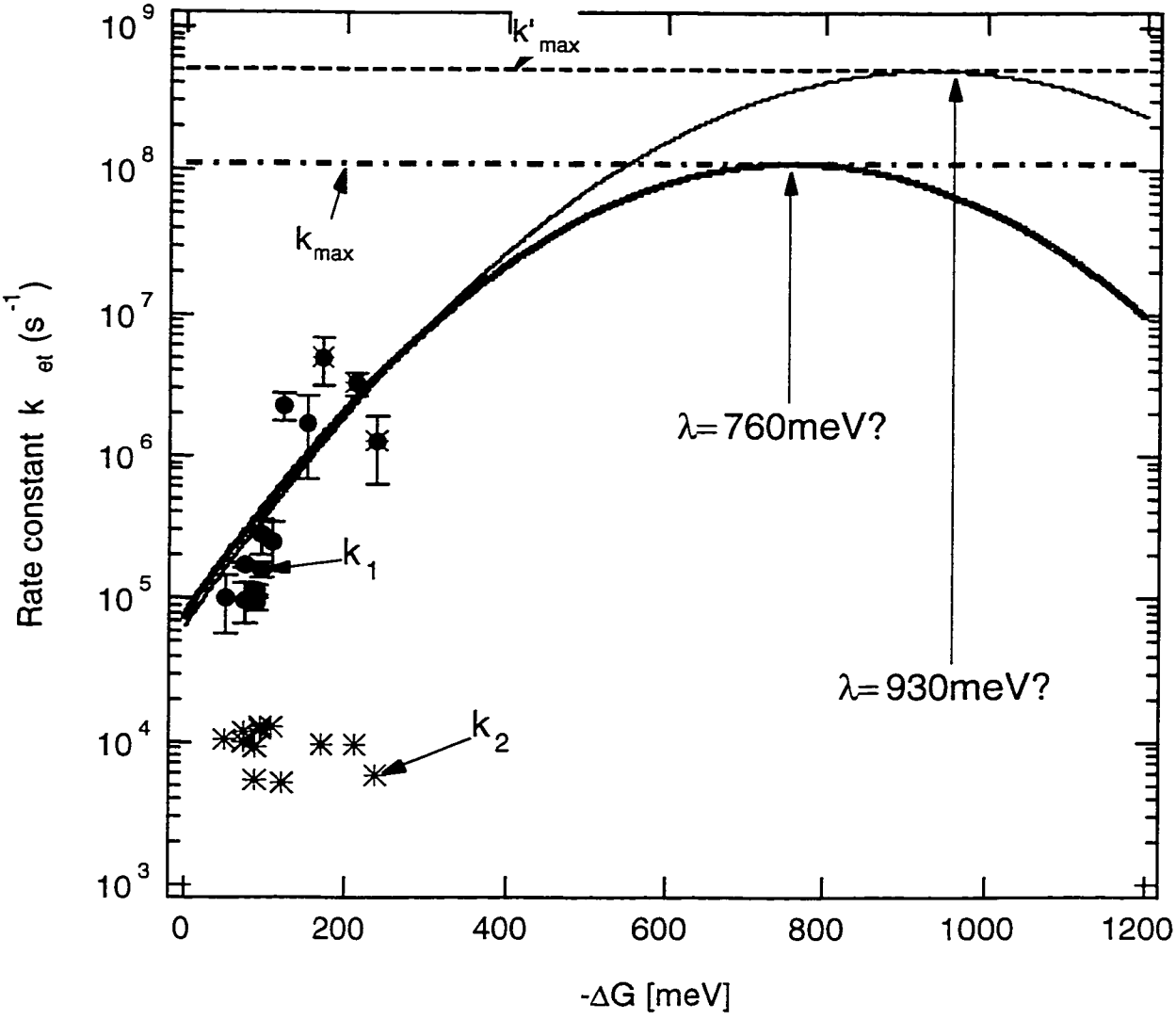

FIGURE 5.3. ΔG^0_{AB} dependence of the rate constant of the fast phase (τ_1) and slow phase (τ_2) at 22±1°C . See the text for the assumptions in evaluating the free energy changes. When several measurements were available, the average value of the rate constants has been plotted. The experimently observed rate k_1 as a function of ΔG^0_{AB} was fitted by equation 5.3 with λ=759±31 meV and $T_{AB} = 1.1\times10^8 s^{-1}$ (theoretical estimated by C.C. Moser and P.L. Dutton, here $V(r) = 7.6\times10^{-8}$ eV), or λ=931±32 meV and $T_{AB} = 5\times10^8 s^{-1}$ (Measured from Magnetic Coupling by Calvo et al. , here $V(r) = 1.7\times10^{-7}$ eV).

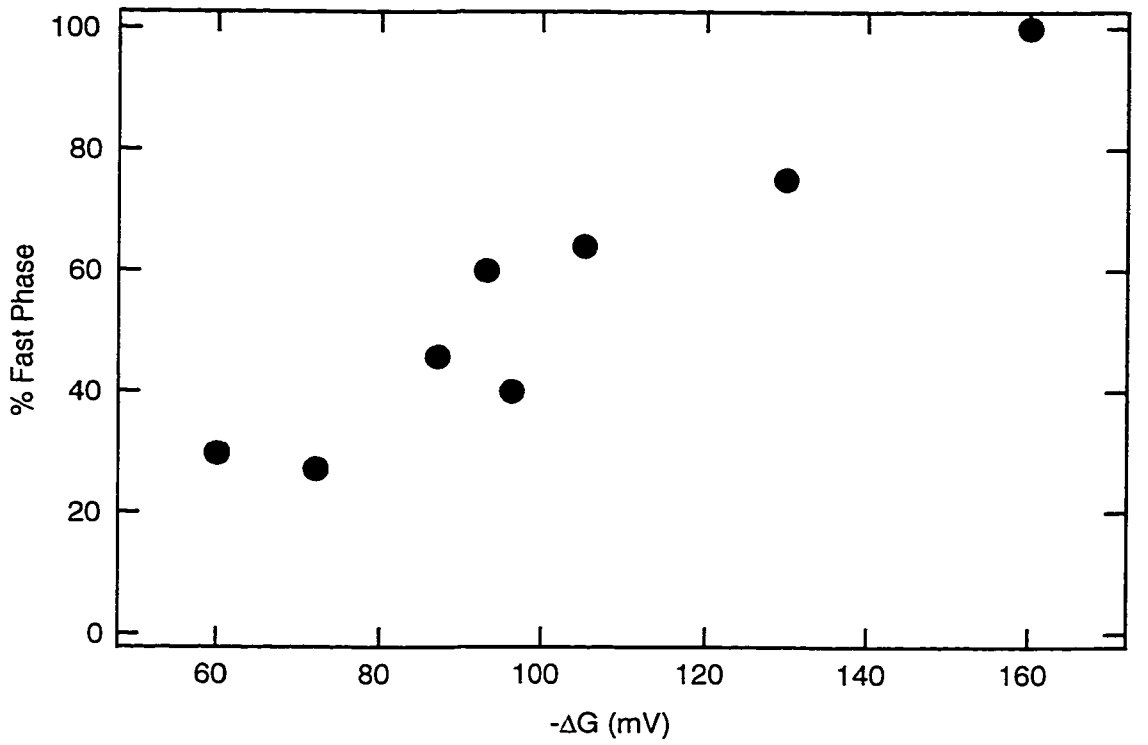

FIGURE 5.4. The fraction of the electron transfer reaction that occurs in the fast phase A_1 as a function of - ΔG^0_{AB}. Most of these data were measured at 406 or 470 nm.

k_{BAP}s are the same within experimental error (see table 1). So ΔG_{AB} is the same in this series of RCs. Changing the tail length of the menaquinone at Q_A does produce a small affect on the rate constant k_1 and its relative amplitude. The rate constant k_1 increases by a factor of 2 as the tail lengthens from 2 to 10 isoprene units (Fig.5.5). At the same time the fraction of the reaction that occurs at k_1 decreases and that at k_2 increases (Fig.5.5).

Influence of number of ubiquinone isoprene units at the Q_B site on the rate of electron transfer from XQ_A^- to UQ_B. When ubiquinone with 0, 1, 2, 4 or 10 isoprene units as Q_A the rate of charge recombination (k_{AP}) changes from 6.9 to 9 s^{-1}. With the same series of quinones at both the Q_A and Q_B sites k_{BAP} ranges from 1.7 s^{-1} to 0.86 s^{1}. Using Eqn. 5.1 to determine ΔG_{AB} a small dependence of ΔG_{AB} on the UQ_B tail length is found. Measurements of k_{BAP} with MQ (VK1) at Q_A shows the same variation of the midpoint of UQ_B with the tail length. Thus when MQ is Q_A, $-\Delta G^0_{AB}$ increases from 72 meV with UQ_1 to 93 meV with UQ_{10} as Q_B (Table 5.1). With MQ as Q_A, k_1 increases as the number of the tail of UQ_B is lengthened ($-\Delta G^0_{AB}$ increases). The rate of the slower reaction (k_2) is independent of the tail length of UQ_B.

The electron transfer to UQ_0 is slow and shows a negligible amount of electron transfer at k_1. This is because the affinity of this quinone for the Q_B site is so small that the site is not fully occupied. Here binding to the Q_B site is the rate limiting step, and the electron transfer rate is now concentration dependent (24).

pH Dependence of the Electron Transfer from Q_A to Q_B in MQ_AUQ_B RCs. The fast reaction was measured as a function of pH in MQ_AUQ_B RCs. The rate is pH independent (6-11.2) (Fig.5.7). This is similar to the behavior of the 20 μs phase of electron transfer in *Rps. viridis* chromatophores where MQ_A is the native quinone(26). This indicates that proton binding is not the rate limiting step. The slower components are pH dependent, k_2 is essentially constant $\approx 10^4$ s^{-1} at low pH and decreases when pH is higher than 8. At high

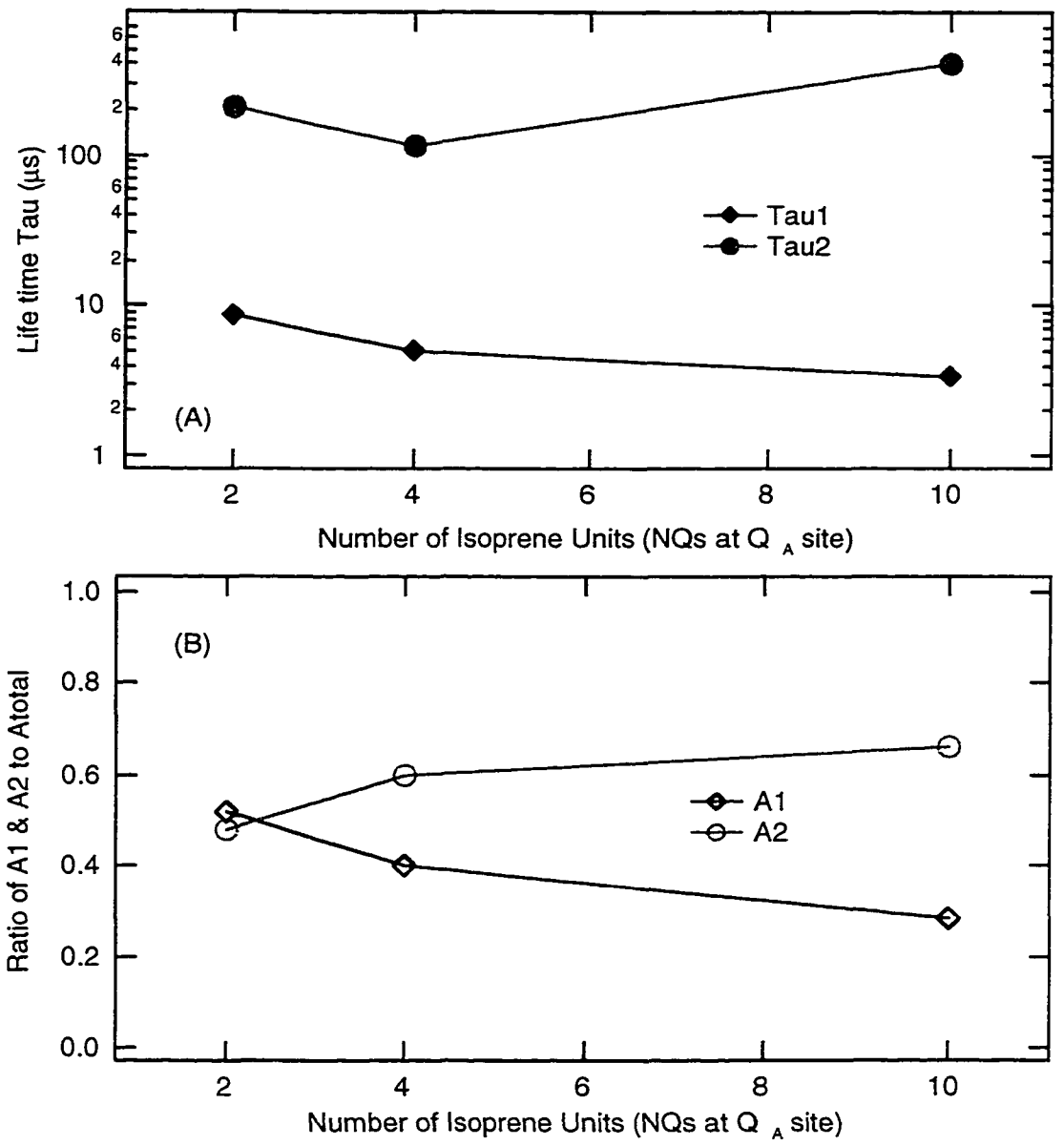

FIGURE 5.5. Influence of number of napthoquinone isoprene units at the Q_A site in R-26 RCs. Condition: Q_A: menaquinone with different tail length, Q_B: UQ_{10}. Measured at 400 nm and pH 8. Plot of (A) Life time τ_1 ($=1/k_1$) and Life time τ_2 ($=1/k_2$), (B) Ratio of A_1 and A_2 as a function of number of napthoquinone isoprene units.

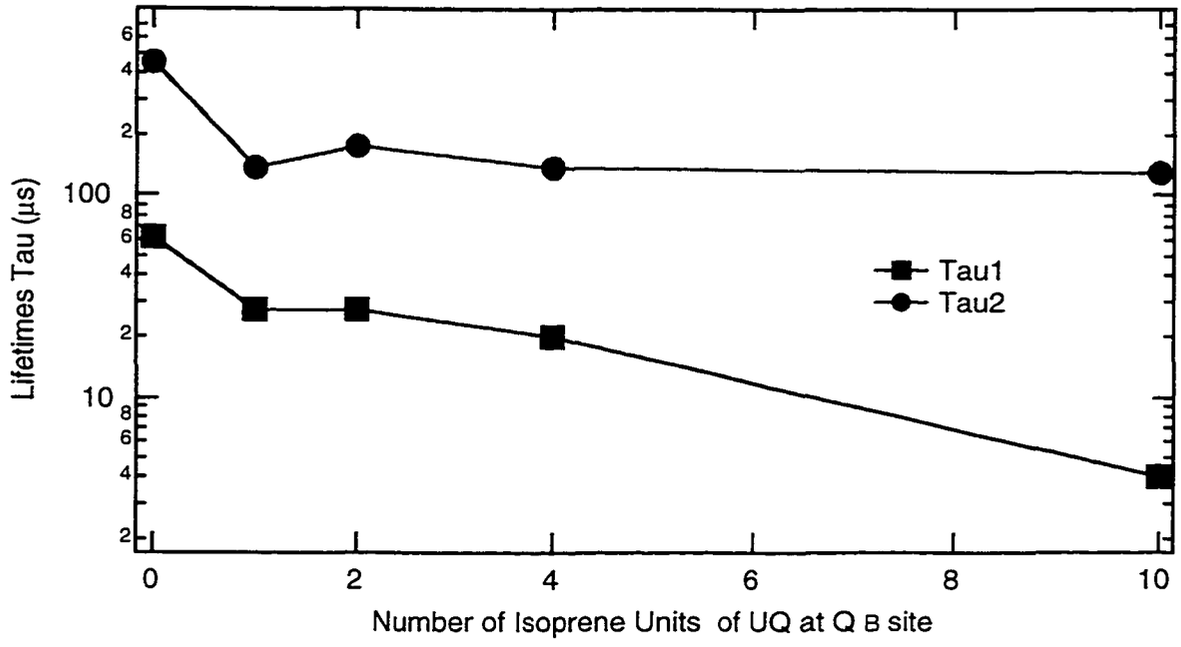

FIGURE 5.6. Influence of number of ubiquinone isoprene units at the Q_A site in R-26 RCs. Condition: Q_A: MQ (VK1), Q_B: Ubiquinone with different tail length. Measured at 406nm and pH 8. Life time Tau1 ($=1/k_1$) and Life time Tau2 ($=1/k_2$) as a function of number of napthoquinone isoprene units.

pH, the rate constant k_3 decreases at high pH (the life time is on the order of ms). The pH dependence of the k_2, k_3, A_2 and A_3 are consistent with previous studies (23, 27).

DISCUSSION

In this work, we investigated the reaction $P^+Q_A^-UQ_B \rightarrow P^+Q_AUQ_B^-$,to determine whether the rate constants of the 2 electron transfer phases (τ_1 and

τ_2)(6) change with the driving force ΔG^0_{AB}, with pH and tail length of Q_A and Q_B, This was accomplished by substituting naphthoquinone molecules with redox potentials lower than that of native UQ into the Q_A site in the R-26 and M265IT RCs. The naphthoquinones have to bind at least several times tighter than the UQ (used to reconstitute Q_B)does at the Q_A site. The experimental results show that the rate constant of the fast phase ($k_1=1/\tau_1$) is dependent on the electron transfer driving force ΔG^0_{AB}, the slow phase ($k_2=1/\tau_2$) is independent of ΔG^0_{AB}(Fig.5.3). In MQ_AUQ_B reaction centers, the rate constant k_1 is pH independent, k_2 is pH dependent. The results for k_2 are consistent with previous measurements on the dependence of ΔG^0_{AB} (3) and on the dependence of pH (23, 28).

Analysis of k_1 Dependence on ΔG^0_{AB}.

Many electron transfer studies in the RC protein have been modeled by theories derived from Marcus electron transfer theory (Equation 1.4) (29, 30):

$$k_{ET} = \frac{4\pi^2 |V(r)|^2}{h\sqrt{4\pi\lambda k_B T}} \exp - \left[\frac{(\Delta G^0_{ET} + \lambda)^2}{4\lambda k_B T} \right] \ldots\ldots \qquad (5.3)$$

where ΔG^0_{ET} is the free energy for electron transfer (defined as the energy of the final minus the initial state, ΔG^0_{AB}, in this work), V(r) is the electronic coupling factor between the initial and final states. In this model, it is assumed that the electron transfer process is in the high temperature limit, where the thermal energy ($k_B T$) is much larger than the energy of the modes coupled to the process ($h\nu$) (i. e. $k_B T >> h\nu$).

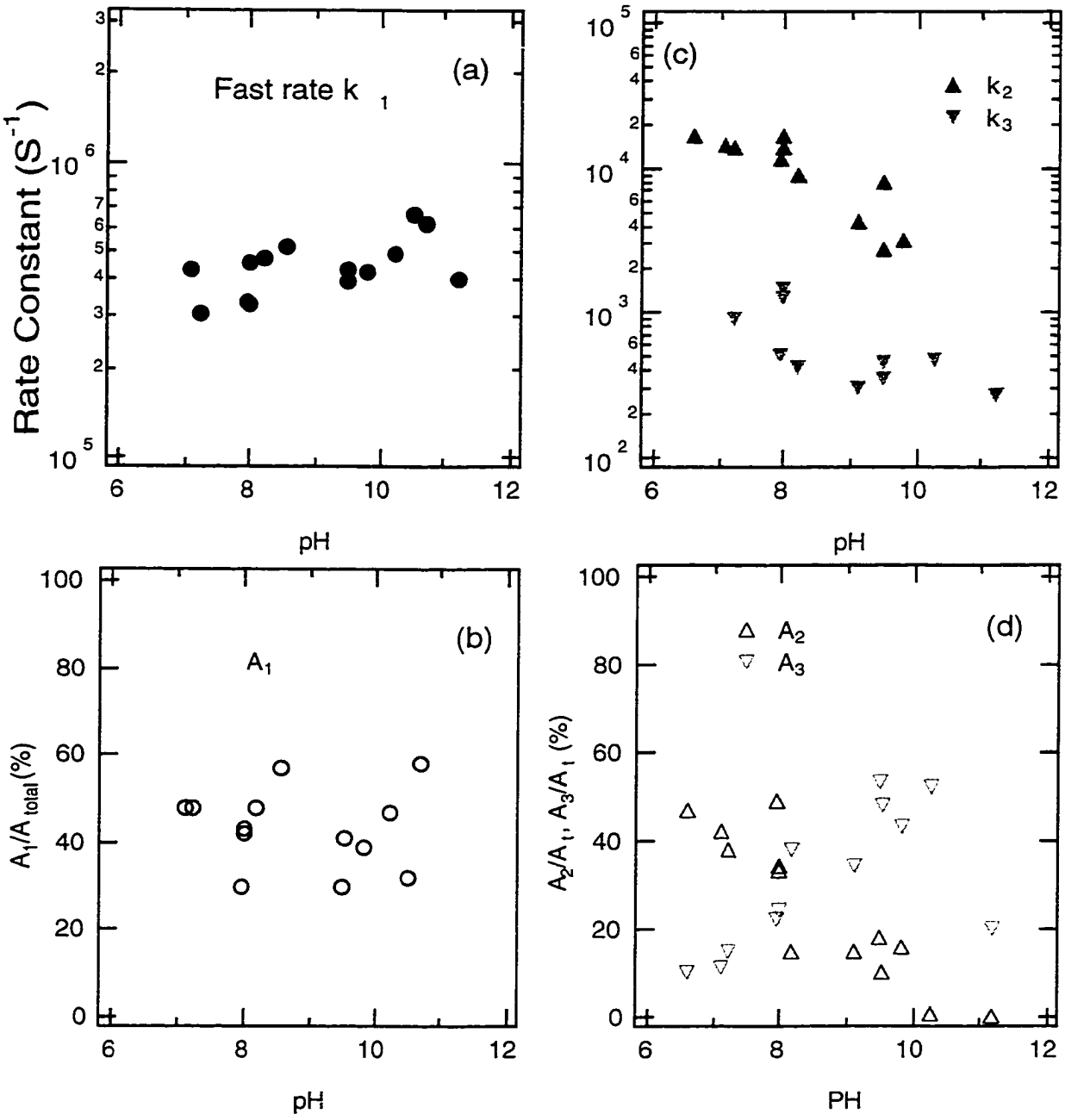

FIGURE 5.7. pH dependence of rate constants of the electron transfer components in MQ_AUQ_B RCs. (a) and (c), rate constant changes with pH: (◆) $\kappa_1 \approx 3$ μs; (▲) $\kappa_2 \approx 80$ μs and (▼) κ_3. (b) and (d), amplitudes change with pH: (○) A_1, (△)A_2 and (▽) A_3. Measured at 400 nm.

If we assume that only the driving force is changed in the NQ substituted R-26 or M265 mutant RCs due to the altered midpoint potentials, the calculated free energy difference between the final and initial states, ΔG^0_{AB} ranges from -50 to -240 meV. Then the relationship between the rate of electron transfer, k_{et} and ΔG^0_{AB} can be modeled using conventional electron transfer theory .

Equation (x) can be simplified as:

$$k^{(1)}_{AB} = k_{\max} \exp - \left[\frac{(\Delta G^0_{AB} + \lambda)^2}{4\lambda k_B T} \right] \quad \ldots\ldots \quad (5.4)$$

here $k_{\max}$ is the maximum rate of electron transfer from Q_A to Q_B when the atoms of the system are correctly arranged for reaction (when $-\Delta G^0_{AB} = \lambda$).

With ΔG^0_{AB} varying from -50 to -240 meV, we can not fit freely to extract a reasonable reorganization energy. So the estimated values of the maximum rate of electron transfer from Q_A to Q_B were used here. The experimentally observed rate k_1 as a function of ΔG^0_{AB} was fitted by equation (5.4) with λ=759±31 meV and $k_{\max} = 1.1 \times 10^8 s^{-1}$ (estimated by C.C. Moser and P.L. Dutton where $V(r) = 7.6 \times 10^{-8}$ eV), or λ=931±32 meV and $k_{\max} = 5 \times 10^8 s^{-1}$ (Measured from Magnetic Coupling by Calvo et al. Biophysical J. A392, here $V(r) = 1.7 \times 10^{-7}$ eV). The estimated errors are based upon standard deviations of the least squares fit. The electronic coupling matrix element V(r) here is larger compared with the V(r) used to fit the results for λ_{AD} and λ_{BD} (31, 32, 33). This is expected given the 14Å distance between Q_A and Q_B compared with the ≈23Å distance from the quinones to P. The results show that k_1 is rate limited by electron transfer. The independence of k_1 on pH (Fig. 5.6) indicates that k_1 is not rate limited by proton binding to the RC.

Analysis of k_2 dependence on ΔG^0_{AB} and pH.

The experimental results show that the rate constants of $k_2 \approx 110$ μs are independent of the electron transfer driving force ΔG^0_{AB} within the range of experimental error (Fig. 5.3). This is consistent with the results measured by Graige et al. with a similar method (3). Thus k_2 is not rate limited by electron transfer. The dependence of k_2 on pH (Fig.5.7), independent below pH 8.5 and slow down at high pH, suggests that k_2 may be limited by proton uptake to the RC or rearrangment inside the RC. Both experiment (34) and calculation shows that protonation state of residues changes with pH in both Q_A^- and Q_B^- states. This implies that the gating of k_2 may be the proton uptake or rearrangement in the vicinity of Q_A or Q_B pocket.

Structure Change and Tail Length Of UQ_B.

Structural changes has been found by comparing the x-ray crystal structure of the RC cooled to cryogenic (90K) temperatures under illumination (light structure, $P^+Q_AQ_B^-$, proximal state) with the structure of the RC cooled in the dark (dark structure, PQ_AQ_B, Distal state) (35). In the light structure, Q_B had moved closer to Q_A and undergone a 180° propeller twist about the isoprenoid chain. The movement of Q_B from distal state to the proximal state could be a light initiated reaction, it may happen after the laser flash and before the electron transfer from Q_A^- to Q_B. The X-ray structure showed that the UQ_2 binds closer to Q_A site than UQ_{10}. Graige et al. had proposed that the conformational change or the Q_B movement controlled $k^{(1)}_{AB}$ (k_2 here) (3). One

hypothesis is that the need for the propeller twist of Q_B suggested that the Q_B could move and flip faster with shorter ubiquinone tail. We tested this hypothesis with UQ_1, UQ_2, UQ_4, UQ_{10} at Q_B site and with MQ at Q_A site. The results (Fig. 5.6) showed that k_2 is independence of the tail length. This is consistent with results from McComb et al. (24). This implies that the movement and the flip may not be the rate limiting step for k_2, or there is no relation between the movement and the tail length, or that the movement and the flip is much fast than k_2.

Kinetic Models That Yield 2 Rates for Electron Transfer from Q_A^- to Q_B

Based on the arguments above, electron transfer may be the rate limited step for k_1, and proton uptake or rearrangement at Q_B site may be the rate limited step for k_2. The fraction of k_1 and k_2 is found to change with ΔG^0_{AB}.

Models can be constructed that may explain the connection between the faction of the RCs that react at k_1 and ΔG_{AB}. We assume: (1). before electron transfer to Q_B, Q_B has two protonation states, protonated and unprotonated at pH 8. This is supported by both experiments and calculations (36). (2). The fraction at each protonation state is sensitive to the Q_A midpoint potential. This becomes reasonable since several studies have indicated that the quinone protein pockets functionally interact with each other (37, 38, 39, 40). It was recently reported that residue L212Glu, situated near the secondary quinone acceptor Q_B, modulates the free energy level of the reduced primary quinone molecule Q_A^- at high pH. Even though the distance between L212Glu and Q_A is 17Å, the interaction energy between L212Glu and Q_A is significant

(30meV) (34). Kalman et al also reported that there were interactions of Q_A^- and the cluster of ionizable residues around L212Glu in the Q_B binding pocket(41). More important, that the proton uptake after formation of PQ_A^- changes at high pH when the native ubiquinone10 was replaced by different NQs or AQs with different midpoint potentials or when the key protonable residues (L212Glu and L213Asp) were replaced by non-protonable alanines in the Q_B binding site. This leads to the model (Scheme 5.1).

Scheme 5.I.

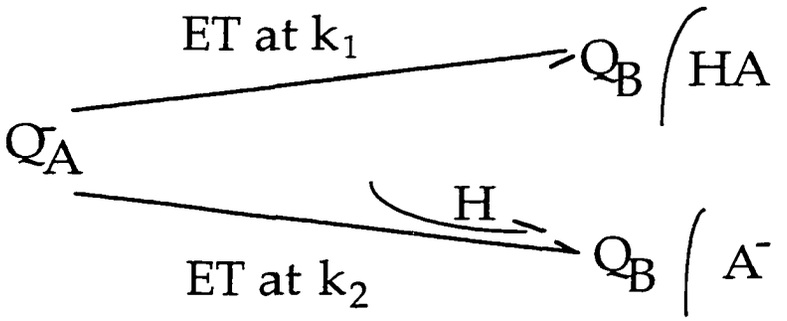

In this model, the RC with pre-protonated state at Q_B favors fast electron transfer k_1. In the unprotonated state, the electron transfer is rate limited by other processes, probably proton uptake or conformational gating. This model can explain the pH data for k_2 above pH9. but it requires that when the - ΔG^0_{AB} is larger, the faction of k_1 increases or the fraction of protonated states increases.

An alternative, Scheme II can explain the observed branching ratio where the faction of k_1 increases when the - ΔG^0_{AB} is larger, here the Q_A^- is formed in a state that is capable of electron transfer to Q_B at k_1. However, within

microseconds Q_A^- induces changes in the protein that block this electron transfer. This requires that the relaxation or the conformation change rate kc is comparable to k_1. Since 50% of the protein reacts at τ_1 when τ_1 is 3 μs this implies that the relaxation occurs in ~3μs. In this model, if k_1 increases as the free energy $-\Delta G^0_{AB}$ increases, the fraction of k_1 increases.

Scheme 5.II.

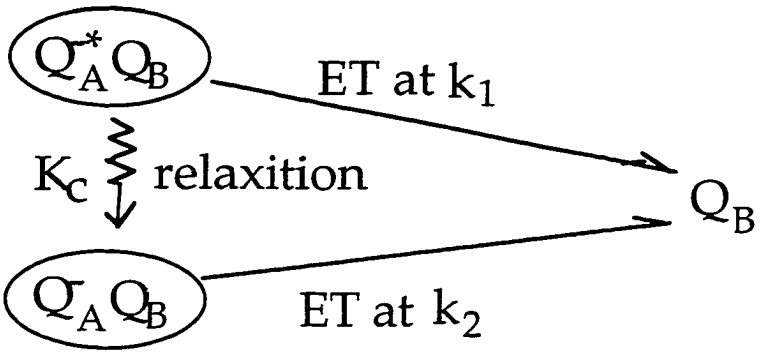

Electron transfer from τ_2 is conformationaly gated. This occurs at 80-100 microseconds in a process that is very weakly dependent on the quinone in the Q_A site or the free energy of the reaction. This latter process does depend on pH above pH 9. This indicates the role of proton transfers may contribute to the gated process. It may be that below pH 9 protons transfers involve only intra-protein protons. At higher pH proton uptake from solution is required to stabilize the Q_B^- state.

Why The Fast Phase (<20μS) Was Not Observed In The Native UQ_AUQ_B RCs? The following reasons can be helpful to explain why: A. There is no

reliable signal from UQ_A to UQ_B. B. The longer the isoprene tail at Q_A site, the smaller the fraction of the fast phase (Fig. 5.4). C. The driving force is small in isolated RCs ($\Delta G^0_{AB} \approx 60$ mV). Electrochromic response measurements on chromatophores of Rb. capsulatus and Rb. sphaeroides (5) have found that electron transfer events were faster than in isolated RCs. These authors have observed a fast component of 4 μs (60%-70%) in chromatophores RCs. Roger prince and P.L. Dutton showed in the 1970's that the operating redox midpoint of Q_A is lower in chromatophores than isolated RCs. At pH 8, in chromatophores Em (Q_A) =-95 mV as opposed to about -50 mV in detergents (42, 43). The redox potential of Q_B doesn't change. Thus the driving force is: $\Delta G^0_{AB} \approx 105$ mV in chromatophores.

REFERENCES

1. Kleinfeld, D., Okamura, M. Y., and Feher, G. (1985) *Biochim. Biophys. Acta 809*, 291-310.
2. Field, M. J., Bash, P. A., and Karplus, M. (1990) *J. Comput. Chem. 113*, 4491.
3. Graige, M. S., Feher, G., and Okamura, M. Y. (1998) *Proc. Natl. Acad. Sci. USA 95*, 11679-11684.
4. Tiede, D. M., Vazquez, J., Cordova, J., and Marone, A. P. (1996) *Biochemistry 35*, 10763-10775.
5. Tiede, D. M., Utschig, L., Hanson, D. K., and Gallo, D. M. (1998) *Photosynth. Res 55*, 267-273.
6. Li, J., Gilroy, D., Tiede, D. M., and Gunner, M. R. (1998) *Biochemistry 37*, 2818-2829.

7. Gunner, M. R. (1991) *Current Topics in Bioenergetics 16*, 319-367.

8. Okamura, M. Y., and Feher, G. (1992) *Annu. Rev. Biochem. 61*, 861-896.

9. Vermeglio, A., and Clayton, R. K. (1977) *Biochim. Biophys. Acta 461*, 159-165.

10. Lubitz, W., Abresch, E. C., Debus, R. J., Isaacson, R. A., Okamura, M. Y., and Feher, G. (1985) *Biochim. Biophys. Acta 808*, 464-469.

11. Maroti, P., and Wraight, C. A. (1988) *Biochim. Biophys. Acta 934*, 314-328.

12. McPherson, P. H., Okamura, M. Y., and Feher, G. (1988) *Biochim. Biophys. Acta 934*, 348-368.

13. Hienerwadel, R., Thibodeau, D., Lenz, F., Nabedryk, E., Breton, J., Kreutz, W., and Mantele, W. (1992) *Biochemistry 31*, 5799-5808.

14. Hienerwadel, R., Grzybek, S., Fogel, C., Kreutz, W., Okamura, M. Y., Paddock, M. L., and Breton, J. (1995) *Biochemistry 34*, 2832-2843.

15. Gunner, M. R., and Honig, B. (1992) in *The Photosynthetic Bacterial Reaction Center: Structure, Spectroscopy and Dynamics II* (Breton, J., and Vermeglio, A., Eds.) pp 403-410, Plenum, New York.

16. Nabedryk, E., Brenton, J., Hienderwadel, R., Fogel, C., Mantele, W., Paddock, M. L., and Okamura, M. Y. (1995) *Biochemistry 34*, 14722-14732.

17. Patel, K. B., and Willson, R. L. (1973) *J. Chem. Soc.(Faraday I) 69*, 814-825.

18. Swallow, A. J. (1982) in *Function of Quinones in Energy Conserving Systems* (Trumpower, B. L., Ed.) pp 59-72, Academic Press, New York.

19. Shopes, R. J., and Wraight, C. A. (1985) *Biochim. Biophys. Acta 806*, 348-356.

20. Woodbury, N. W., Parson, W. W., Gunner, M. R., Prince, R. C., and Dutton, P. L. (1986) *Biochim. Biophys. Acta. 851*, 6-22.

21. Gunner, M. R., and Dutton, P. L. (1989) *J. Am. Chem. Soc. 111*, 3400-3412.

22. Mancino, L. J., Dean, D. P., and Blankenship, R. E. (1984) *Biochim. Biophys. Acta 764*, 46-54.

23. Kleinfeld, D., Okamura, M. Y., and Feher, G. (1984) *Biochim. Biophys. Acta 766*, 126-140.

24. McComb, J. C., Stein, R. R., and Wraight, C. A. (1990) *Biochim. Biophys. Acta 1015*, 156-171.

25. Warncke, K., Gunner, M. R., Braun, B. S., Gu, L., Yu, C., Bruce, J. M., and Dutton, P. L. (1994) *Biochemistry 33*, 7830-7841.

26. Leibl, W., and Breton, J. (1991) *Biochemistry 30*, 9634-9642.

27. Takahashi, E., and Wraight, C. A. (1992) *Biochemistry 31*, 855-866.

28. Takahashi, E., Maroti, P., and Wraight, C. A. (1992) in *Electron and Proton Transfer in Chemistry and Biology* (Muller, A., Ed.) pp pgs. 219-236, Elsevier.

29. Marcus, R. A., and Sutin, N. (1985) *Biochim. Biophys. Acta 811*, 265-322.

30. DeVault, D. (1980) *Q. Rev. Biophys. 13*, 387-564.

31. Allen, J. P., Williams, J. C., Graige, M., Paddock, M. L., Labahn, A., Feher, G., and Okamura, M. Y. (1998) *Photosynth. Res. 55*, 227-233.

32. Labahn, A., Paddok, M. L., McPherson, P. H., Okamura, M. Y., and Feher, G. (1994) *J. Phys. chem. 98*, 3417-3423.

33. Labahn, A., Bruce, J. M., Okamura, M. Y., and Feher, G. (1995) *Chem. Phys. 97*, 355-366.

34. Miksovska, J., Maroti, P., Tandori, J., Schiffer, M., Hanson, D. K., and Sebban, P. (1996) *Biochemistry 35*, 15411-15417.

35. Stowell, M. H. B., McPhillips, T. M., Rees, D. C., Soltis, S. M., Abresch, E., and Feher, G. (1997) *Science 276*, 812-816.

36. Alexov, E. G., and Gunner, M. R. (1997) *Biophys. J. 72*, 2075-2093.

37. Tiede, D. M., and Hanson, D. K. (1992) in *The Photosynthetic Reaction Center II* (Breton, J., and Vermeglio, A., Eds.) pp 341-350, Plenum Press, New York.

38. Brzezinski, P., Okamura, M. Y., and Feher, G. (1992) *Structural changes following the formation of D+QA- in bacetrial reaction centers: measurement of light-induced electrogenic events in RCs incorporated in a phospholipid monolayer*, Plenum Press, New York.

39. Baciou, L., and Sebban, P. (1995) *Photochem. and Photobio. 62*, 271-278.

40. Maroti, P., Hanson, D. K., Schiffer, M., and Sebban, P. (1995) *Nature Struc. Biology 2*, 1057-1059.

41. Kalman, L., Sebban, P., Hanson, D. K., Schiffer, M., and Maroti, P. (1998) *Biochim Biophys Acta 1365*, 513-521.

42. Dutton, P. L., Leigh, J. S., and Wraight, C. A. (1973) *FEBS Lett. 36*, 169-173.

43. Prince, R., and Dutton, P. L. (1976) *Arch. Biochem. Biophys. 172*, 329-334.

Appendix 1-competitive binding to Q_A and Q_B.

The model for XQ and UQ binding to Q_A and Q_B site can be simplified by

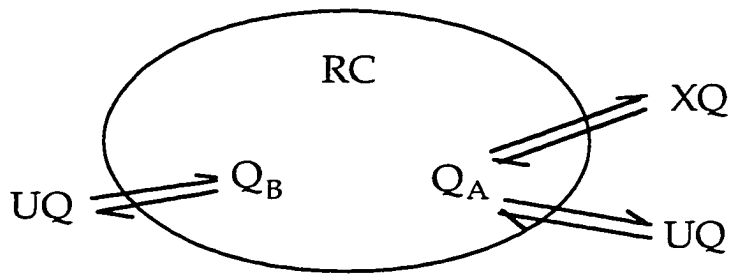

The problem to prepare samples with the maximum fraction of RCs with XQ_A and UQ_B is: XQ and UQ compete for the Q_A site, In addition, UQ binds more tightly to the Q_A site than to the Q_B site and binds more tightly then some XQs to the Q_A site. Thus, a fraction of the Q_A site was occupied by a UQ. The calculation is done to help to find the best ratio of XQ and UQ to achieve the maximum fraction of RCs with XQ_AUQ_B. The equilibrium dissociation constants (K_d) are known for XQ at Q_A site (K_x), UQ at Q_A site (K_u) and UQ at Q_B site (K_b). In this calculation we assume: (1). The binding of a UQ to Q_B does not depend on whether a UQ or XQ is at Q_A. (2). the possibility of a UQ binds at Q_B and with Q_A site unoccupied is close zero. (3). Naphthoquinones (XQ) do not bind to the Q_B site or the binding of XQ to Q_B is negligible. The binding equations and conditions at equilibrium are written by

$X + R \longleftrightarrow Rx$ (XQ binds to Q_A) $\qquad Kx = \frac{X_f \cdot R_f}{Rx}$

$U + R \longleftrightarrow Ru$ (UQ binds to Q_A) $\qquad K_u = \frac{U_f \cdot R_f}{Ru}$

$U + (Rx + Ru) \longleftrightarrow Rb$ (UQ binds to Q_B) $\qquad K_b = \frac{U_f \cdot (Rx + Ru)_f}{Rb}$

$Rt = Rf + Rx + Ru$

$Xt = Xf + Rx$

$Ut = Uf + Ru + Rb$

$$(Rx + Ru)_f = Rx + Ru - Rb$$

Here X is the concentration of XQ, R is RC, Rx is the RC with XQ bound at Q_A, K is dissociation constant, U is UQ, Ru is RCs with UQ bound at Q_A, Rb is RCs with XQ or UQ bound at Q_A and UQ bound at Q_B, Rt is the total RC concentration, Rf is the RCs with no quinone bound, Xt is the total XQ quinone concentration in the solution, Xf is the free quinone XQ concentration, Ut is the total UQ quinone concentration, Uf is the free quinone UQ concentration. The percentage of XQ_AUQ_B RCs is $\frac{Rx \cdot Ru}{(Rx+Ru)R_t}$.

Rearranging so that the unknowns are at same side

$$Rf = Rt - Rx - Ru \quad (1)$$

$$Xf = Xt - Rx \quad (2)$$

$$Uf = Ut - Ru - Rb \quad (3)$$

$$Rf \cdot Xf = K_x \cdot Rx \quad (4)$$

$$Rf \cdot Uf = K_u \cdot Ru \quad (5)$$

$$Uf \cdot (Rx + Ru - Rb) = K_b \cdot Rb \quad (6)$$

Simplified further,

$$Ut - Ru - Rb = \frac{K_b \cdot Rb}{(Rx + Ru - Rb)} \quad (7)$$

$$Rt - Rx - Ru = \frac{K_u \cdot Ru}{K_b \cdot Rb}(Rx + Ru - Rb) \quad (8)$$

$$Xt - Rx = \frac{Kx \cdot Kb \cdot Rx \cdot Rb}{Ku \cdot Ru \cdot (Rx + Ru - Rb)} \quad (9)$$

Equation for Rx:

$$
\begin{aligned}
0=&-(b^2c^3s^2)\\
&+(abc^2rs-2b^2c^2rs+3b^2c^2s^2+2bc^3s^2+2bc^2rs^2-bc^2rst)\mathrm{Rx}\\
&+(-2abcrs+4b^2crs-ac^2rs+3bc^2rs-acr^2s+4bcr^2s-3b^2cs^2-6bc^2s^2-c^3s^2\\
&-4bcrs^2-2c^2rs^2-cr^2s^2+acr^2t-bcr^2t+2bcrst+c^2rst+cr^2st)\mathrm{Rx}^2\\
&+(abrs-2b^2rs+2acrs-6bcrs-c^2rs+ar^2s-4br^2s-3cr^2s-2r^3s+b^2s^2+6bcs^2\\
&+3c^2s^2+2brs^2+4crs^2+r^2s^2+ar^2t+br^2t+cr^2t+r^3t-brst-2crst-r^2st)\mathrm{Rx}^3\\
&+(-(ars)+3brs+2crs+3r^2s-2bs^2-3cs^2-2rs^2-r^2t+rst)\mathrm{Rx}^4\\
&+(-(rs)+s^2)\mathrm{Rx}^5
\end{aligned}
$$

Where a=Ut, b=Rt, c=Xt, r=K_x, s=K_u, t=K_b. The numerical solution can be obtained by Mathematica.

$$Ru=\frac{Rt\cdot Rx-(Rt+Xt+Kx)\cdot Rx+Rx^2}{Xt-Rx}$$

$$Rb=\frac{Ku\cdot Rx\cdot(Rx+Ru)}{(Rt-Rx-Ru)\cdot Rb+k_u\cdot Ru}$$

Letting Rt=1 μM, XQ=20μM (TMNQ)

Q_A: K_X=0.06 μM (TMNQ), K_{u4}=0.00024μM (UQ4), K_{U1}=0.085μM (UQ_1)

Q_B: K_{u4}=0.002μM (UQ4), K_{U1}=1μM (UQ_1)

Plot Rx, Ru and Rb as a function of a=Ut given the b=XQ concentration fixed (limited by solubility). The concentrations of RCs with TMNQ as XQ, UQ1 and UQ4 as UQ are shown in the Figure below.

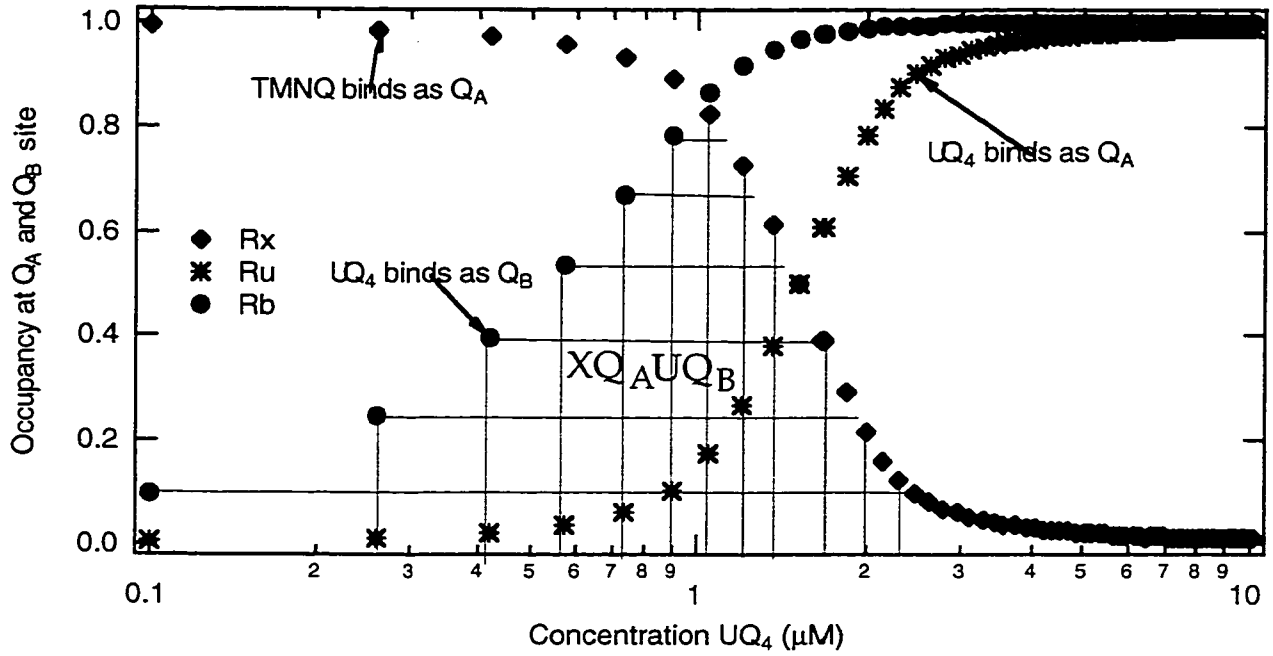

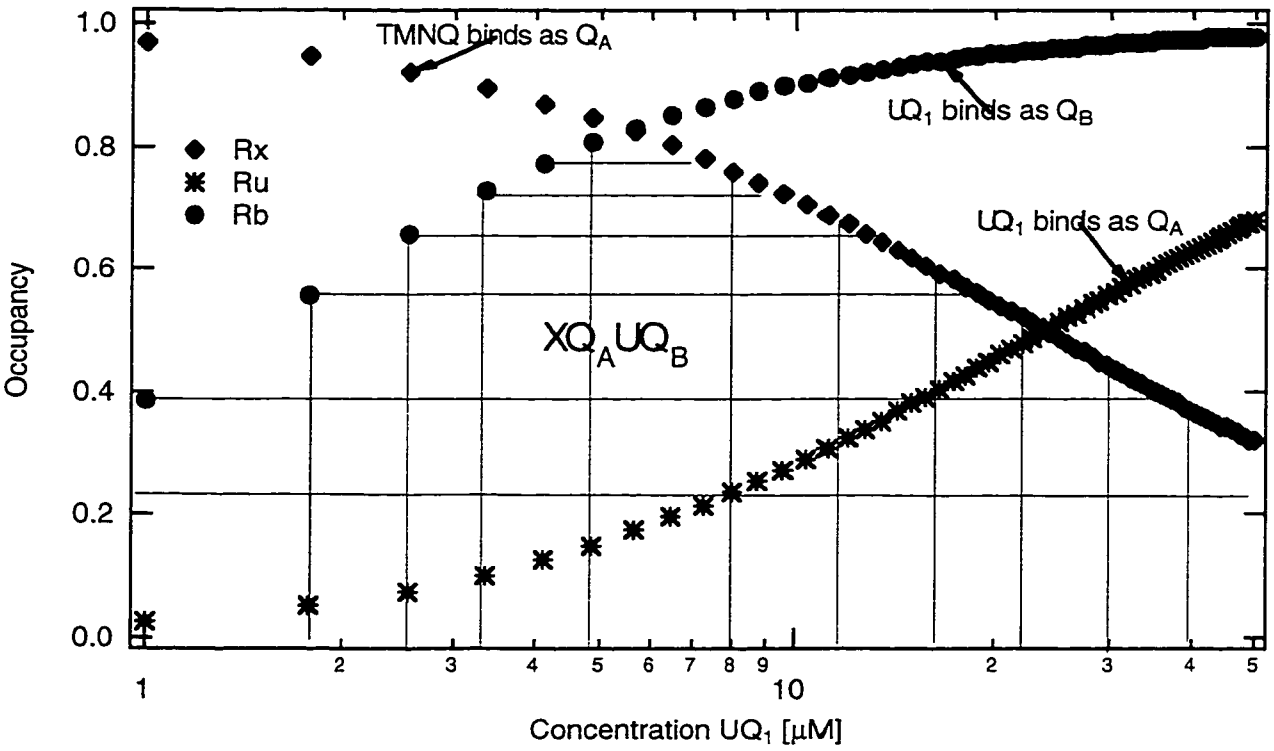

Appendix 2-Electron Transfer Kinetics

A simplified electron transfer scheme in RC is shown below

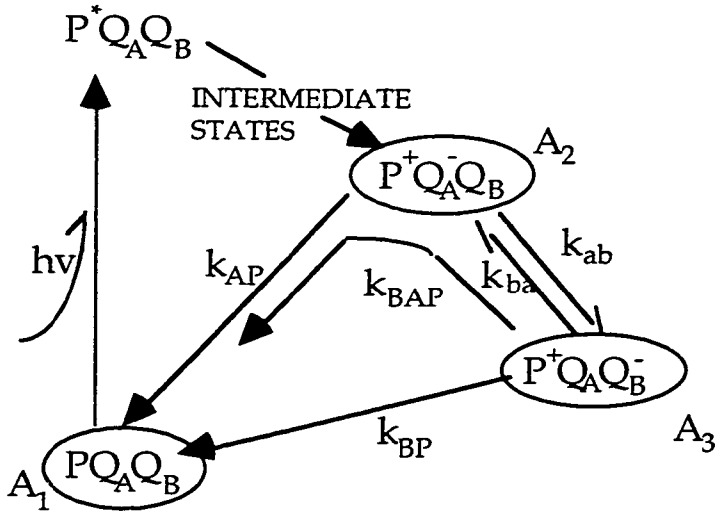

The rate equations governing elelctron transfer kinetics after a single flash in reaction centers for the scheme depicted in Figure 1 are given by:

$$\left.\begin{aligned} \frac{dA_1}{dt} &= k_{AP}\cdot A_2 + k_{BP}\cdot A_3 \\ \frac{dA_2}{dt} &= -(k_{AP}+k_{AB})\cdot A_2 + k_{BA}\cdot A_3 \\ \frac{dA_3}{dt} &= k_{AB}\cdot A_2 - (k_{BP}+k_{BA})\cdot A_3 \end{aligned}\right\} \qquad (1)$$

Let $k_{AP}=k_1$, $k_{BP}=k_2$, $k_{AB}=k_3$ and $k_{BA}=k_4$, so that

$$\frac{d}{dt}\begin{pmatrix} A_1 \\ A_2 \\ A_3 \end{pmatrix} = \begin{pmatrix} 0 & k_1 & k_2 \\ 0 & -(k_1+k_3) & k_4 \\ 0 & k_3 & -(k_2+k_4) \end{pmatrix}\begin{pmatrix} A_1 \\ A_2 \\ A_3 \end{pmatrix} \qquad (2)$$

The general solutions of above equations are:

$$A_i = \sum_{i=1}^{3} B_{ir}\Theta_r e^{-\lambda_r t}$$

$$= B_{i1}\Theta_1 e^{-\lambda_1 t} + B_{i2}\Theta_2 e^{-\lambda_2 t} + B_{i3}\Theta_3 e^{-\lambda_3 t} \qquad (3)$$

(3) to (2)

$$\sum_{r=1}^{3} -\lambda_r \mathrm{I}\begin{pmatrix} B_{1r} \\ B_{2r} \\ B_{3r} \end{pmatrix}\Theta_r e^{-\lambda_r t} = \sum_{r=1}^{3}\begin{pmatrix} 0 & k_1 & k_2 \\ 0 & -(k_1+k_3) & k_4 \\ 0 & k_3 & -(k_2+k_4) \end{pmatrix}\begin{pmatrix} B_{1r} \\ B_{2r} \\ B_{3r} \end{pmatrix}\Theta_r e^{-\lambda_r t}$$

or

$$\sum_{r=1}^{3}\begin{pmatrix} \lambda_r & k_1 & k_2 \\ 0 & \lambda_r-(k_1+k_3) & k_4 \\ 0 & k_3 & \lambda_r-(k_2+k_4) \end{pmatrix}\begin{pmatrix} B_{1r} \\ B_{2r} \\ B_{3r} \end{pmatrix}\Theta_r e^{-\lambda_r t} = 0 \qquad (4)$$

The secular equation is

$$\begin{vmatrix} \lambda_r & k_1 & k_2 \\ 0 & \lambda_r-(k_1+k_3) & k_4 \\ 0 & k_3 & \lambda_r-(k_2+k_4) \end{vmatrix} = 0$$

or when expanded

$$\lambda_r[(\lambda_r^2 - (k_1+k_2+k_3+k_4)\lambda_r + (k_1k_4+k_2k_3+k_2k_1)] = 0$$

The three solutions for λ_r are

$$\lambda_1 = 0$$

$$\lambda_{2.3} = \frac{k_1+k_2+k_3+k_4}{2} \pm \sqrt{\left(\frac{k_1+k_2+k_3+k_4}{2}\right)^2 - (k_1k_4+k_2k_3+k_2k_1)} \qquad (\lambda_2 = \lambda_+ \text{ here})$$

from (4), the equations for B_{ir} ae given by

$$\begin{pmatrix} \lambda_r & k_1 & k_2 \\ 0 & \lambda_r-(k_1+k_3) & k_4 \\ 0 & k_3 & \lambda_r-(k_2+k_4) \end{pmatrix}\begin{pmatrix} B_{1r} \\ B_{2r} \\ B_{3r} \end{pmatrix} = 0$$

or

$$\left.\begin{aligned} &\lambda_r B_{1r} + k_1 B_{2r} + k_2 B_{3r} = 0 \\ &(\lambda_r - k_1 - k_3)B_{2r} + k_4 B_{3r} = 0 \\ &k_3 B_{2r} + (\lambda_r - k_2 - k_4)B_{3r} = 0 \end{aligned}\right\} \qquad (5)$$

Letting B_{1r}=1 (B_{1r} is arbitrary) then

$$B_{2r} = \frac{\lambda_r k_4}{(\lambda_r - k_1 - k_3)k_2 - k_1 k_4}$$

$$B_{3r} = \frac{-\lambda_r(\lambda_r - k_1 - k_3)}{(\lambda_r - k_1 - k_3)k_2 - k_1 k_4}$$

For the general solution

$$A_i = \sum_{i=1}^{3} B_{ir}\Theta_r e^{-\lambda_r t}$$

Initial condition: after a saturated short flash, at t=0, all electrons are at $P^+Q_A^-Q_B$ state, that is

$$A_1^0(t=0) = [PQ_AQ_B] = 0 \quad A_2^0(t=0) = [P^+Q_A^-Q_B] = N_0 \quad A_3^0(t=0) = [P^+Q_AQ_B^-] = 0$$

so at t=0,

$$\begin{cases} \Theta_1 + \Theta_2 + \Theta_3 = 0 \\ B_{22}\Theta_2 + B_{23}\Theta_3 = N_0 \\ B_{32}\Theta_2 + B_{33}\Theta_3 = 0 \end{cases}$$

at t=∞, with λ_1=0, $A_1(t=\infty) = N_0$, so

$$\Theta_1 = N_0$$

$$\Theta_2 = -N_0\left[1 + \frac{1 + B_{22}}{B_{23} - B_{22}}\right]$$

$$\Theta_3 = N_0\left[\frac{1 + B_{22}}{B_{23} - B_{22}}\right]$$

So with B_{1r}=1, B_{21}=B_{31}=0 , the solutions of the equations are

$$\begin{cases} A_1 = \Theta_1 + \Theta_2 e^{-\lambda_2 t} + \Theta_3 e^{-\lambda_3 t} \\ A_2 = B_{22}\Theta_2 e^{-\lambda_2 t} + B_{23}\Theta_3 e^{-\lambda_3 t} \\ A_3 = B_{32}\Theta_2 e^{-\lambda_2 t} + B_{33}\Theta_3 e^{-\lambda_3 t} \end{cases} \qquad (9)$$

The charge recombination process P+->P we monitored is A_1 as a function of time t.

Example of computer simulation of electron transfer reaction starting from Q_A in RC protein is shown bellow:

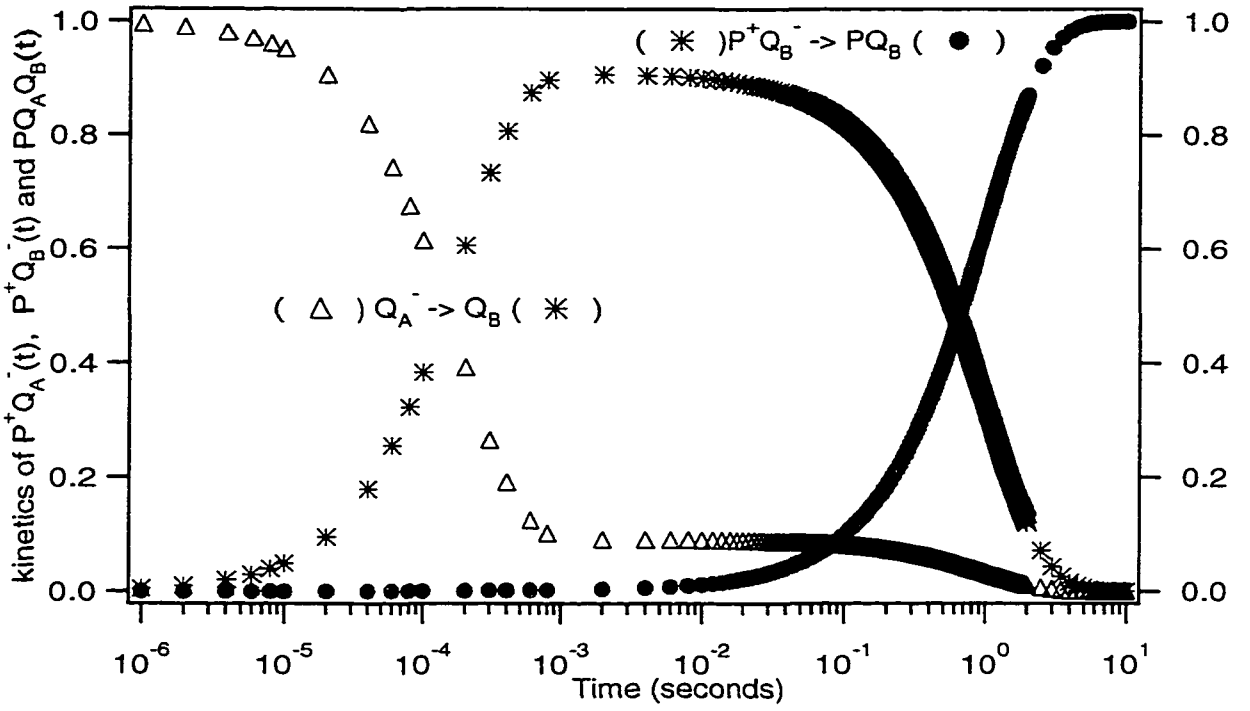

Simulated reaction kinetics in UQ_AUQ_B RCs. Parameters are given: $N_0=1$, $k_1=k_{AP}=10\ s^{-1}$, $k_2=k_{BP}=0.12\ s^{-1}$, $k_3=k_{AB}=5000\ s^{-1}$, $k_4=k_{BA}\ s^{-1}$. $A_1(t)=P^+Q_A^-Q_B(t)$ (Δ), $A_2(t)=P^+Q_AQ_B^-(t)$ (*), $A_3(t)=PQ_AQ_B(t)$ (•).

REFERENCES

Chapter 1

1. Cramer, W. A., and Knaff, D. B. (1991) *Energy Transduction in Biological Membranes: A Textbook of Bioenergetics*, Springer-Verlag, New York.
2. Feher, G., and Okamura, M. Y. (1978) in *The Photosynthetic Bacteria* (Clayton, R. K., and Sistrom, W. R., Eds.) pp 349-386, Plenum Press, New York.
3. Prince, R. C., and Youvan, D. C. (1987) *Biochim. Biophys. Acta 890*, 286-291.
4. Reed, D. W., and Clayton, R. K. (1968) *Biochim. Biophys. Res. Commun. 30*, 471.
5. Reed, D. W. (1969) *J. Biol. Chem. 244*, 4936.
6. Williams, J. C., Steiner, L. A., and Feher, G. (1986) *Proteins 1*, 312-325.
7. Deisenhofer, J., and Michel, H. (1989) *Science 245*, 1463-1473.
8. Okamoto, Y. (1994) *Biopolymers 34*, 529-539.
9. Moser, C. C., Keske, J. M., Warncke, K., Farid, R., and Dutton, P. L. (1992) *Nature 355*, 796-802.
10. Marcus, R. A., and Sutin, N. (1985) *Biochim. Biophys. Acta 811*, 265-322.
11. Gunner, M. R. (1991) *Current Topics in Bioenergetics 16*, 319-367.
12. Kirmaier, C., and Holten, D. (1987) *Photosynthesis Research 13*, 225-260.

13. Kirmaier, C., and Holten, D. (1993) in *The Photosynthetic Reaction Center* (Deisenhofer, J., and Norris, J. R., Eds.) pp 49-70, Academic Press, San Diego.

14. Feher, G., Allen, J. P., Okamura, M. Y., and Rees, D. C. (1989) *Nature 339*, 111-116.

15. Wraight, C. A., and Clayton, R. K. (1973) *Biochim. Biophys. Acta 333*, 246-260.

Chapter 3

1. Coleman, W. J., and Youvan, D. C. (1993) *Nature 366*, 517-518.

2. Prince, R. C., and Youvan, D. C. (1987) *Biochim. Biophys. Acta 890*, 286-291.

3. Takahashi, E., and Wraight, C. A. (1992) *Biochemistry 31*, 855-866.

4. Paddock, M. L., Rongey, S. H., McPherson, P. H., Juth, A., Feher, G., and Okamura, M. Y. (1994) *Biochemistry 33*, 734-745.

5. Mancino, L. J., Dean, D. P., and Blankenship, R. E. (1984) *Biochim. Biophys. Acta 764*, 46-54.

6. Baciou, L., Bylina, E. J., and Sebban, P. (1993) *Bipphysical J. 65*, 652-660.

7. Giangiacomo, K. M., and Dutton, P. L. (1989) *Proc. Natl. Acad. Sci. USA 86*, 2658-2662.

8. Paddock, M. L., Rongey, S. H., Feher, G., and Okamura, M. Y. (1989) *Proc. Natl. Acad. Sci. USA 86*, 6602-6606.

9. Paddock, M. L., McPherson, P. H., Feher, G., and Okamura, M. Y. (1990) *Proc. Natl. Acad. Sci. 87*, 6803-6807.

10. Bylina, E. J., and Youvan, D. C. (1987) *Z. Naturforsch. 42c*, 769-774.

11. Maroti, P., Hanson, D. K., Baciou, L., Marianne, S., and Sebban, P. (1994) *Proc. Natl. Acac. Sci. 91*, 5617-5621.
12. Wraight, C. A. (1977) *Biochim. Biophys. Acta 495*, 525-531.
13. Maroti, P., and Wraight, C. A. (1988) *Biochim. Biophys. Acta 934*, 329-347.
14. McPherson, P. H., Okamura, M. Y., and Feher, G. (1993) *Biochim. Biophys. Acta 1144*, 309-324.
15. Kleinfeld, D., Okamura, M. Y., and Feher, G. (1984) *Biochim. Biophys. Acta 766*, 126-140.
16. Debus, R. J., Feher, G., and Okamura, M. Y. (1985) *Biochemistry 24*, 2488-2500.
17. Gunner, M. R., and Honig, B. (1992) in *The Photosynthetic Bacterial Reaction Center: Structure, Spectroscopy and Dynamics II* (Breton, J., and Vermeglio, A., Eds.) pp 403-410, Plenum, New York.
18. Takahashi, E., and Wraight, C. A. (1994) *Advances in Molecular and Cell Biology 10*, 197-251.
19. Okamura, M. Y., and Feher, G. (1992) *Annu. Rev. Biochem. 61*, 861-896.
20. Moser, C. C., Keske, J. M., Warncke, K., Farid, R., and Dutton, P. L. (1992) *Nature 355*, 796-802.
21. Deisenhofer, J., and Michel, H. (1989) *The EMBO Journal 8*, 2149-2170.

Chapter 4

1. Feher, G., Allen, J. P., Okamura, M. Y., and Rees, D. C. (1989) *Nature 339*, 111-116.
2. Gunner, M. R. (1991) *Current Topics in Bioenergetics 16*, 319-367.

3. Blankenship, R. E., Madigan, M. T., and Bauer, C. E. (1995) *Anoxygenic Photosynthetic Bacteria*, Vol. 2, Kluwer Academic Publishers.

4. Maroti, P., and Wraight, C. A. (1988) *Biochim. Biophys. Acta 934*, 314-328.

5. McPherson, P. H., Okamura, M. Y., and Feher, G. (1988) *Biochim. Biophys. Acta 934*, 348-368.

6. Graige, M. S., Paddock, M. L., Bruce, J. M., Feher, G., and Okamura, M. Y. (1996) *J. Am. Chem. Soc. 118*, 9005-9016.

7. Wraight, C. A. (1979) *Biochim. Biophys. Acta 548*, 309-327.

8. Wraight, C. A. (1977) *Biochim. Biophys. Acta 495*, 525-531.

9. Kleinfeld, D., Okamura, M. Y., and Feher, G. (1985) *Biochim. Biophys. Acta 809*, 291-310.

10. Okamura, M. Y., and Feher, G. (1995) in *Anoxygenic Photosynthetic Bacteria* (Blankenship, R. E., Madigan, M. T., and Bauer, C. E., Eds.) pp 231-257, Kluwer Academic Publishers.

11. Cramer, W. A., and Knaff, D. B. (1991) *Energy Transduction in Biological Membranes: A Textbook of Bioenergetics*, Springer-Verlag, New York.

12. Nicholls, D. G., and Ferguson, J. S. (1992) *Bioenergetics 2*, Academic Press Limited, London.

13. Takahashi, E., and Wraight, C. A. (1994) *Advances in Molecular and Cell Biology 10*, 197-251.

14. Breton, J., and Verméglio, A. (1988) *The Photosynthetic Bacterial Reaction Center: Structure and Dynamics*, Plenum Press, New York.

15. Beroza, P., Fredkin, D. R., Okamura, M. Y., and Feher, G. (1995) *Biophys. J. 68*, 2233-2250.

16. Lancaster, C. R. D., Michel, H., Honig, B., and Gunner, M. R. (1996) *Biophys. J. 70*, 2469-2492.

17. Verméglio, A., and Clayton, R. K. (1977) *Biochim. Biophys. Acta 461*, 159-165.

18. Hales, B. J., and Case, E. E. (1981) *Biochim. Biophys. Acta 637*, 291-302.

19. Lubitz, W., Abresch, E. C., Debus, R. J., Isaacson, R. A., Okamura, M. Y., and Feher, G. (1985) *Biochim. Biophys. Acta 808*, 464-469.

20. Hienerwadel, R., Thibodeau, D., Lenz, F., Nabedryk, E., Breton, J., Kreutz, W., and Mantele, W. (1992) *Biochemistry 31*, 5799-5808.

21. Hienerwadel, R., Grzybek, S., Fogel, C., Kreutz, W., Okamura, M. Y., Paddock, M. L., and Breton, J. (1995) *Biochemistry 34*, 2832-2843.

22. Gunner, M. R., and Honig, B. (1992) in *The Photosynthetic Bacterial Reaction Center: Structure, Spectroscopy and Dynamics II* (Breton, J., and Vermeglio, A., Eds.) pp 403-410, Plenum, New York.

23. Nabedryk, E., Brenton, J., Hienderwadel, R., Fogel, C., Mantele, W., Paddock, M. L., and Okamura, M. Y. (1995) *Biochemistry 34*, 14722-14732.

24. Okamura, M. Y., and Feher, G. (1992) *Annu. Rev. Biochem. 61*, 861-896.

25. Bensasson, R., and Land, E. J. (1973) *Biochim. Biophys. Acta*, 176-181.

26. Tiede, D. M., Vazquez, J., Cordova, J., and Marone, P. A. (1996) *Biochemistry 35*, 10763-10775.

27. Takahashi, E., Maroti, P., and Wraight, C. A. (1992) in *Electron and Proton Transfer in Chemistry and Biology* (Muller, A., Ed.) pp pgs. 219-236, Elsevier.

28. Tiede, D. M., and Hanson, D. K. (1992) in *The Photosynthetic Reaction Center II* (Breton, J., and Vermeglio, A., Eds.) pp 341-350, Plenum Press, New York.

29. Parson, W. W. (1969) *Biochim. Biophys. Acta 189*, 384-396.

30. Kleinfeld, D., Okamura, M. Y., and Feher, G. (1984) *Biochim. Biophys. Acta 766*, 126-140.

31. Patel, K. B., and Willson, R. L. (1973) *J. Chem. Soc. 69*, 814-825.

32. Swallow, A. J. (1982) in *Function of Quinones in Energy Conserving Systems* (Trumpower, B. L., Ed.) pp 59-72, Academic Press, New York.

33. Shopes, R. J., and Wraight, C. A. (1985) *Biochim. Biophys. Acta 806*, 348-356.

34. Woodbury, N. W., Parson, W. W., Gunner, M. R., Prince, R. C., and Dutton, P. L. (1986) *Biochim. Biophys. Acta. 851*, 6-22.

35. Lancaster, C. R. D., Ermler, U., and Michel, H. (1995) in *Anoxygenic Photosynthetic Bacteria* (Blankenship, R. E., Madigan, M. T., and Bauer, C. E., Eds.) pp 503-526, Kluwer, Dordrecht.

36. Breton, J., and Nabedryk, E. (1996) *Biochim. Biophys. Acta 1275*, 84-90.

37. Warncke, K., Gunner, M. R., Braun, B. S., Gu, L., Yu, C., Bruce, J. M., and Dutton, P. L. (1994) *Biochemistry 33*, 7830-7841.

38. Giangiacomo, K. M., and Dutton, P. L. (1989) *Proc. Natl. Acad. Sci. USA 86*, 2658-2662.

39. Clayton, R. K., and Wang, R. T. (1971) *Methods Enzymol 23*, 696-704.

40. Okamura, M. Y., Isaacson, R. A., and Feher, G. (1975) *Proc. Natl. Acad. Sci, USA 72*, 3492-3496.

41. McComb, J. C., Stein, R. R., and Wraight, C. A. (1990) *Biochim. Biophys. Acta 1015*, 156-171.

42. Mancino, L. J., Dean, D. P., and Blankenship, R. E. (1984) *Biochim. Biophys. Acta 764*, 46-54.

43. Slooten, L. (1972) *Biochim. Biophys. Acta 275*, 208-218.

44. Clayton, R. K., and Straley, S. C. (1972) *Biophys. J 12*, 1221-1234.

45. Tiede, D. M., Gallo, D. M., and Hanson, D. K. (1997) *Biophys. J. 72*, A248.

46. Tiede, D. M., Utschig, L., Hanson, D. K., and Gallo, D. M. (1997) *submitted to Photosynthesis Research.*

47. Carithers, R. P., and Parson, W. W. (1975) *Biochim. Biophys. Acta 387*, 194-211.

48. Leibl, W., Sinning, I., Ewald, G., Michel, H., and Breton, J. (1993) *Biochemistry 32*, 1958-1964.

49. Maróti, P., and Wraight, C. A. (1997) *Biophys. J. 73*, 367-381.

50. Brzezinski, P., Okamura, M. Y., and Feher, G. (1992) in *The Photosynthetic Bacterial Research Center II* (Brenton, J., and Vermeglio, A., Eds.) pp 321-330, Plenum Press, New York.

51. Devault, D. (1980) *Q. Rev. Biophys. 13*, 387-564.

52. Marcus, R. A., and Sutin, N. (1985) *Biochim. Biophys. Acta 811*, 265-322.

53. Moser, C. C., Keske, J. M., Warncke, K., Farid, R., and Dutton, P. L. (1992) *Nature 355*, 796-802.

54. Onuchic, J. N., Beratan, D. N., Winkler, J. R., and Gray, H. B. (1992) *Ann. Rev. Biophys. Biomol. Struct. 21*, 349-377.

55. Labahn, A., Paddock, M. L., McPherson, P. H., Okamura, M. Y., and Feher, G. (1994) *J. Phys. Chem. 98*, 3417-3423.

56. Breton, J., Burie, J., Berthomieu, C., Berger, G., and Nabedryk, E. (1994) *Biochemistry 33*, 4953-4965.

57. Gunner, M. R., and Dutton, P. L. (1989) *J. Am. Chem. Soc. 111*, 3400-3412.

58. Gunner, M. R., Robertson, D. E., and Dutton, P. L. (1986) *J. Phys. Chem. 90*, 3783-3795.

59. Brudler, R., de Groot, J. M., van Liemt, W. B. S., Steggerda, W. F., Esmeijer, R., Gast, P., Hoff, A. J., Lugtenburg, J., and Gerwert, K. (1994) *EMBO J. 13*, 5523-5530.

60. Breton, J., Claude, B., Burie, J., Nabedryk, E., and Mioskowski, C. (1994) *Biochemistry 33*, 14378-14386.

61. Morrison, L. E., and Loach, P. A. (1978) *Photochem. Photobiol. 27*, 751-757.

62. Parot, P., Thiery, J., and Vermèglio, A. (1987) *Biochim. Biophys. Acta 893*, 534-543.

63. Gao, J., Shopes, R. J., and Wraight, C. A. (1991) *Biochim. Biophys. Acta. 1056*, 259-272.

64. Baciou, L., and Sebban, P. (1995) *Photochem. and Photobiol. 62*, 271-278.

65. Sebban, P. (1988) *Biochim. Biophys. Acta 936*, 124-132.

66. Sebban, P., and Wraight, C. A. (1989) *Biochim. Biophys. Acta 974*, 54-65.

67. Gunner, M. R., Tiede, D. M., Prince, R. C., and Dutton, P. L. (1982) in *Function of Quinones in Energy Conserving Systems* (Trumpower, B. L., Ed.) pp 265-269, Academic Press, New York.

68. Kleinfeld, D., Okamura, M. Y., and Feher, G. (1985) *Biophys. J. 48*, 849-852.

69. Franzen, S., Goldstein, R. F., and Boxer, S. G. (1990) *J. Phys. Chem. 94*, 5135-5149.

70. Shopes, R. J., and Wraight, C. A. (1987) *Biochim. Biophys. Acta 893*, 409-425.

71. Gunner, M. R., Braun, B. S., Bruce, J. M., and Dutton, P. L. (1985) in *Antennas and Reaction Centers of Photosynthetic Bacteria* (Michel-Beyerle, M. E., Ed.) pp 298-305, Springer-Verlag, Berlin.

72. Warncke, K., and Dutton, P. L. (1993) *Biochemistry 32*, 4769-4779.

73. Moser, C. C., Page, C. C., Chen, X., and Dutton, P. L. (1997) *Journal of Biological Inorganic Chemistry*, in press.

74. Brudler, R., de Groot, H. J. M., van Liemt, W. B. S., Hoff, A. J., Lugtenburg, J. L., and Gerwert, K. (1995) *FEBS letter*, 2-14.

75. Deisenhofer, J., Epp, O., Miki, R., and Michel, H. (1985) *Nature 318*, 618-624.

76. Allen, J. P., Feher, G., Yeates, T. O., Komiya, H., and Rees, D. C. (1988) *Proc. Natl. Acad. Sci. USA 85*, 8487-8491.

77. El-Kabbani, O., Chang, C.-H., Tiede, D., Norris, J., and Schiffer, M. (1990) *Biochemistry 30*, 5361-5369.

78. Ermler, U., Fritzsch, G., Buchanan, S. K., and Michel, H. (1994) *Structure 2*, 925-936.

79. Abresch, E. C., Stowell, M. H. B., McPhillips, T. M., Rees, D. C., Soltis, S. M., and Feher, G. (1997) *Biophysical Journal 72*, A8.

80. Stowell, M. H. B., McPhillips, T. M., Rees, D. C., Soltis, S. M., Abresch, E. C., and Feher, G. (1997) *Science 276*, 812-816.

81. Paddock, M. L., Rongey, S. H., Feher, G., and Okamura, M. Y. (1989) *Proc. Natl. Acad. Sci. USA 86*, 6602-6606.

82. Mathis, P., Sinning, I., and Michel, H. (1992) *Biochim. Biophys. Acta 1098*, 151-158.

Chapter 5

1. Kleinfeld, D., Okamura, M. Y., and Feher, G. (1985) *Biochim. Biophys. Acta 809*, 291-310.
2. Field, M. J., Bash, P. A., and Karplus, M. (1990) *J. Comput. Chem. 113*, 4491.
3. Graige, M. S., Feher, G., and Okamura, M. Y. (1998) *Proc. Natl. Acad. Sci. USA 95*, 11679-11684.
4. Tiede, D. M., Vazquez, J., Cordova, J., and Marone, A. P. (1996) *Biochemistry 35*, 10763-10775.
5. Tiede, D. M., Utschig, L., Hanson, D. K., and Gallo, D. M. (1998) *Photosynth. Res 55*, 267-273.
6. Li, J., Gilroy, D., Tiede, D. M., and Gunner, M. R. (1998) *Biochemistry 37*, 2818-2829.
7. Gunner, M. R. (1991) *Current Topics in Bioenergetics 16*, 319-367.
8. Okamura, M. Y., and Feher, G. (1992) *Annu. Rev. Biochem. 61*, 861-896.
9. Vermeglio, A., and Clayton, R. K. (1977) *Biochim. Biophys. Acta 461*, 159-165.
10. Lubitz, W., Abresch, E. C., Debus, R. J., Isaacson, R. A., Okamura, M. Y., and Feher, G. (1985) *Biochim. Biophys. Acta 808*, 464-469.
11. Maroti, P., and Wraight, C. A. (1988) *Biochim. Biophys. Acta 934*, 314-328.

12. McPherson, P. H., Okamura, M. Y., and Feher, G. (1988) *Biochim. Biophys. Acta 934*, 348-368.
13. Hienerwadel, R., Thibodeau, D., Lenz, F., Nabedryk, E., Breton, J., Kreutz, W., and Mantele, W. (1992) *Biochemistry 31*, 5799-5808.
14. Hienerwadel, R., Grzybek, S., Fogel, C., Kreutz, W., Okamura, M. Y., Paddock, M. L., and Breton, J. (1995) *Biochemistry 34*, 2832-2843.
15. Gunner, M. R., and Honig, B. (1992) in *The Photosynthetic Bacterial Reaction Center: Structure, Spectroscopy and Dynamics II* (Breton, J., and Vermeglio, A., Eds.) pp 403-410, Plenum, New York.
16. Nabedryk, E., Brenton, J., Hienderwadel, R., Fogel, C., Mantele, W., Paddock, M. L., and Okamura, M. Y. (1995) *Biochemistry 34*, 14722-14732.
17. Patel, K. B., and Willson, R. L. (1973) *J. Chem. Soc.(Faraday I) 69*, 814-825.
18. Swallow, A. J. (1982) in *Function of Quinones in Energy Conserving Systems* (Trumpower, B. L., Ed.) pp 59-72, Academic Press, New York.
19. Shopes, R. J., and Wraight, C. A. (1985) *Biochim. Biophys. Acta 806*, 348-356.
20. Woodbury, N. W., Parson, W. W., Gunner, M. R., Prince, R. C., and Dutton, P. L. (1986) *Biochim. Biophys. Acta. 851*, 6-22.
21. Gunner, M. R., and Dutton, P. L. (1989) *J. Am. Chem. Soc. 111*, 3400-3412.
22. Mancino, L. J., Dean, D. P., and Blankenship, R. E. (1984) *Biochim. Biophys. Acta 764*, 46-54.

23. Kleinfeld, D., Okamura, M. Y., and Feher, G. (1984) *Biochim. Biophys. Acta 766*, 126-140.
24. McComb, J. C., Stein, R. R., and Wraight, C. A. (1990) *Biochim. Biophys. Acta 1015*, 156-171.
25. Warncke, K., Gunner, M. R., Braun, B. S., Gu, L., Yu, C., Bruce, J. M., and Dutton, P. L. (1994) *Biochemistry 33*, 7830-7841.
26. Leibl, W., and Breton, J. (1991) *Biochemistry 30*, 9634-9642.
27. Takahashi, E., and Wraight, C. A. (1992) *Biochemistry 31*, 855-866.
28. Takahashi, E., Maroti, P., and Wraight, C. A. (1992) in *Electron and Proton Transfer in Chemistry and Biology* (Muller, A., Ed.) pp pgs. 219-236, Elsevier.
29. Marcus, R. A., and Sutin, N. (1985) *Biochim. Biophys. Acta 811*, 265-322.
30. DeVault, D. (1980) *Q. Rev. Biophys. 13*, 387-564.
31. Allen, J. P., Williams, J. C., Graige, M., Paddock, M. L., Labahn, A., Feher, G., and Okamura, M. Y. (1998) *Photosynth. Res. 55*, 227-233.
32. Labahn, A., Paddok, M. L., McPherson, P. H., Okamura, M. Y., and Feher, G. (1994) *J. Phys. chem. 98*, 3417-3423.
33. Labahn, A., Bruce, J. M., Okamura, M. Y., and Feher, G. (1995) *Chem. Phys. 97*, 355-366.
34. Miksovska, J., Maroti, P., Tandori, J., Schiffer, M., Hanson, D. K., and Sebban, P. (1996) *Biochemistry 35*, 15411-15417.
35. Stowell, M. H. B., McPhillips, T. M., Rees, D. C., Soltis, S. M., Abresch, E., and Feher, G. (1997) *Science 276*, 812-816.
36. Alexov, E. G., and Gunner, M. R. (1997) *Biophys. J. 72*, 2075-2093.

37. Tiede, D. M., and Hanson, D. K. (1992) in *The Photosynthetic Reaction Center II* (Breton, J., and Vermeglio, A., Eds.) pp 341-350, Plenum Press, New York.

38. Brzezinski, P., Okamura, M. Y., and Feher, G. (1992) *Structural changes following the formation of D+QA- in bacetrial reaction centers: measurement of light-induced electrogenic events in RCs incorporated in a phospholipid monolayer*, Plenum Press, New York.

39. Baciou, L., and Sebban, P. (1995) *Photochem. and Photobio. 62*, 271-278.

40. Maroti, P., Hanson, D. K., Schiffer, M., and Sebban, P. (1995) *Nature Struc. Biology 2*, 1057-1059.

41. Kalman, L., Sebban, P., Hanson, D. K., Schiffer, M., and Maroti, P. (1998) *Biochim Biophys Acta 1365*, 513-521.

42. Dutton, P. L., Leigh, J. S., and Wraight, C. A. (1973) *FEBS Lett. 36*, 169-173.

43. Prince, R., and Dutton, P. L. (1976) *Arch. Biochem. Biophys. 172*, 329-334.